Technical Report Documentation Page

1. Report No. FHWA/TX-08/0-4586-1	2. Government Accession No.	3. Recipient's Catalog No.
4. Title and Subtitle Field Tests and Analytical Studies of the Dynamic Behavior and the Onset of Galloping in Traffic Signal Structures		5. Report Date March 2007, Rev. November 2007 6. Performing Organization Code
7. Author(s) Micah J. Florea, Lance Manuel, Karl H. Frank, Sharon L. Wood		8. Performing Organization Report No. 0-4586-1
9. Performing Organization Name and Address Center for Transportation Research The University of Texas at Austin 3208 Red River, Suite 200 Austin, TX 78705-2650		10. Work Unit No. (TRAIS) 11. Contract or Grant No. 0-4586
12. Sponsoring Agency Name and Address Texas Department of Transportation Research and Technology Implementation Office P.O. Box 5080 Austin, TX 78763-5080		13. Type of Report and Period Covered Technical Report 9/1/2003 – 8/31/2006 14. Sponsoring Agency Code

15. Supplementary Notes
Project performed in cooperation with the Texas Department of Transportation and the Federal Highway Administration.

16. Abstract
Unpredictable fatigue failures of cantilevered traffic signal structures in Texas and throughout the United States in recent years have created the need to study their fatigue behavior. Based on recent research, the American Association of State Highway and Transportation Officials (AASHTO) specification has adopted a design equation for galloping loads that is overly conservative in many cases. The Texas Department of Transportation (TxDOT) is interested in establishing design criteria for galloping that more accurately represents galloping potential and provides a more efficient design. In this study, three signal structures in Texas were monitored for a total of 9 months to detect the magnitude of galloping forces experienced in the field. Although large-amplitude displacements were measured in the field, sustained galloping did not occur. In addition to the field tests, an analytical model was developed and used to perform a parametric study for predicting the galloping potential of traffic signal structures with various properties. The analytical model suggests that modifying the aerodynamic properties of the sign and signal attachments may be the most effective way to handle galloping.

17. Key Words Traffic signal structures, signs, luminaires, fatigue, galloping, field tests.	18. Distribution Statement No restrictions. This document is available to the public through the National Technical Information Service, Springfield, Virginia 22161; www.ntis.gov.

19. Security Classif. (of report) Unclassified	20. Security Classif. (of this page) Unclassified	21. No. of pages 128	22. Price

Form DOT F 1700.7 (8-72) Reproduction of completed page authorized.

Field Tests and Analytical Studies of the Dynamic Behavior and the Onset of Galloping in Traffic Signal Structures

Micah J. Florea
Lance Manuel
Karl H. Frank
Sharon L. Wood

CTR Technical Report:	0-4586-1
Report Date:	March 2007, Rev. November 2007
Project:	0-4586
Project Title:	Revision of AASHTO Fatigue Design Loading for Signs, Luminaries, and Traffic Signal Structures for Use in Texas
Sponsoring Agency:	Texas Department of Transportation
Performing Agency:	Center for Transportation Research at The University of Texas at Austin

Project performed in cooperation with the Texas Department of Transportation and the Federal Highway Administration.

Center for Transportation Research
The University of Texas at Austin
3208 Red River
Austin, TX 78705

www.utexas.edu/research/ctr

Disclaimers

Author's Disclaimer: The contents of this report reflect the views of the authors, who are responsible for the facts and the accuracy of the data presented herein. The contents do not necessarily reflect the official view or policies of the Federal Highway Administration or the Texas Department of Transportation (TxDOT). This report does not constitute a standard, specification, or regulation.

Patent Disclaimer: There was no invention or discovery conceived or first actually reduced to practice in the course of or under this contract, including any art, method, process, machine manufacture, design or composition of matter, or any new useful improvement thereof, or any variety of plant, which is or may be patentable under the patent laws of the United States of America or any foreign country.

Engineering Disclaimer

NOT INTENDED FOR CONSTRUCTION, BIDDING, OR PERMIT PURPOSES.

Project Engineer: Lance Manuel, Ph.D., P.E.
Professional Engineer License State and Number: Texas No. 95990
P.E. Designation: Research Supervisor

Acknowledgments

The authors wish to acknowledge financial support received from the Texas Department of Transportation (TxDOT) engineers that made this research project possible. In addition, they thank the following TxDOT engineers who served on the project team and provided valuable assistance: Scott Walton, P.E., Ronald D. Medlock, P.E., Jim Yang, P.E., and Timothy Bradberry, P.E. They also express their gratitude to the production staff at the Center for Transportation Research for assistance in preparing this report.

Products

Product 1, "Suggested Revisions to the AASHTO Standard Specifications for Structural Supports for Highway Signs, Luminaires, and Traffic Signals (Section 11: Fatigue Design)," is included as an appendix to this report.

Abstract

Unpredictable fatigue failures of cantilevered traffic signal structures in Texas and throughout the United States in recent years have created the need to study their fatigue behavior. Based on recent research, the American Association of State Highway and Transportation Officials (AASHTO) specification has adopted a design equation for galloping loads that is overly conservative in many cases. The Texas Department of Transportation (TxDOT) is interested in establishing design criteria for galloping that more accurately represents galloping potential and provides a more efficient design. In this study, three signal structures in Texas were monitored for a total of 9 months to detect the magnitude of galloping forces experienced in the field. Although large-amplitude displacements were measured in the field, sustained galloping did not occur. In addition to the field tests, an analytical model was developed and used to perform a parametric study for predicting the galloping potential of traffic signal structures with various properties. The analytical model suggests that modifying the aerodynamic properties of the sign and signal attachments may be the most effective way to handle galloping.

Table of Contents

List of Tables

List of Figures

Notation

A	projected area of the cross section on a plane perpendicular to the wind direction
C_D	drag coefficient of the cross section
C_{Fy}	vertical force coefficient of the cross section
C_L	lift coefficient of the cross section
c_e	equivalent viscous damping coefficient of the structure
d	height of the signal structure attachment
F_D	drag force
F_L	lift force
F_y	resultant force in the vertical direction
F_{ye}	equivalent aerodynamic damping of the structural system
I_F	importance Factor
k_e	equivalent stiffness of the structure
L	length of sign or signal attachment or length of arm
M	moment at the connection
t_{pole}	wall thickness of pole
t_{arm}	wall thickness of arm
m_e	equivalent mass of the structure
$m(x)$	mass per unit length of the structure
P_G	equivalent static pressure (psf) to be applied to the horizontal surface area of all rigid attachments
S	section modulus
t	variable representing time
U	wind speed
u	displacement in the vertical direction
$\dot{u}$	velocity in the vertical direction
$\ddot{u}$	acceleration in the vertical direction
$U_{\min}$	minimum sustained perpendicular wind speed required to cause galloping
x	coordinate used to define position along the structural members comprising the traffic signal structure
$z(t)$	generalized coordinate used to describe displacement at any time
$\dot{z}(t)$	time derivative of the generalized coordinate used to describe displacement
α	angle of attack of the wind on the cross section
ρ	mass density of air (taken as 0.00237 slug/ft^3 at 15°C and 760 mm of mercury)
σ	longitudinal stress range of interest
ω_e	equivalent natural angular frequency
$\psi(x)$	assumed function describing the displaced shape of the structure
$\psi''(x)$	second derivative with respect to x of the assumed function describing the displaced shape of the structure
ζ	damping ratio of the structure

Chapter 1. Introduction

1.1 Background

Cantilevered traffic signal structures are used extensively in Texas and throughout the United States as a practical and economical solution for support of traffic signals and certain other traffic control devices, especially in urban areas. Due to their innate flexibility and low mechanical damping properties, these cantilevered structures are extremely susceptible to cyclic fatigue loading. Once a wind gust or some other transient force initiates motion of the mast arm, the structures undergo a large number of cycles before the motion decays. The structures accumulate many stress cycles with each such event.

Unpredictable fatigue failures of many cantilever traffic signal structures around the country over the past several years have created a need to study traffic signal support structure fatigue behavior. In the state of Missouri, a dozen traffic signal mast arms failed in a recent 5-year period, most of which occurred after only 1 to 2 years in service (Wu et al., 2000). A visual inspection of 840 signal structures in Wyoming determined that over a third of them had fatigue cracks at the pole-to-arm connection, ranging from ¼ in. to 20 in. in length (Hamilton et al., 2000). Texas has also witnessed fatigue failures, including one each in the cities of Pflugerville and Lubbock. The Pflugerville failure can be seen in Figures 1.1 and 1.2. Several studies over the past decade have addressed the loading conditions of traffic signal structures, attempting to determine if the failures have been due to inadequate design load assumptions.

Figure 1.1: Failure of traffic signal structure in Pflugerville

Figure 1.2: Failure due to fatigue crack initiated at top of mast arm

1.2 Galloping

Cantilevered mast arms are assumed to be susceptible to four different wind phenomena that can induce vibrations and lead to fatigue failure. These four phenomena include vortex shedding, galloping, natural wind gusts, and truck-induced wind gusts. Cyclical displacements at the tip of the mast arm up to 48 in. have been witnessed under steady wind conditions perpendicular to the mast arm (Kaczinski et al., 1998). Previous studies have concluded that large-magnitude displacements of tapered mast arms are not generally caused by vortex shedding (McDonald et al., 1995). Continuous large-amplitude displacements have sometimes occurred when trucks are not present, and the behavior of mast arms, moving vertically in an across-wind direction, matches the expected response brought about by galloping. Galloping has been thought to be the cause of the largest displacements of traffic signal structures in the field, and is potentially the most damaging type of load experienced by traffic signal structures.

Galloping is an aeroelastic motion-induced phenomenon created by a perpendicular wind acting on a non-symmetric cross section. In the case of traffic signals, the wind is horizontal and the motion of the signal is vertical. The lateral wind velocity couples with the relative velocity caused by the vertical motion of the cross section to create a wind resultant with a constantly changing angle of attack. Once galloping initiates, the structure can experience increased displacements with each cycle in a sustained wind until a specific amplitude is reached, which is determined by the aerodynamic properties of the sign and signal attachments and the mechanical properties of the structure. Only certain specific cross sections have the potential to gallop, and the lateral wind speed must be greater than a critical value for it to occur. Circular cross sections, used for most mast arms, cannot experience galloping, and therefore only the attachments on the mast arms can help induce galloping. In order for a cross section to experience galloping, there must be the potential for negative aerodynamic damping to occur. Commonly referred to as the Den Hartog stability criterion, the overall damping of the structure must be negative to lead to instability. The phenomenon of galloping was first studied to describe the large-displacement

behavior of transmission lines, but the principles have since been applied to many other structures to describe instability (Den Hartog, 1956). The galloping phenomenon is explained in more detail in Chapter 2.

1.3 Motivation

In 1995, tow tank tests were performed at Texas Tech University (McDonald et al., 1995) to measure the susceptibility to galloping of several traffic signal configurations. It was determined that traffic signals with back plates were more susceptible in general than signals without back plates. More specifically, a signal located below the mast arm with a back plate and subjected to wind from the rear was extremely unstable. The results of these tow tank tests are utilized in the analytical model developed in Chapter 2.

Several wind-tunnel tests and field tests were performed for NCHRP Report 412 (Kaczinski et al., 1998) to determine the loads caused by galloping. Measured moment data was used to back-calculate an equivalent static pressure, which was multiplied by the horizontal projection of the attachments on the mast arm and applied as vertical loads on the arm. The resulting equivalent static loads varied from 16.2 psf to 38.9 psf. It is apparent that the loads caused by galloping forces can vary quite drastically and can depend on the configuration and properties of the specific structure subjected to the proper wind flow. It was concluded that, since galloping is suspected to be a rare occurrence, a low-end value of 21 psf was sufficient to use for design purposes. This value, which can be reduced by up to 70 percent by applying importance factors, was adopted by AASHTO for design (AASHTO, 2003).

According to the latest AASHTO specification, traffic signals must be designed to resist galloping in the following manner:
"Overhead cantilevered sign and traffic signal support structures shall be designed for galloping-induced cyclic loads by applying an equivalent static shear pressure vertically to the surface area, as viewed in normal elevation of all sign panels and/or traffic signal heads and back plates rigidly mounted to the cantilevered horizontal support. The magnitude of this vertical shear pressure range shall be equal to the following:" (AASHTO, 2003)

Equation 1-1: $P_G = 21 \cdot I_F$

where:

P_G: The equivalent static pressure (psf) to be applied to the horizontal surface area of all rigid attachments

I_F: Importance Factor as explained in Table 1.1

Table 1.1: Importance Factors for Galloping

Fatigue Category	Importance Factor, I_F	Structures that apply
I	1.0	Critical cantilevered support structures installed on major highways
II	0.65	Other cantilevered support structures installed on major highways and all cantilevered support structures installed on secondary highways
III	0.30	Cantilevered support structures installed at all other locations

The current AASHTO provisions for galloping have at least two inherent flaws: they assume that all structures gallop, and they assume very simplified galloping forces that do not accurately capture the true loading behavior of a galloping structure. The member sizes currently required to resist galloping forces are quite often very large and govern many designs. The design equation must be applied to all traffic signal structures because currently there is not sufficient aerodynamic data from a variety of traffic signals to determine which structures will definitely not gallop. In an attempt to confirm the design criteria currently used for galloping, Texas Tech University measured stresses on a traffic signal structure with a 48-ft arm. After back-calculating from the measured moments at the pole, the maximum equivalent static pressure was determined to be 19.9 psf. This pressure compared quite well with the 21 psf currently used for design.

The current design equations for galloping are thought by many agencies and design engineers across the country to vastly overestimate the expected galloping loads, and thus require heavy sections and cause needless cost burdens for new traffic signal structures. However, it is also evident from the research studies cited above that this is not the case for all traffic signal structures. In fact, for some structures, the current equations appear to underdesign for galloping. It is clear that the problem is not that the loads experienced during galloping are being overestimated, but rather that most structures do not gallop and therefore should not be required to resist the galloping design loads specified in the code.

1.4 Project Scope and Objectives

The University of Texas at Austin and Texas Tech University teamed up to investigate the loading effects of galloping and truck-induced wind gusts on traffic signal structures for the Texas Department of Transportation (TxDOT). The use of analytical models to explain galloping potential, and the monitoring of signal structures in field test studies focusing on the galloping phenomenon are reported here.

The theory behind the phenomenon of galloping was studied. A mathematical model was derived and a computer program was developed to analyze traffic signal structures with arbitrary member sizes and attachments. Parametric studies were carried out to evaluate the effects of varying the structural characteristics of signal structures and assess the effectiveness of the application of a damping wing, which had been studied previously for structures in the field (McDonald et al., 1995) and in a wind tunnel (Pulipaka et al., 1998). A study of traffic signal structures at three field sites was carried out to determine the wind speeds expected to cause galloping at each site. In a preliminary field test, a signal structure was temporarily instrumented to test equipment and to develop methods for analyzing the response of the structure. Three traffic signal structures at distinct locations were later monitored for a total of 9 months to gather large-amplitude displacement data. The results of these investigations are discussed in this report, and recommendations are made to establish an appropriate path to resolution of the current inconsistency in galloping design.

Chapter 2. Analytical Model

2.1 Introduction

Only a small fraction of traffic signal structures have the potential to gallop. This statement is reinforced by Texas Tech's tow tank test findings that most traffic signal configurations provide positive aerodynamic damping and hence cannot experience galloping (McDonald et al., 1995). Therefore, it is conservative to design all signal structures to withstand galloping oscillations, which is the controlling design criterion in many cases. Since galloping can only occur with sustained wind above certain critical velocities (Dyrbye and Hansen, 1997), one way to eliminate the possibility of galloping for a particular structure is to design the structure to ensure that the onset wind velocity is higher than the maximum wind velocity typically experienced at the site.

Many tests and analyses have been carried out previously to determine if a constant cross section with a single degree of freedom will gallop, but these studies cannot be directly applied to predict if a traffic signal structure will gallop. Therefore, the principles of galloping need to be extended to an entire traffic signal structure, an infinite-degree-of-freedom system where each component may bring about its own unique aerodynamic loads on the structure. Analytical models were developed to determine which signal structures have the possibility of galloping. A corresponding program was written in MathCAD to facilitate a parametric study.

2.2 Background

The Den Hartog criterion has traditionally been used to determine the minimum wind speed required to cause a constant cross section with a single degree of freedom to gallop (Dyrbye and Hansen, 1997):

$$\textit{Equation 2-1:}\quad U_{\min} = \frac{-4m_e\zeta\omega_e}{\rho A}\frac{1}{\left(\frac{\partial C_L}{\partial \alpha} + C_D\right)\Big|_{\alpha=0}};\ \text{and}\ \left(\frac{\partial C_L}{\partial \alpha} + C_D\right)\Big|_{\alpha=0} < 0$$

where:

- U_{min}: minimum sustained perpendicular wind speed required to cause the cross section to gallop,
- m_e: equivalent mass of the structure,
- ζ: damping ratio of the structure,
- ω_e: equivalent natural angular frequency,
- ρ: mass density of air (taken as 0.00237 slug/ft^3 at 15°C and 760 mm of mercury),
- A: the projected area of the cross section on a plane perpendicular to the wind direction,
- C_L: lift coefficient of the cross section,

C_D: drag coefficient of the cross section,

α: the angle of attack of the wind on the cross section.

As mentioned previously, traffic signal structures are not comprised of one constant cross section, but rather have continuously varying cross sections along the length of the mast arm. One must take a closer look at the cause of galloping and the development of the Den Hartog criterion to form an appropriate model that can be applied to signal structures used by TxDOT. The models must be able to incorporate variable member sizes made of tapered circular tubes and several signal and sign attachments located at arbitrary locations along the arm, each with its own properties (Figure 2.1).

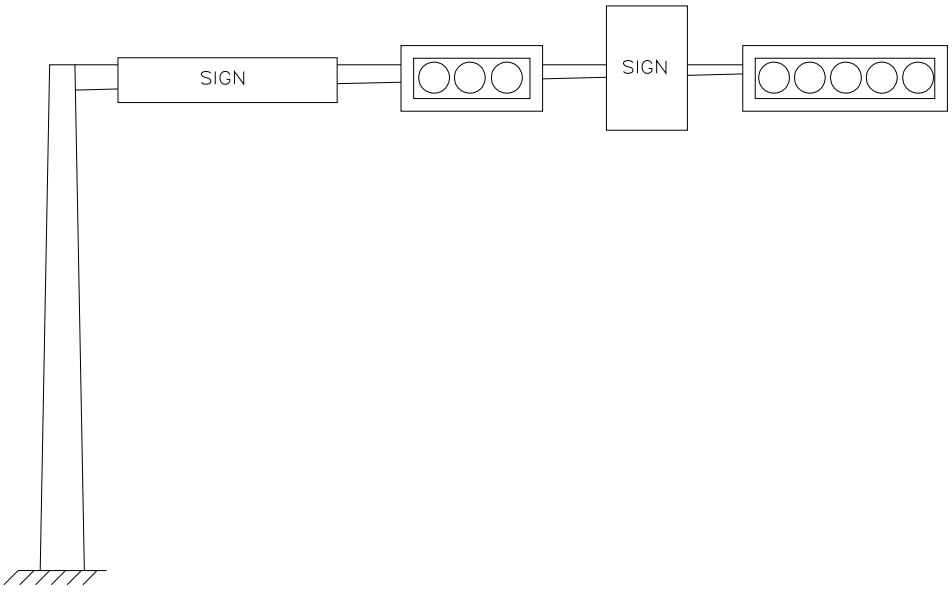

Figure 2.1: A typical TxDOT cantilever mono-tube traffic signal structure with various sign and signal attachments along its mast arm

Galloping is a motion-induced phenomenon. Therefore, galloping requires a separate source of loading to initiate it, which can come from natural wind gusts, vortex shedding, or, in the case of traffic signals, truck gusts. Once the cross section begins moving perpendicular to the wind vertically, the horizontal wind velocity, u, combines with the vertical velocity of the cross section, $\dot{u}$, to form a resultant wind vector with a vertical component relative to the structure and a constantly changing angle of attack, α. This scenario is demonstrated in Figure 2.2.

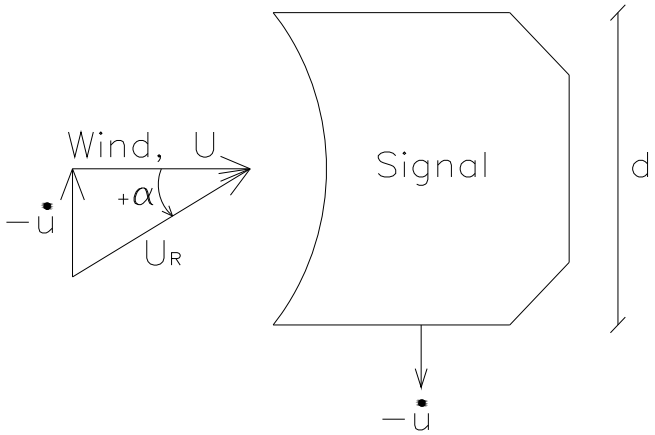

Figure 2.2: The vertical velocity of the traffic signal adds to the horizontal wind velocity to create a relative wind velocity resultant

If the angle of attack, α, is set equal to zero with a horizontal wind resultant, then as the cross section moves downward, the resultant wind vector forms a positive angle. Conversely, as the cross section moves upward, the resultant wind vector forms a negative angle. The resultant upward vertical force coefficient, C_{Fy}, can be plotted against α to determine the possibility of galloping. Plots of this type have been produced for several traffic signal configurations during a study by Texas Tech University (McDonald et al., 1995). A positive slope, as in , means that as the cross section moves upward, a relative downward force is applied. The actual value and direction of the applied force is irrelevant to galloping; only the change in force is important. As the cross section moves downward, a relative upward force acts on it. Termed positive aerodynamic damping, this adds to the structural damping and helps reduce the motion of the structure. If the slope of the C_{Fy} vs. α plot is negative, as in Figure 2.4, the effect is the opposite. As the cross section moves downward, a relative downward force is applied, and as it moves upward, a relative upward force is applied. This acts to promote motion and is known as negative aerodynamic damping. In a single-degree-of-freedom system with a single cross section, if the negative aerodynamic damping of the cross section exceeds the structural damping, then the structure will gallop.

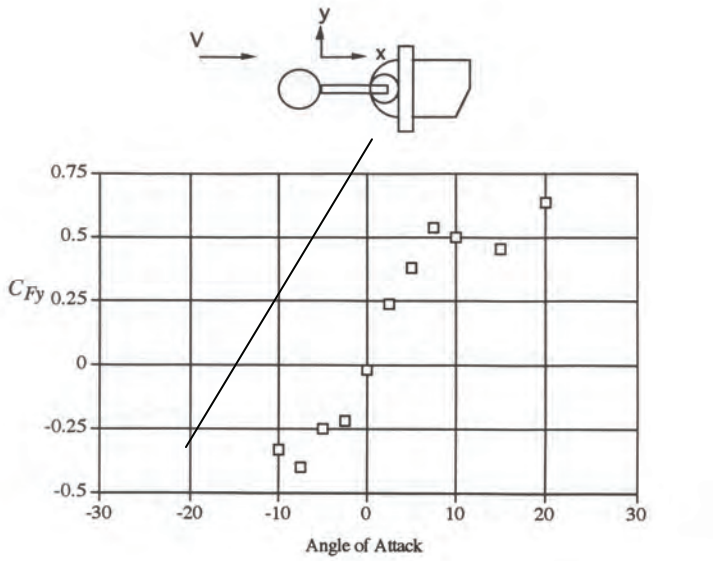

Figure 2.3: Vertical force coefficient, C_{Fy}, vs. angle of attack, α, forms a positive slope (McDonald et al., 1995)

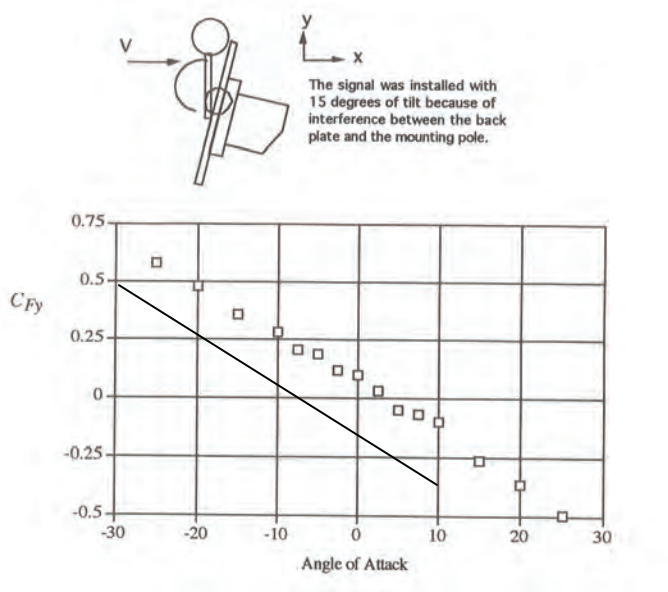

Figure 2.4: Vertical force coefficient, C_{Fy}, vs. angle of attack, α, forms a negative slope (McDonald et al., 1995)

With a constant wind velocity, once galloping initiates, the motion-induced forces will act in phase with the structural response and create larger displacements with each cycle until one of three things occurs:

1. The wind changes velocity or direction, creating a sudden disturbance in the angle of attack and potentially creating forces that act out of phase with the motion of the structure. This may cause the galloping to cease, allowing the structural damping to damp out the motion. Depending on the new direction of wind, this could even create positive aerodynamic damping forces to accompany the structural damping forces, damping out the motion more quickly.

2. The structure's damping ratio increases as the displacements become larger, and eventually the structural damping becomes equal to the motion-induced aerodynamic damping, causing constant-amplitude galloping. In this case, galloping will continue, but the amplitude will not keep increasing.

3. The angle of attack changes sufficiently to exit the region with a negative slope on the C_{Fy} vs. α plot. In a galloping situation, the total change in the angle of attack increases as the displacement to wind speed ratio increases.

2.3 Mathematical Model

The mathematical model assumes a constant horizontal wind velocity flowing perpendicular to the mast arm of the structure. Although wind may flow parallel to the mast arm, the area of the signal attachments normal to that direction is considered small enough to not have a significant effect on galloping. A constant damping ratio of the structure and a constant slope on the C_{Fy} vs. α plot for each sign or signal attachment in the zone where galloping will initiate is also assumed. Neglecting the influence of turbulence, drag and lift forces are expressed by the following equations (Dyrbye and Hansen, 1997):

Equation 2-2: $$F_D = \frac{1}{2}\rho U^2 A C_D$$

Equation 2-3: $$F_L = \frac{1}{2}\rho U^2 A C_L$$

As mentioned earlier, when the signal moves downward it has a negative velocity, and the angle of attack is positive. This creates the following relationship:

Equation 2-4: $$\tan(\alpha) = \frac{-\dot{u}}{U}$$

The force that causes galloping is the resultant force in the vertical direction. This force can be seen in Figure 2.5 to be related to F_D and F_L in the following manner:

Equation 2-5: $$F_y = F_D \sin(\alpha) + F_L \cos(\alpha)$$

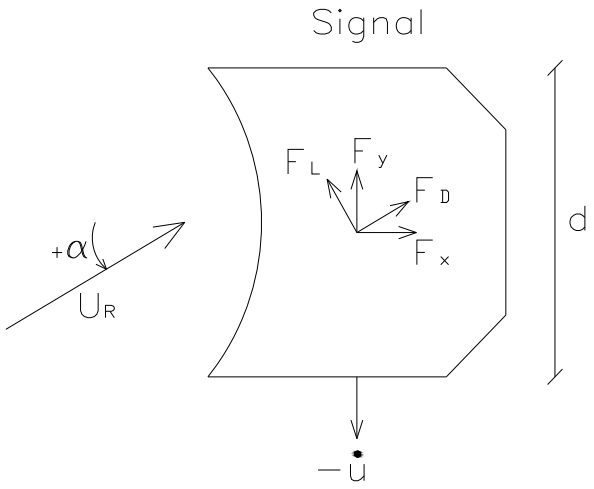

Figure 2.5: A traffic signal showing the relationship of the various forces acting on it due to the resultant wind vector

The vertical force coefficient, C_{Fy}, can be related to the velocity of the wind in the same form as the lift and drag force coefficients are:

Equation 2-6: $$F_y = \frac{1}{2}\rho U^2 A C_{Fy}$$

This allows for a relationship between the force coefficients. Typically, lift and drag coefficients of an object are measured in wind tunnel tests. The following relationship is used to relate the vertical force coefficient to the lift and drag force coefficients:

Equation 2-7: $$C_{Fy} = \left(C_L + C_D \tan(\alpha)\right)\frac{1}{\cos(\alpha)}$$

The computational model will be developed here in terms of the vertical force coefficient. This way, the final equations will be ready to incorporate results from the Texas Tech report (McDonald et al., 1995), which used a tow tank to directly measure the vertical force coefficient at various angles of attack (Figure 2.3 and Figure 2.4). By taking the MacLaurin Series expansion of *Equation 2-6* and retaining only the first two terms, the following equation is derived:

Equation 2-8: $$F_y = \frac{1}{2}\rho U^2 A \left.\frac{\partial C_{Fy}}{\partial \alpha}\right|_{\alpha=0} \alpha$$

Combining *Equation 2-4* and *Equation 2-8* and applying the small angle of attack approximation, namely that $\lim_{\alpha\to 0}\frac{\alpha}{\tan(\alpha)} = 1$, the aerodynamic damping force may be related to the relative wind velocity resultant as follows:

Equation 2-9: $$F_y = -\frac{1}{2}\rho \dot{u} U A \left.\frac{\partial C_{Fy}}{\partial \alpha}\right|_{\alpha=0}$$

Although the structure has infinite degrees of freedom, it can be simplified for the purpose of analysis and design. An acceptable approximation employed in similar dynamic analysis studies is to assume a deflected shape for the structure (Chopra, 2001), and then develop a generalized single-degree-of-freedom system based on this shape. For the MathCAD program developed for

this study, a generalized shape was derived based on the deflected shape of a structure consisting of a cantilevered vertical pole rigidly connected to a horizontal arm, with a vertical force at the tip of the arm (Figure 2.6). For this shape derivation, Bernoulli beam theory was employed, and each member's cross section was assumed prismatic and equal to the cross section at its midpoint. Only in-plane deformations were considered. This is expected to be a sufficiently accurate representation of the shape of the structure when galloping, based on visual images of a galloping structure and the natural in-plane mode shape of the structure. The assumed shape function $\psi(x)$ was multiplied by a time-dependent generalized displacement $z(t)$ to determine the displacement at any place along the structure at a given time. Note that x is used as a coordinate to define points along both structural element members and all the attachments.

Equation 2-10: $u = \psi(x)z(t)$

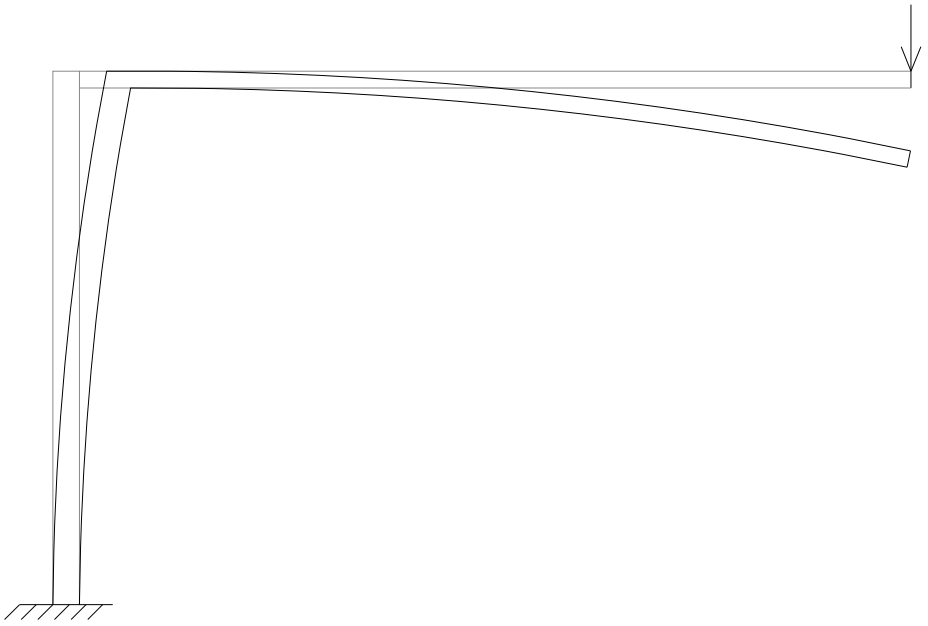

Figure 2.6: The assumed deflected shape of the structure during a galloping event

Allowing the displacement, u, to vary along the length of the structure and requiring the height, d, and the term $\left.\frac{\partial C_{Fy}}{\partial \alpha}\right|_{\alpha=0}$ to remain constant over the length of each attachment, *Equation 2-9* can be rewritten to describe the vertical force caused by aerodynamic damping per unit length for each attachment:

Equation 2-11: $F_y(x) = -\frac{1}{2}\rho U d \left.\frac{\partial C_{Fy}}{\partial \alpha}\right|_{\alpha=0} \psi(x)\dot{z}(t)$

Applying the principle of virtual work to derive an equivalent system, the equation of motion in terms of the generalized displacement, $z(t)$, can be expressed as follows:

Equation 2-12: $m_e\ddot{z} + c_e\dot{z} + k_e z = F_{ye}\dot{z}$

where:

m_e: the equivalent mass of the system, $\sum\int m(x)\left(\psi(x)\right)^2 dx$, where *m(x)* is the mass per unit length, the summation includes both structural members and all attachments, and the integration is performed over the length of each structural member and the length of each attachment,

k_e: the equivalent stiffness of the system, $\sum\int EI(x)\left(\psi''(x)\right)^2 dx$, where *E* is taken as 29,600 ksi for steel, *I(x)* is the moment of inertia, the summation includes only the two structural members, and the integration is performed over the length of each structural member,

c_e: the equivalent structural damping coefficient of the system, $2\zeta m_e \omega_e$, where ω_e is the equivalent natural frequency of the system, equal to $\sqrt{\frac{k_e}{m_e}}$,

F_{ye}: the equivalent aerodynamic damping of the system, $-\frac{1}{2}\rho U\sum\left(d\frac{\partial C_{Fy}}{\partial\alpha}\bigg|_{\alpha=0}\int\left(\psi(x)\right)^2 dx\right)$, where the summation includes only the sign and signal attachments, and the integration is only performed over the length of each attachment, since the term $\frac{\partial C_{Fy}}{\partial\alpha}$ is zero for a circular cross section.

The inertia and restoring forces in *Equation 2-12* are not of interest for galloping. Of interest is the sum of the structural and aerodynamic damping forces, F_d:

Equation 2-13: $$F_d = \left(2m_e\zeta\omega_e + \frac{1}{2}\rho U\sum\left(d\frac{\partial C_{Fy}}{\partial\alpha}\bigg|_{\alpha=0}\int\left(\psi(x)\right)^2 dx\right)\right)\dot{z}(t)$$

In *Equation 2-13*, all terms except $\frac{\partial C_{Fy}}{\partial\alpha}\bigg|_{\alpha=0}$ are positive. Therefore, it is clear that the total damping force can only be negative if at least one of the signal or sign attachments complies with the following:

Equation 2-14: $$\frac{\partial C_{Fy}}{\partial\alpha}\bigg|_{\alpha=0} < 0$$

For galloping to be possible, not only must *Equation 2-14* be true, but the attachments that produce negative aerodynamic damping must exceed the structural damping and the potential positive aerodynamic damping of other attachments. Solving for the critical wind velocity required for this to occur results in the following equation:

Equation 2-15: $$U_{\min} = \frac{-4m_e\zeta\omega_e}{\rho} \frac{1}{\sum\left(d \left.\frac{\partial C_{Fy}}{\partial \alpha}\right|_{\alpha=0} \int (\psi(x))^2 dx \right)}$$

2.4 Qualitative Analysis

To understand how the properties of a traffic signal structure influence its potential to gallop, it is worth examining *Equation 2-15* qualitatively. The following relationships between the minimum wind speed required for galloping and the parameters of the structure can be used to tune the system:

- $U_{\min}$ is proportional to $\sqrt{m_e}$, so it is desirable to increase the generalized mass of the system. The generalized mass includes the term $(\psi(x))^2$; therefore, the mass near the tip of the structure has a much greater effect than the mass near the pole in increasing $U_{\min}$.
- $U_{\min}$ is proportional to $\sqrt{k_e}$, so a stiffer system is less likely to gallop.
- $U_{\min}$ is linearly proportional to the structural damping ratio, ζ, so an increase in structural damping is beneficial.
- $U_{\min}$ is inversely proportional to the sum of the aerodynamic damping caused by each attachment. Here again, since the term $(\psi(x))^2$ is included, the sign and signal attachments near the tip of the structure have the greatest impact on the required wind speed for the onset of galloping. Although the mass, stiffness, and damping can be predicted fairly accurately, the term $\left.\frac{\partial C_{Fy}}{\partial \alpha}\right|_{\alpha=0}$ for each attachment is not as well known.

2.5 Quantitative Analysis

The MathCAD program written to determine the minimum wind velocity required for galloping can efficiently analyze traffic signal structures with various parameters. It was utilized for a parametric study and for the analysis of three signal structures tested in the field. The program is included in Appendix A. From the Texas Tech tow tank tests mentioned previously (McDonald et al., 1995), the worst-case traffic signal configuration can be seen in Figure 2.4 to have a $\left.\frac{\partial C_{Fy}}{\partial \alpha}\right|_{\alpha=0}$ value of -1.3. Note that this particular configuration is the only one out of the eight traffic signals tested by researchers at Texas Tech University that had an obvious negative slope at an angle of attack near zero degrees. The other configurations either had a definite positive slope or a slope of approximately zero. This discrepancy between the majority of the data with a slope of practically zero and the one test with a large negative slope had a very significant effect

on the wind speeds required for galloping to occur. Since the term $\frac{\partial C_{Fy}}{\partial \alpha}$ can vary considerably depending on the orientation of each signal on the mast arm, it is allowed to vary in many of the following studies.

Although the following plots appear to suggest a high probability of galloping for many values of $\frac{\partial C_{Fy}}{\partial \alpha}$, there has not been sufficient research carried out to determine what the actual value of $\frac{\partial C_{Fy}}{\partial \alpha}$ is for most traffic signals. Based on the limited research performed in the tow tank tests as stated above, the vast majority of traffic signals may have values of $\frac{\partial C_{Fy}}{\partial \alpha}$ that are either positive or close to zero, which would not induce galloping, as the following plots suggest. Furthermore, if there is more than one attachment on a mast arm, one of them could induce galloping while the other ones cancel it out with their positive aerodynamic damping effects. For the purposes of this study, all of the signs and signals attached to the arm are assumed to share the same aerodynamic properties in each case.

2.5.1 Parametric Study

Control Specimen

For the parametric study, the signal at the Pflugerville site (described in more detail in Chapter 4) was used as the control specimen. A plot comparing U_{min} estimates based on the value of $\frac{\partial C_{Fy}}{\partial \alpha}$ can be found in Figure 2.7. Note that for low values of $\frac{\partial C_{Fy}}{\partial \alpha}$, galloping is not possible. However, as the value of $\frac{\partial C_{Fy}}{\partial \alpha}$ increases, the wind speed required to induce galloping is very low, and galloping is more likely to occur.

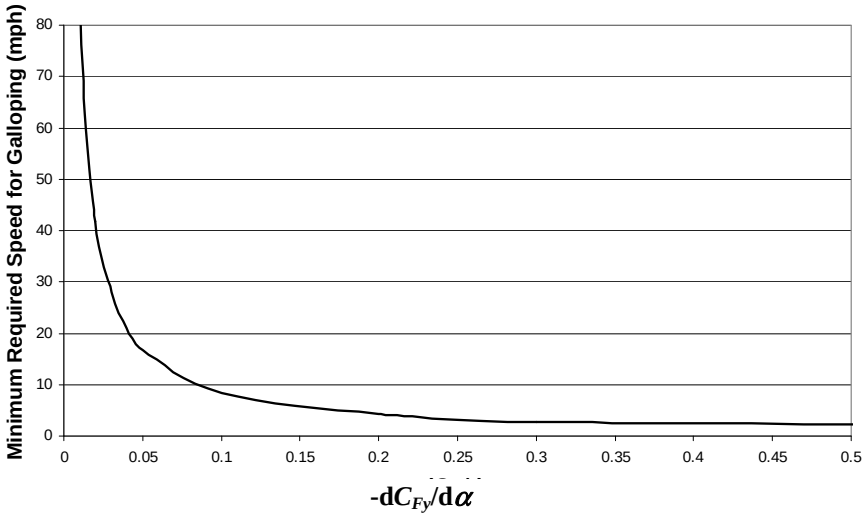

Figure 2.7: Pflugerville test site

Effect of Mass

The galloping onset velocity of the structure can be increased by increasing the generalized mass of the structure. This is most effectively done by adding mass to the tip of the mast arm. It is evident from Figure 2.8 that it would require an unsafe amount of weight at the tip of the mast arm to have a noticeable effect on the structure's potential for galloping. Another problem with increasing the mass of the structure is that, although the onset wind speed increases with increased mass for a given value of $\frac{\partial C_{Fy}}{\partial \alpha}$, the $\frac{\partial C_{Fy}}{\partial \alpha}$ value is much more critical in determining galloping potential. If a $\frac{\partial C_{Fy}}{\partial \alpha}$ value of -0.5 is assumed, which is not even the worst case for galloping, then the added mass to the structure has negligible effect. Therefore, adding mass may not be an effective manner to counter galloping potential.

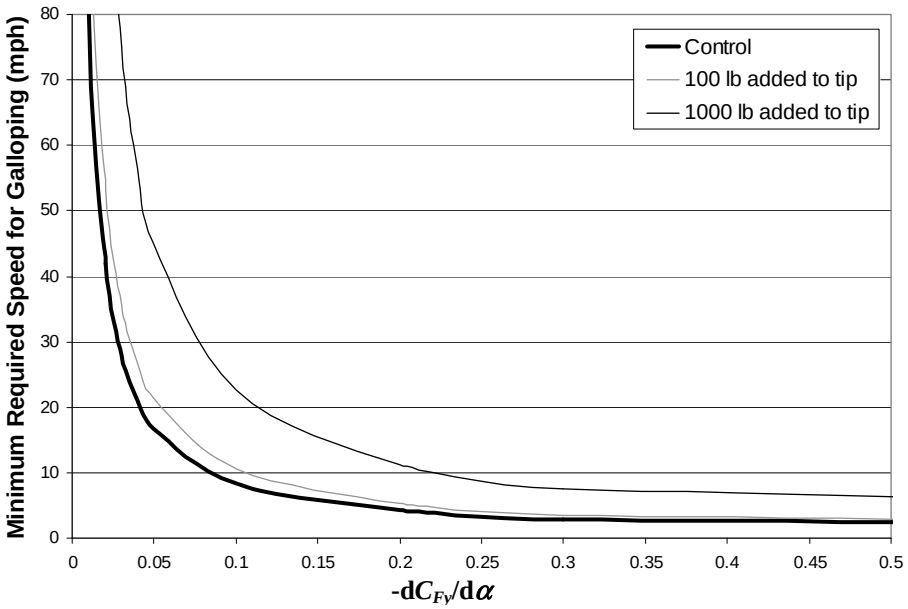

Figure 2.8: The effect of mass (weight) on galloping

Effect of Stiffness

Another possible way to increase the onset velocity for galloping is to increase the stiffness of the structure. If the pole is assumed to be rigid, creating a fixed-end cantilever mast arm, Figure 2.9 suggests that not much is gained towards preventing galloping. This is because the arm still deflects with a similar shape as before. If the arm is considered to be rigid, the deflected shape of the arm is linear, and this is slightly more effective at preventing galloping. However, as in the case of adding mass, neither of these options is effective for eliminating the possibility of galloping, especially since the $\frac{\partial C_{Fy}}{\partial \alpha}$ values are not well known.

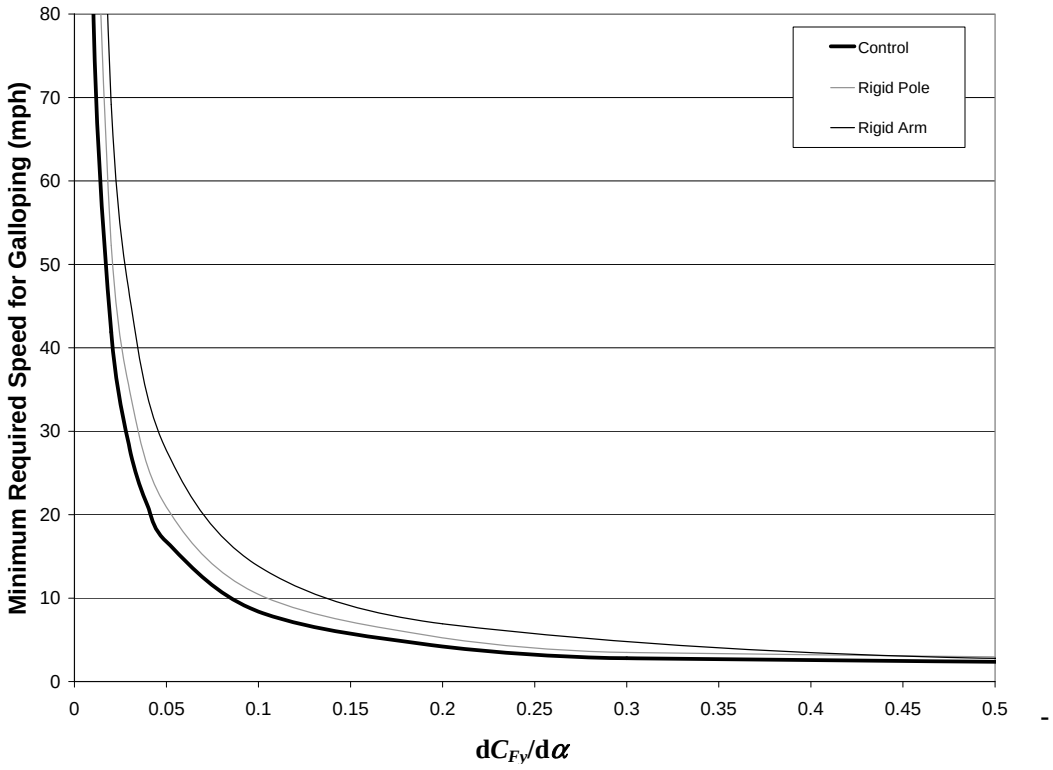

Figure 2.9: The effect of structural stiffness on galloping

Effect of Structural Damping

The wind speed required for galloping is directly proportional to the structural damping of the system. Partly due to this, many structural damping systems have been developed and tested, including tuned-mass dampers, friction dampers, etc. (Cook and Bloomquist, 2000 and Hamilton et al., 2000). Although increasing the structural damping can increase the wind speed required for galloping, this change effectively shifts the curves in Figure 2.10 vertically. However, the increase in damping required to make a noticeable difference in the wind speed required for galloping is quite large, and the aerodynamic properties of the attachments still typically govern. Currently, no cost-effective solution that can sufficiently increase the structural damping has been developed. Once again, these changes are most effective if the sign and signal attachments have aerodynamic properties very close to a specific value, which is not easily predictable. One other advantage of increasing the structural damping of a system is that the number of large amplitude cycles caused by any type of gust loading can be greatly reduced. Therefore, increased structural damping is helpful to lengthen fatigue life, but it is not a very effective solution to eliminate the possibility of galloping.

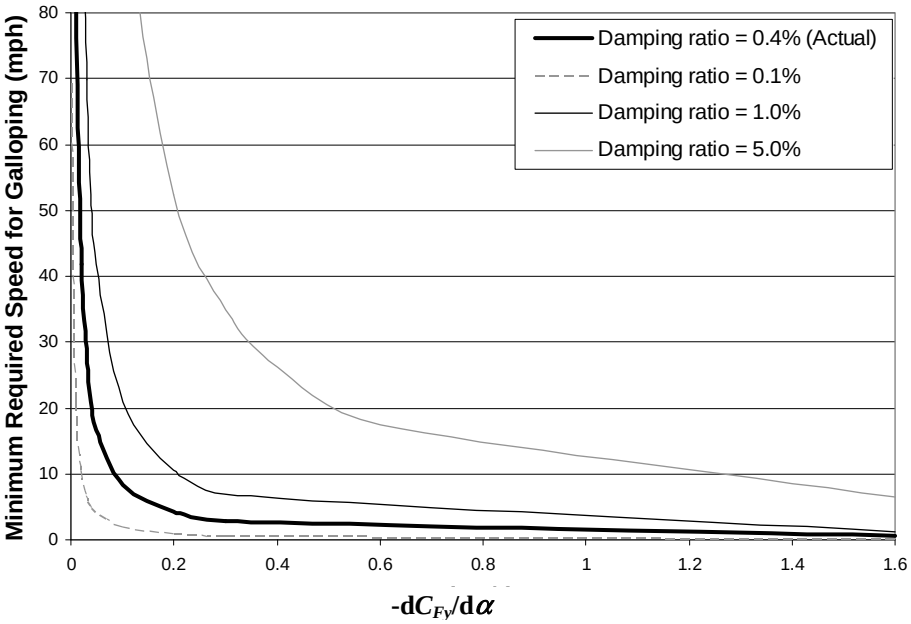

Figure 2.10: The effect of structural damping on galloping

Modification of Aerodynamic Properties

The most effective solution to eliminate the possibility of galloping is to modify the aerodynamic properties of the structure. One way to do this is to only install traffic signals that have positive aerodynamic damping properties or very little negative aerodynamic damping potential. Currently in Texas, some signals in service have rounded backs, some have V-shaped backs, and some are more squared-off. The effect of these differences has not been studied; however, if it were determined that one particular type of signal backing always provided positive aerodynamic damping, then this type of signal could always be used to avoid galloping.

One factor related to aerodynamic damping that has been studied, though not extensively, is the orientation of the signal attached to the mast arm. It appears that the orientation can have severe and unpredictable effects on galloping, but it is unclear whether or not small changes to a given orientation can make a large difference in galloping potential. Extremely precise orientation of traffic signals is difficult to control when installing them in the field, and therefore it may be necessary to assume a worst-case scenario for signal orientation.

The effect of back plates has also been studied briefly, and in general, traffic signals with back plates were found to have more severe negative aerodynamic damping potential than traffic signals without them (McDonald et al., 1995). In a discussion with personnel at TxDOT, the author was informed that all future traffic signals may have back plates. Therefore, TxDOT must design all of their traffic signal structures to resist the additional forces caused by the back plates. Both configurations of traffic signals with back plates that were studied by Texas Tech in the tow tank tests (below the mast arm and in-line with the mast arm) have the potential to cause negative aerodynamic damping. Therefore, to eliminate the possibility of galloping, an additional attachment with positive aerodynamic damping to counteract the negative aerodynamic damping may need to be installed.

The horizontal sign blank, or wing, which has been tested previously under controlled conditions, can be a very effective damping device, and appears to be a cost-effective solution. It consists of mounting a blank traffic sign horizontally above the mast arm, typically near the tip of the arm. Researchers at Texas Tech University have performed tow tank tests on one sign blank configuration to determine its positive aerodynamic damping potential. Its dimensions and layout are given in Figure 2.11, and its vertical force coefficient is plotted against angle of attack in Figure 2.12. This is the only data currently available for determining the necessary length of wing required to eliminate the possibility of galloping. The effect of adjusting the distance between the mast arm and the wing, moving the wing laterally relative to the mast arm, or changing the width of the wing are not completely understood. More testing to determine the effects of these modifications could offer more effective options for design. Because of this limitation, the analytical studies of the effects of the wing included herein only consider the dimensions and layout shown in Figure 2.11 of 4.6 for $\frac{\partial C_{Fy}}{\partial \alpha}$ based on Figure 2.12.

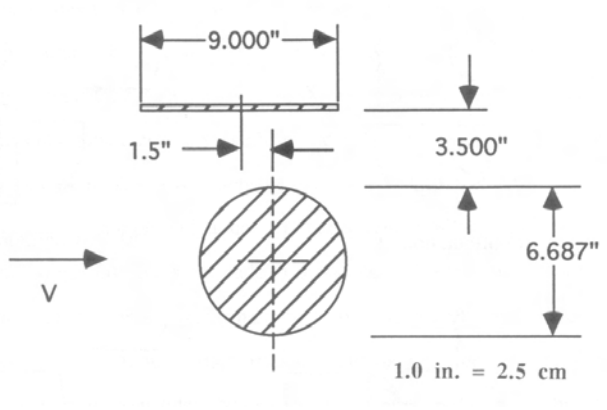

Figure 2.11: Dimensions and configuration of the wing tested at Texas Tech University and included in this parametric study (Source: McDonald et al., 1995)

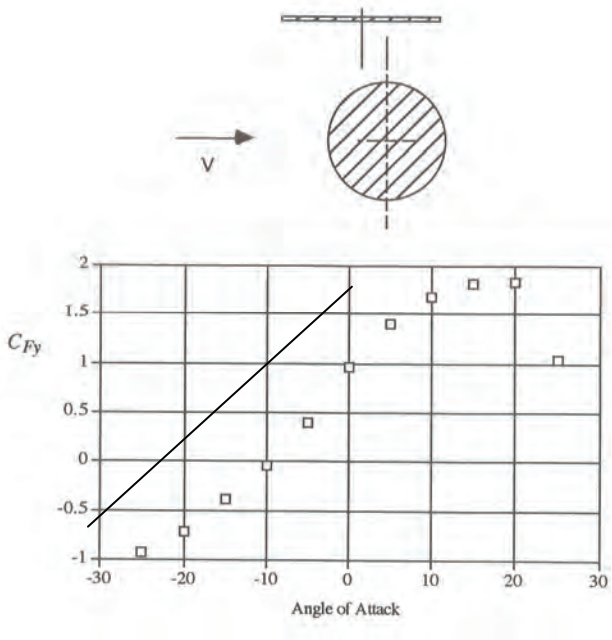

Figure 2.12: Positive aerodynamic damping potential of wing attached to mast arm (Source: McDonald et al., 1995)

The wing is most beneficial for eliminating galloping when located at the end of the mast arm. In Figure 2.13, the location of the center of a 36-in. wing is plotted against the wind speed required to cause galloping of the structure. Several values of $\frac{\partial C_{Fy}}{\partial \alpha}$ were assumed for the signals and attachments, and they are included in the plot. The figure clearly demonstrates that the location of the wing is important; for maximum benefit, the wing should be located as far out toward the tip of the mast arm as possible. If the aerodynamic properties of the traffic signals are excessively large in the sense of negative aerodynamic potential for the size of wing used, the wing will not help regardless of its location. Also, Figure 2.13 shows that there are nearly vertical portions of the curves showing U_{min} versus distance to wing. If the wing is located beyond a certain point for a specific signal configuration, the structure will not gallop. For example, if $\frac{\partial C_{Fy}}{\partial \alpha}$ is -0.2, a 36-in. wing placed at or beyond 70 percent of the arm length will not gallop.

The length of the wing is also very crucial. In general, a longer wing needs a higher wind speed to initiate galloping. As Figure 2.14 demonstrates, the length of wing required to prevent galloping at a given wind speed varies considerably for different aerodynamic properties of the signals. It also varies considerably with small changes in location of the wing: flush with the end of the mast arm, or with its center lined up with the end of the arm and extending beyond the arm. This assumes that the aerodynamic properties of the wing stay the same when extended beyond the arm. These calculations also ignore the interaction of the wing over a traffic signal, which has not been studied extensively.

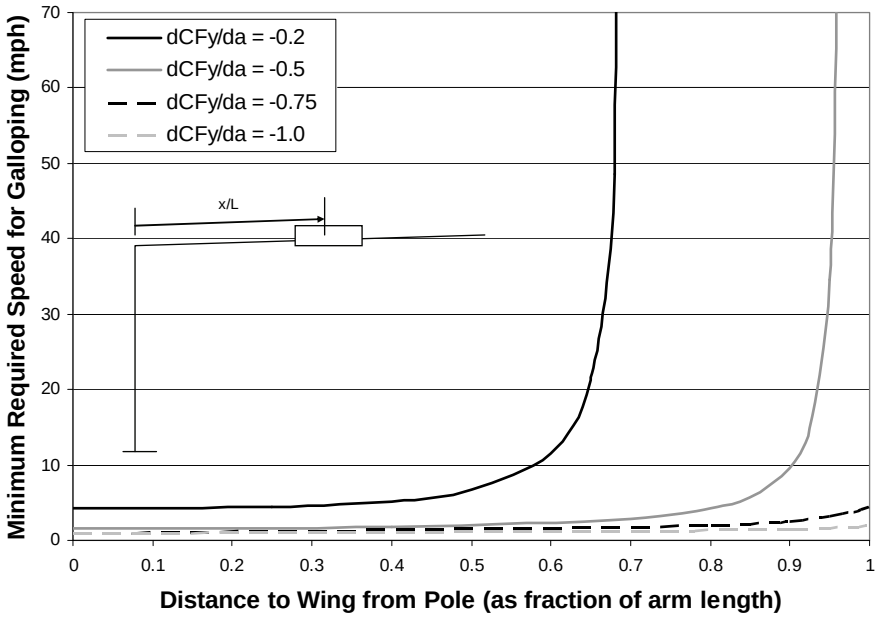

Figure 2.13: Effect of wing location on galloping

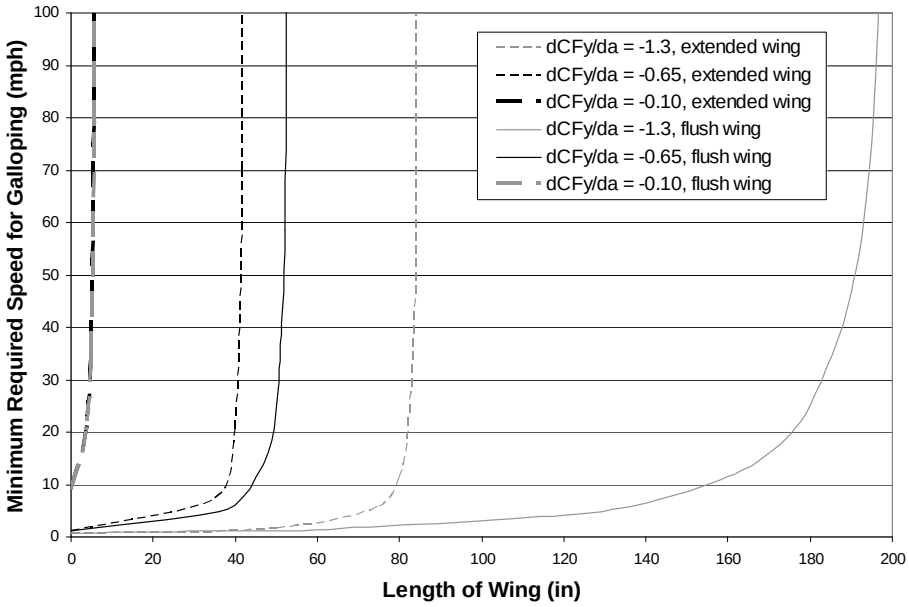

Figure 2.14: Effects of wing length and wing alignment with the tip of the mast arm on galloping

2.5.2 Signal Structures from Field Tests

The three sites that were monitored in the field included a site in Pflugerville, one in Round Rock, and one in Lubbock. They all had unique member sizes and different sign and signal configurations along their mast arms. The member sizes are summarized in Table 2.1 using the

layout description in Figure 2.15. The sign and signal attachments are summarized in Table 2.2 using the description in Figure 2.16. The minimum sustained wind speed perpendicular to the mast arm required for each structure to gallop is shown in Figure 2.17. It is clear that the potential for each structure to gallop varies depending on the value of $\frac{\partial C_{Fy}}{\partial \alpha}$ assumed for the attachments.

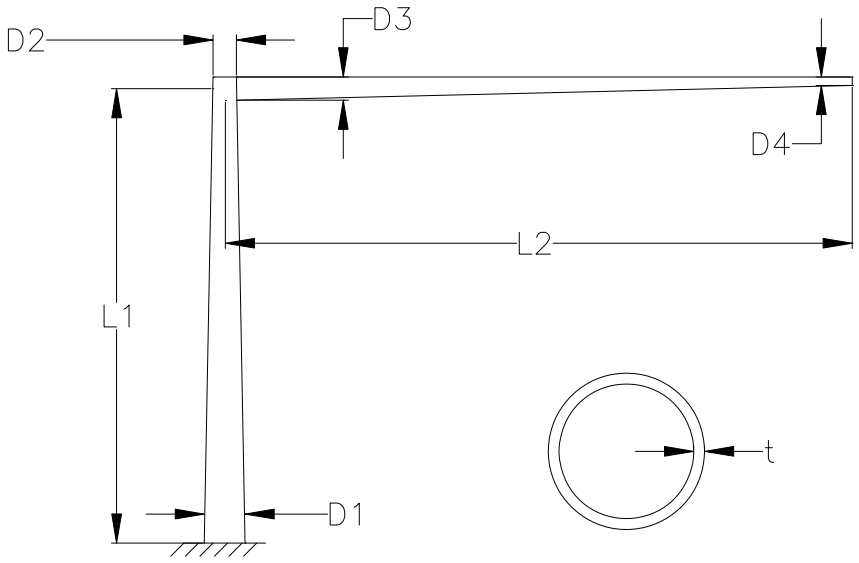

Figure 2.15: Nomenclature for dimensions of traffic signal structure members at the three field sites

Table 2.1: Dimensions of traffic signal structure members as defined in Figure 2.15

Site	L1 (in)	L2 (in)	D1 (in)	D2 (in)	D3 (in)	D4 (in)	t (in)
Pflugerville	218	340	11.62	9.29	8.26	4.20	0.179
Round Rock	201	412	11.70	9.35	8.30	4.20	0.179
Lubbock	214	538	11.95	8.86	8.92	4.10	0.239

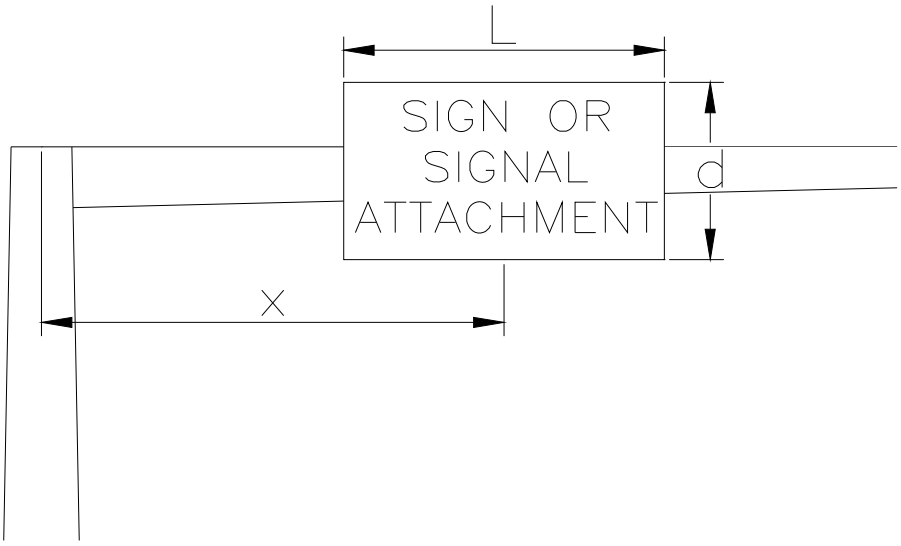

Figure 2.16: Nomenclature for dimensions of mast arm attachment at the three field sites

Table 2.2: Dimensions of mast arm attachments as defined in Figure 2.16

Attachment Number	Pflugerville			Round Rock			Lubbock		
	x (in)	L (in)	d (in)	x (in)	L (in)	d (in)	x (in)	L (in)	d (in)
Attachment 1	68	102	16	189	78	11	86	90	18
Attachment 2	166	52	23	325	50	23	209	50	23
Attachment 3	263	52	23	419	50	23	362	50	23
Attachment 4	348	80	23	N/A	N/A	N/A	443	29	33
Attachment 5	N/A	N/A	N/A	N/A	N/A	N/A	526	80	23

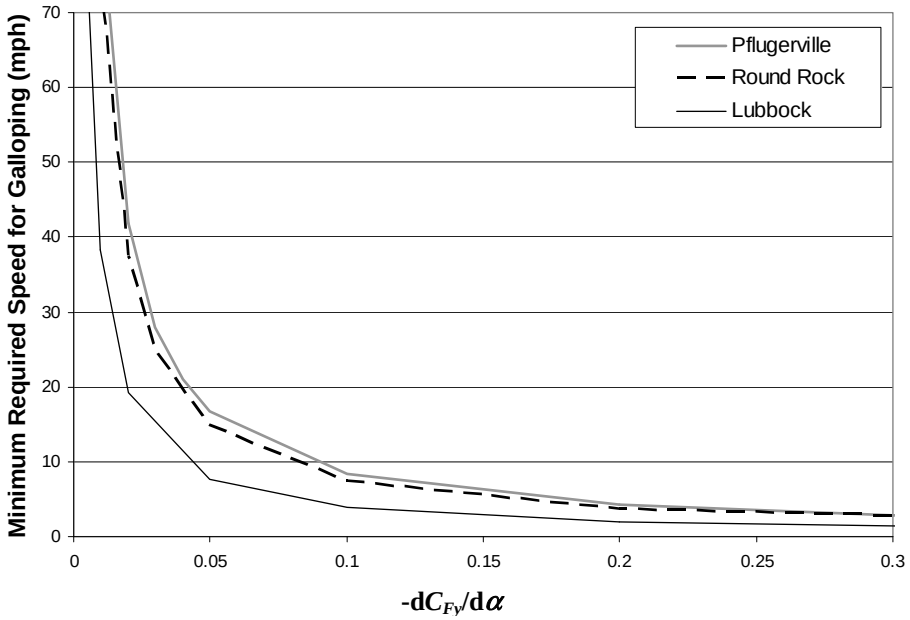

Figure 2.17: Required wind speed for structure at each site to gallop based on assumed aerodynamic properties of sign and signal attachments

A damping wing, as described earlier, could be added to each of these three structures to eliminate the possibility of galloping. To ensure there is no negative aerodynamic damping, the structural damping is irrelevant. Only the aerodynamic forces of the mast arm and its attachments must be considered. A worst-case scenario of -1.3 and a moderate-case scenario of -0.3 are assumed for the values of $\frac{\partial C_{Fy}}{\partial \alpha}$ for each sign and signal attachment. The wing is assumed to be located at the tip of the mast arm for each case, flush with the end of the arm. The length of wing required for each traffic signal structure to eliminate galloping for the two scenarios at each site is presented in Table 2.3. At these three sites, no simple and easily detectable pattern is obvious, although the area of the sign and signal attachments near the tip of the mast arm plays a significant role in determining the wing length required.

Table 2.3: Length of wing required at each site to prevent galloping

Site of Traffic Signal Structure	Length of Wing Required (in)	
	$\frac{\partial C_{Fy}}{\partial \alpha}$ = -0.3	$\frac{\partial C_{Fy}}{\partial \alpha}$ = -1.3
Pflugerville	22	206
Round Rock	14	79
Lubbock	21	117

2.6 Conclusions

Traffic signal structures are prone to galloping because of their flexibility, their extremely light structural damping, and the potentially poor aerodynamic damping properties of their

attachments. Although all of these play a role, the aerodynamic damping of the structure has the greatest impact on its potential to gallop. Therefore, signals that can only produce positive aerodynamic damping should be used, if possible. If signals with negative aerodynamic damping potential are used, then additional attachments that create positive aerodynamic damping to offset the effects of the signals should be installed to avoid galloping of the structure. Sign blanks, or wings, mounted on the tip of the mast arm seem to be a cost-effective solution; however, more research studies may need to be carried out to be able to specify their dimensions to effectively eliminate galloping.

Chapter 3. Preparations for Field Tests

3.1 Computational Study of Traffic Signal Behavior

Before designing a data acquisition system and instrumenting traffic signal structures in the field, a computational study investigating TxDOT's standard structures was performed using the finite element analysis program SAP2000. This was done to evaluate the static and dynamic behavior of typical structures used in Texas. Models were created based on the TxDOT standard design drawing, SMA-80(1)-99, which is shown in Appendix B. The standard drawing lists the properties of each structure based on its mast arm length. Eight models with distinct mast arm lengths were created and analyzed. They all consisted of members with circular cross sections. Their properties are given in Table 3.1 using the nomenclature shown in Figure 3.1.

Each model included masses and gravity forces for attached traffic signals. Each model included between one and three signals, whose quantity and placement matched TxDOT's standards. The signals were assumed to weigh 50 lbs each. All of the members were created using tapered (non-prismatic) pipe cross sections. The pole-to-arm connection was treated as rigid, and the base of the pole was restrained from displacements and rotations in all directions.

Table 3.1: Dimensions of members as defined in Figure 3.1

Nominal Arm Length (ft)	L (ft)	D_1 (in)	D_2 (in)	D_3 (in)	D_4 (in)	t_{pole} (in)	t_{arm} (in)	h (in)
20	19.1	10.5	7.8	6.5	3.8	0.179	0.179	21
24	23.1	11.0	8.3	7.5	4.3	0.179	0.179	22
28	27.1	11.5	8.8	8.0	4.2	0.179	0.179	23
32	31.0	12.5	9.8	9.0	4.7	0.179	0.179	25
36	35.0	12.0	9.3	9.5	4.6	0.239	0.179	28
40	39.0	12.0	9.3	9.5	4.1	0.239	0.239	32
44	43.0	12.5	9.8	10.0	4.1	0.239	0.239	35
48	47.0	13.0	10.3	10.5	4.1	0.239	0.239	40

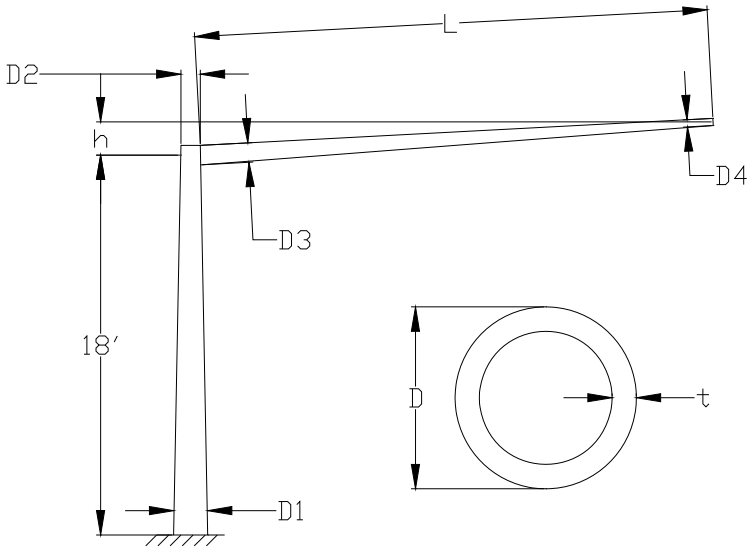

Figure 3.1: Nomenclature for dimensions of models

Several static load cases were run, and the importance of the pole stiffness in the overall structural response investigated. Table 3.2 shows the displacement of the tip of the mast arm under two distinct loading conditions with two structural modeling assumptions. One loading condition was dead load alone, and the other included superimposed load application consisting of a 100-lb vertical force applied to the tip of the mast arm. The structure was modeled with flexible arm and pole in one case and with flexible arm and rigid pole in the other case. As expected, the rigid pole model yielded 50 percent smaller tip deflections under dead load and somewhat smaller differences under the superimposed load.

The dynamic properties of the structures were also investigated. The in-plane behavior was of primary interest, since motion attributed to galloping typically acts in the plane formed by the pole and the arm. The first in-plane vibration mode of each structure, creating a motion sometimes referred to as hatcheting (Connor et al., 2004). The structures generally had lower frequencies as the arm lengths were increased. The frequencies varied from 0.75 Hz for a 48-ft arm to 1.53 Hz for a 20-ft arm. When the out-of plane behavior was included in the study, the overall lowest-energy vibration mode was with the arm bending out of plane combined with twisting of the pole. (Note, though, that the precise material and section properties and the support/connection characteristics at the top and bottom of the pole as they relate to torsional motion may need to be studied in greater detail than was done in this study.) The hatcheting motion was the second mode, though its frequency was almost identical to the first mode frequency. As higher modes were investigated, they appeared to come in pairs of similar energy levels, with the third and fourth modes having a frequency of typically around 2.5 to 4.5 times the first and second mode frequencies, depending on the arm length.

Therefore, the first and second modes were expected to contribute to the majority of the motion experienced by the structures used by TxDOT. Table 3.4 displays the frequencies of the first six modes for the structures with 24-ft and 48-ft mast arms.

Table 3.2: Displacement of mast arm tip under various conditions

Arm Length (ft)	Dead Load Displacement (in)		Live Load Displacement (in)	
	Unmodified Pole	Rigid Pole	Unmodified Pole	Rigid Pole
20	2.60	1.43	2.20	1.34
24	4.27	2.19	2.56	1.51
28	6.01	3.30	3.31	2.09
32	7.66	4.26	3.37	2.17
36	9.94	5.80	4.09	2.76
40	14.39	7.94	4.78	3.14
44	17.67	10.17	5.42	3.70
48	21.29	12.71	6.05	4.26

Table 3.3: First in-plane frequency of each structure

Arm Length (ft)	First In-plane Mode Frequency (Hz)	
	Unmodified Pole	Rigid Pole
20	1.53	2.06
24	1.53	2.24
28	1.30	1.81
32	1.25	1.71
36	1.10	1.46
40	0.91	1.24
44	0.83	1.10
48	0.75	0.98

Table 3.4: First six frequencies of two representative structures

Mode Number	24 ft Arm	48 ft Arm
	Frequency (Hz)	
1 (out-of-plane)	1.48	0.72
2 (in-plane)	1.53	0.75
3	3.70	2.87
4	3.76	2.96
5	8.38	4.45
6	9.59	4.85

3.2 Preliminary Test Setup and Analysis

In February 2004, a data acquisition system was prepared and installed on a traffic signal structure at the intersection of Burnet Road and Ohlen Road in Austin. The signal structure is shown in Figure 3.2. The installation was intended to test the functionality of the equipment, streamline the installation procedure for future field tests, and gather data samples to analyze. A Campbell Scientific CR9000 Datalogger was used to gather information from four strain gauges, two 3-axis accelerometers, and one 3-axis ultrasonic anemometer, placed on the structure as shown in Figure 3.3 and Figure 3.4. Vertical pluck tests were performed by hanging a weight from the tip of the mast arm. After the weight came to a rest, the wire holding the weight was cut, allowing the structure to undergo free vibration motion. Through a series of checks, all of the instrumentation appeared to be operating correctly. The strain gauges located opposite each other on the mast arm measured equal and opposite data. Figure 3.5 and Figure 3.6 show the strain data from one of the strain gauges plotted against the corresponding reversed-sign strain from the opposite side. Figure 3.5 is for strains on the two sides and Figure 3.6 is for strains at the top and bottom of the mast arm. Due to the well-correlated behavior observed in diametrically opposite gauges, only two strain gauges were used in future tests: one on top of the mast arm and one on one side.

Figure 3.2: Traffic signal structure in Austin utilized for preliminary test setup

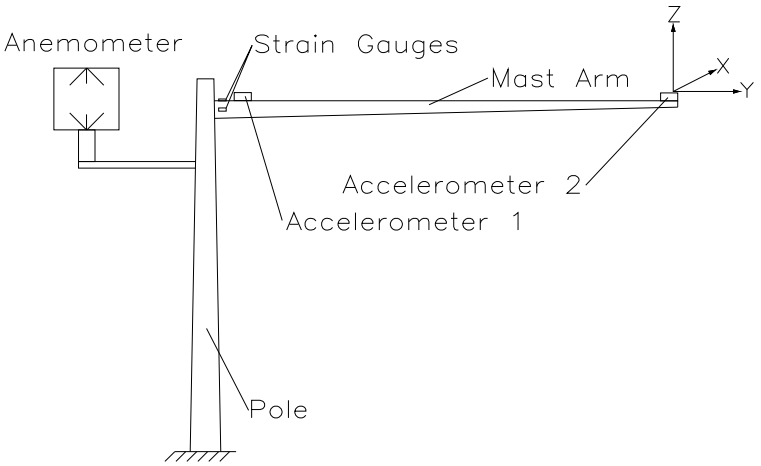

Figure 3.3: Layout of equipment for preliminary test setup

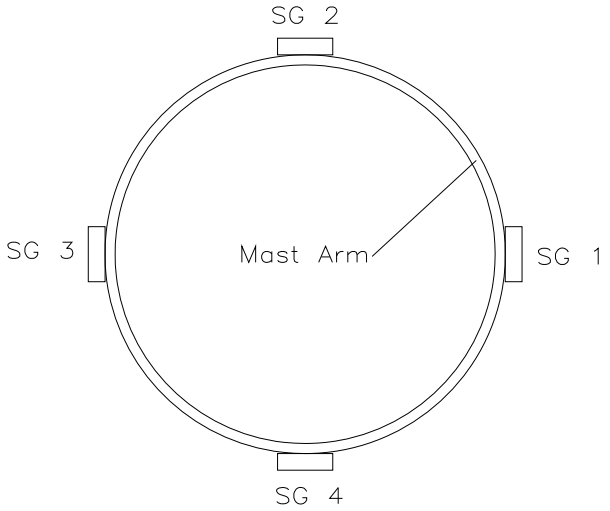

Figure 3.4: Placement of strain gauges on mast arm

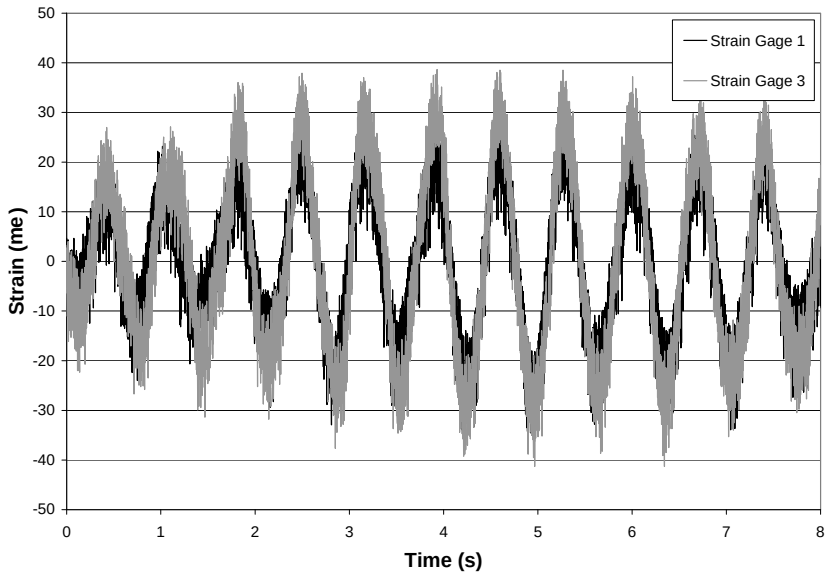

Figure 3.5: Strain measured by strain gauges on sides of the mast arm

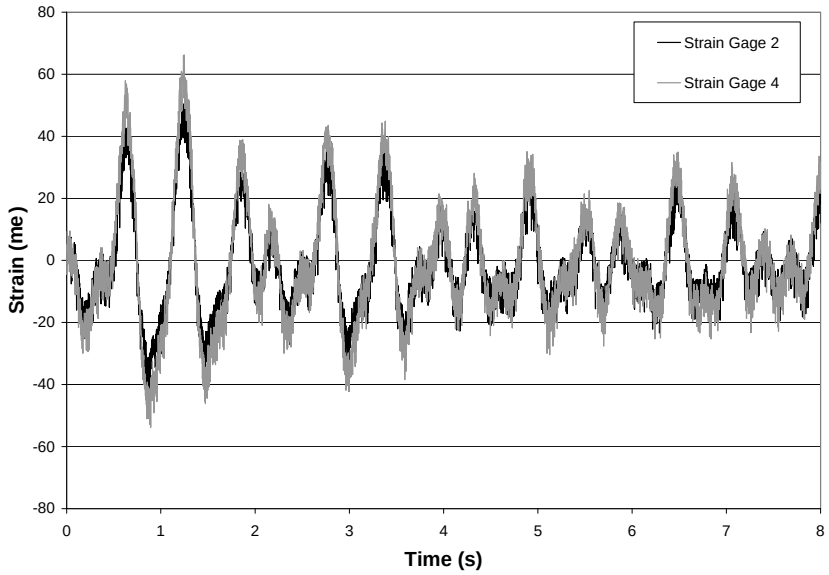

Figure 3.6: Strain measured by strain gauges on top and bottom of mast arm

The same site was revisited in April 2004 to gather more free vibration data because the data from the initial tests were not thought to be sufficient to determine the structure's dynamic characteristics. The behavior of the structure initially appeared to be quite random. When new plucks were applied directly vertically again, the motion of the structure consistently showed significant out-of-plane character. Upon analyzing the acceleration data at the tip of the mast arm, it was evident that energy was swapping between two modes, indicating a beating response. This complex behavior can be confirmed by studying Figure 3.7, where the vertical displacement and lateral out-of-plane displacement, respectively, are plotted against time. The displacements were derived from the acceleration data by the procedure described later in this chapter.

Also in Figure 3.7, the two displacements are plotted together to indicate how they complement each other. Figure 3.8 shows smoothed power spectra of the acceleration at the tip of the mast arm in these two directions. It is evident that several modes participated to varying degrees in the structure's dynamic response. A luminaire that was attached to the signal structure and which extended out of plane over the adjacent roadway might have been the cause of much of the out-of-plane motion. The eccentricity of the traffic signals, which were attached about 6 in. out of the centerline plane created by the pole and the mast arm also may have contributed to out-of-plane motion. This was subsequently confirmed in a finite element analysis of the structure.

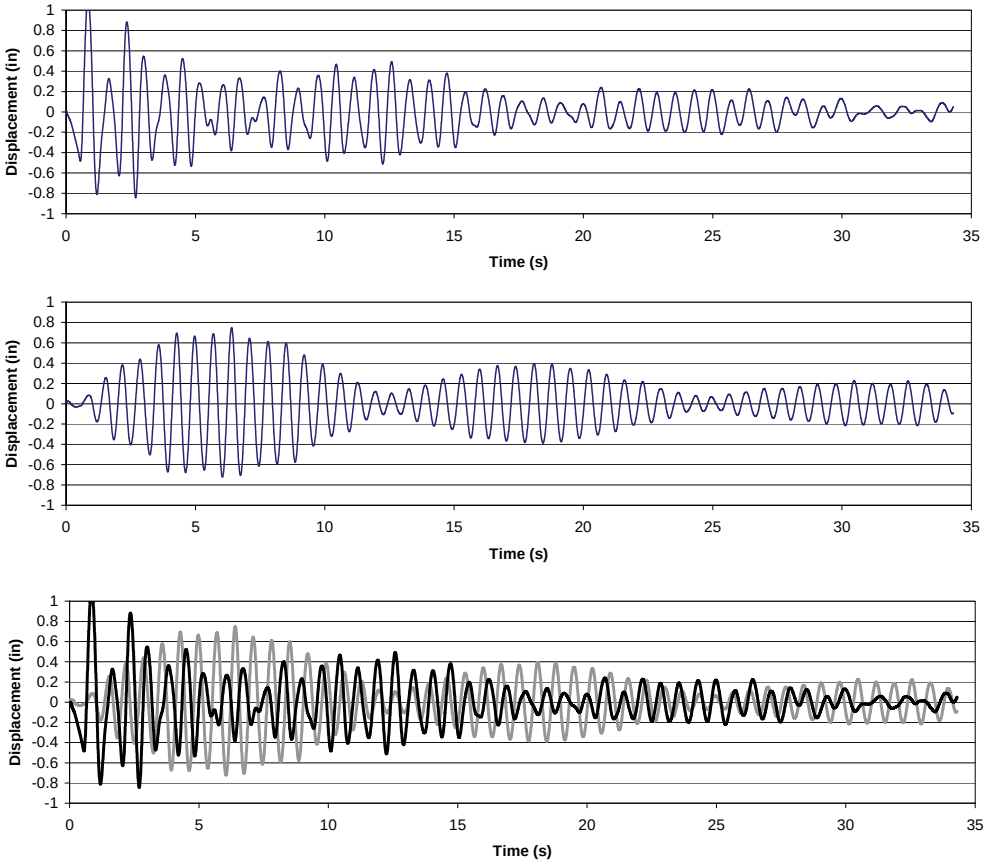

Figure 3.7: Displacement of the mast arm tip vertically (top), laterally out of plane (middle), and both combined (bottom)

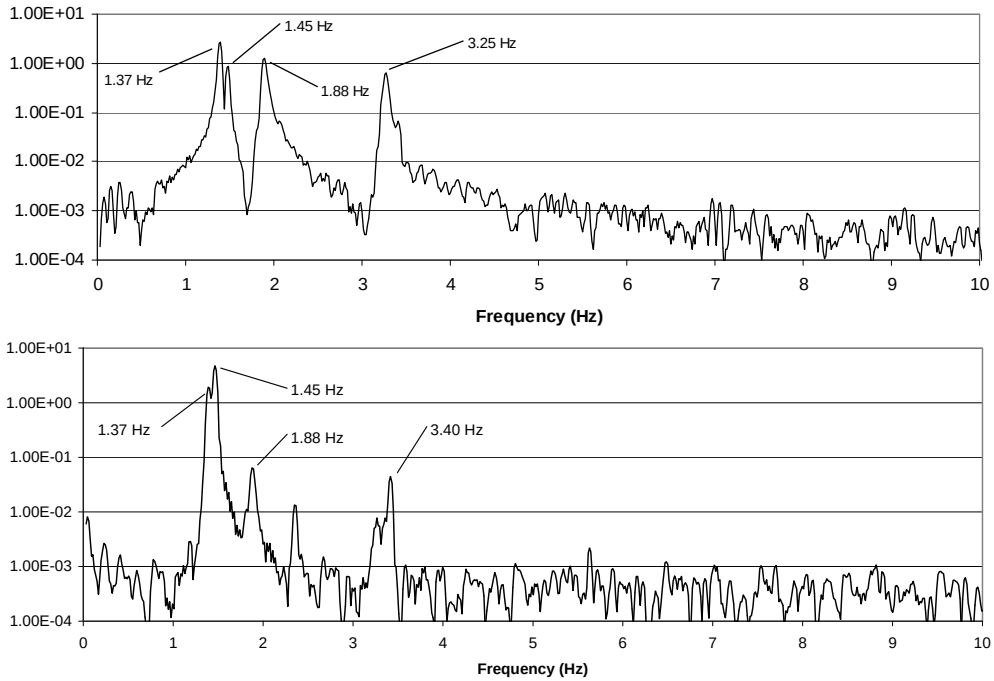

Figure 3.8: Smoothed power spectra of acceleration data at the tip of the mast arm in the vertical direction (top), and lateral out-of-plane direction (bottom)

A finite element model of the traffic signal structure was created in SAP2000. The structure accounted for the offset traffic signals and the luminaire, and a damping ratio of 0.5 percent was assumed for all modes. The first four frequencies of the model closely matched the frequencies seen in the power spectrum for vertical accelerations (Figure 3.8). A time-history video of the dynamic response of the structural model was created to observe its behavior. A simulated pluck test was run on the model by applying a vertical static displacement to the tip of the mast arm and then releasing it, calculating fifty response data points per second. The model appeared to behave very similar to the real structure. The vertical motion of the mast arm tip slowly diminished as the lateral motion increased, and then the vertical motion increased again as the lateral motion appeared to damp out.

This cyclic pattern continued repeatedly with slight randomness, and only very slowly damped out. This behavior was thought to potentially deter galloping—as the vertical motion energy gets swapped to the lateral motion periodically, no motion-induced loads associated with galloping could be sustained for very long on the structure. The majority of traffic signal structures, however, may not have components that contribute significant out-of-plane behavior (such as the luminaire attached to it here); hence, the out-of-plane behavior and its effects on galloping were not studied further.

3.3 Acceleration-to-Displacement Conversion

Galloping can cause very large vertical displacements in traffic signal structures at the tip of the mast arm. It was desired, therefore, to capture the displacement of the mast arm tip during the field tests conducted for this report. One type of system often used to measure displacements includes a video camera. This system was explored, but in order to capture absolute

displacements with a video camera, the camera must remain perfectly still. This system turned out to be impractical for the field tests planned. Therefore, an accelerometer on the tip of the mast arm was used to calculate displacement.

Theoretically, acceleration data can be integrated twice to obtain displacement data. In practice, however, due to limitations of accelerometer equipment, displacements will appear to drift, often quite significantly, after performing the two integrations. The drift imposes a variable offset in the displacement data leading to low-frequency error. This phenomenon is well known, and curve-fitting baseline-correction solutions have been derived for converting earthquake ground accelerations, for example, into displacements. Several different curve-fitting methods were attempted to convert the acceleration data from the field tests in this report into displacements. None of these methods were able to eliminate the drift completely, which often exceeded the actual displacements by several orders of magnitude.

Dr. Connor of Lehigh University faced similar issues with drifts in a study being conducted at the same time as the tests for this report. He employed a method for eliminating drift and obtaining accurate displacement data from acceleration data and shared this method with the author. The method consists of a combination of integrations and high-pass filters, and can be explained in a few steps.

The original acceleration data are first obtained. The data are converted from the time domain to the frequency domain by means of a Fourier Transform. Once in the frequency domain, the acceleration data can be plotted, and evident peaks should appear, which represent natural frequencies of the structural system. A high-pass filter is then applied, eliminating all of the data with frequencies below the base of the first peak. An inverse Fourier Transform is next utilized to convert the data back to the time domain. The filtered acceleration data are then numerically integrated to obtain velocities. The velocity data are then converted to the frequency domain and filtered in a similar way to the acceleration data. When converted back to the time domain, a single integration is performed to obtain displacements. Once again, these data are converted to the frequency domain and filtered to eliminate any drift caused in the last integration. An inverse Fourier Transform results in the final displacement data.

To calibrate this method and ensure its validity, a test was performed at the Ferguson Structural Engineering Laboratory at The University of Texas. An accelerometer was attached to the end of a cantilevered aluminum bar. At the same location as the accelerometer, a linear variable differential transformer (LVDT) with a 6-in. reach was attached to the bar. The LVDT directly measured the vertical displacements of the bar when subjected to vibrations. The acceleration data from the accelerometer was run through a MATLAB program to perform the filtering and integration steps outlined above. In this validation test, a loop was included in the program to optimize the cutoff frequency for each step of high-pass filtering based on a least-squares fit with the directly-measured displacement data. The Fourier amplitude spectrum of the unfiltered acceleration data is plotted in Figure 3.9. There is an obvious peak at 3.75 Hz where the natural frequency of the structure appears. The data were filtered up to the optimum cutoff frequency of 2.81 Hz resulting in the Fourier amplitude spectrum plotted again in Figure 3.10. It is evident that frequencies below the base of the peak were eliminated. The exact cutoff point did not prove to be critical; however, if the cutoff frequency were too much smaller, the displacement data would noticeably drift, and if it were too much higher and included part of the peak of the

spectrum, the displacements would become very small and the displacement frequency would not match the acceleration frequency.

The drift caused by integrating acceleration data twice to obtain displacements without filtering can be seen in Figure 3.11, where the calculated displacements are plotted along with the displacements measured using the LVDT. The displacements derived from the Connor method described above are compared with the directly measured displacements in Figure 3.12. The two data series are perfectly in phase with each other, and the magnitudes of displacement are consistently within 5 percent of each other after the initial abrupt pluck causing the vibrations. This method was determined to be sufficiently accurate for use in the field tests, and was utilized to obtain all the displacement information reported in this report. The MATLAB program employing this method is given in Appendix C.

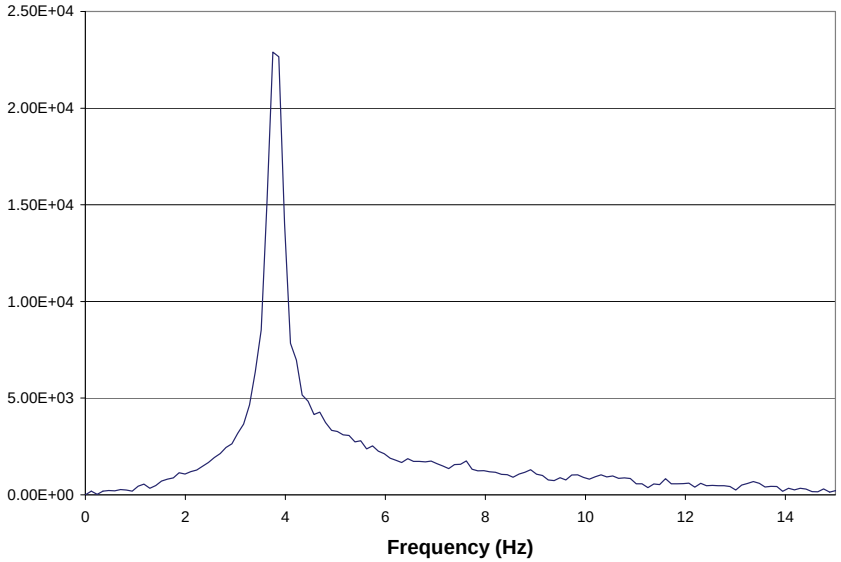

Figure 3.9: Fourier amplitude spectrum of the unfiltered acceleration data plotted in the frequency domain

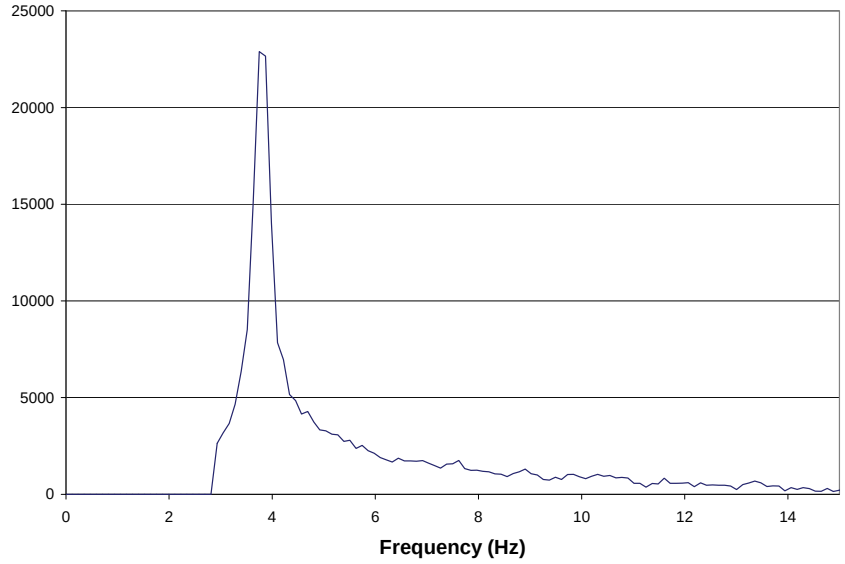

Figure 3.10: Fourier amplitude spectrum of the filtered acceleration data plotted in the frequency domain

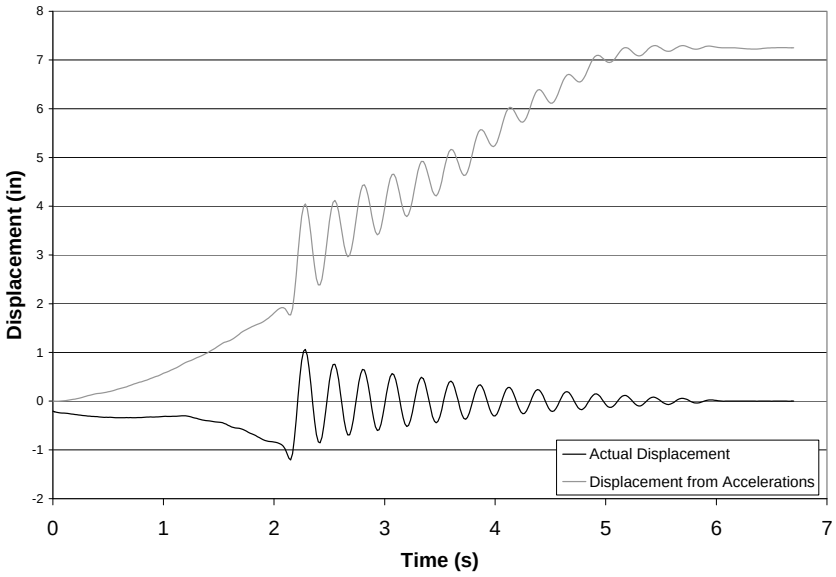

Figure 3.11: Displacements calculated from acceleration data without filtering clearly contains a significant drift

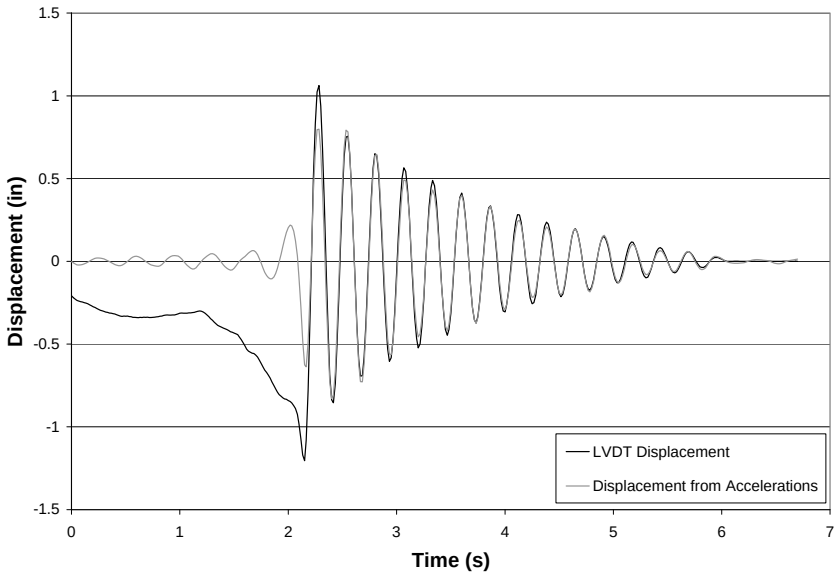

Figure 3.12: Displacements calculated from acceleration data with the described method contain no drift and are sufficiently accurate

Chapter 4. Field Tests

4.1 Introduction

The portion of this research project related to galloping involves two types of tests: controlled tests and field tests. The controlled tests, performed at Texas Tech University, were needed to record galloping events with a variety of sign and signal configurations, allowing for a probabilistic model. The field tests, performed by researchers at The University of Texas at Austin and included herein, were intended to study the actual behavior of traffic signal structures that are currently installed in the field. Although the field tests were not intended to provide sufficient data for developing new design equations for galloping, they were believed to be necessary to investigate how often galloping actually occurs in the field. It was also of interest to determine how the structures behave when subjected to the combination of galloping along with other potential forces seen in the field, and how the loads acting on the signal structures compare with design loads prescribed in the current AASHTO specifications.

It was decided to instrument three distinct sites for field monitoring in order to maximize the length of time each site would be monitored while still including a variety of locations. An attempt was made to acquire a list of signal structures that had been reported to frequently experience large-amplitude displacements throughout the state of Texas. These structures would have been prime candidates to monitor and the data would have been most useful, presumably representing the worst-case scenarios. However, TxDOT does not currently have a system implemented to gather this information easily, so the ideal sites across the state were not studied. Instead, the first site investigated was a local intersection in Pflugerville where a signal structure across the street from the test structure failed in December 2003. The second site was at an intersection in Round Rock, where the signal structure selected for testing was reported to have experienced some large-amplitude displacements. The third site was in Lubbock, and was a site recommended by the City of Lubbock again because of its history of frequent large-amplitude displacements on the test structure selected.
Some basic dynamic properties of the three structures tested are given in Table 4.1.

Table 4.1: Basic dynamic properties of structures monitored for galloping

	Damping Ratio in 2^{nd} mode, ζ	1^{st} mode (out-of-plane) frequency (Hz)	2^{nd} mode (in-plane) frequency (Hz)
Pflugerville Site	0.4%	1.02	1.19
Round Rock Site	N/A	1.11	1.23
Lubbock Site	0.3%	0.69	0.86

4.2 Test Instrumentation and Setup

The same test setup was used for all three field test sites. The equipment was chosen based on the findings from the preliminary tests as discussed in Chapter 3. A total of eight channels were recorded, consisting of two strain gauges, one 3-axis accelerometer and one 3-axis anemometer.

All of the equipment was mounted on the traffic signal structure, including the data acquisition unit. After the data was collected, it was remotely downloaded to the structural computer laboratory at the University of Texas at Austin using wireless modem technology. The location of the equipment on the traffic signal structures can be viewed in the layouts in Figures 4.1 and 4.2.

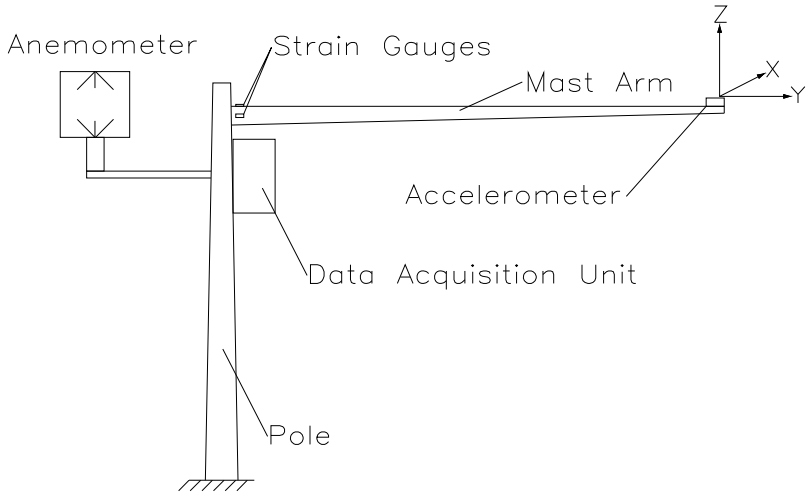

Figure 4.1: Elevation view of equipment layout on typical traffic signal structure (axes shown correspond to accelerometer data)

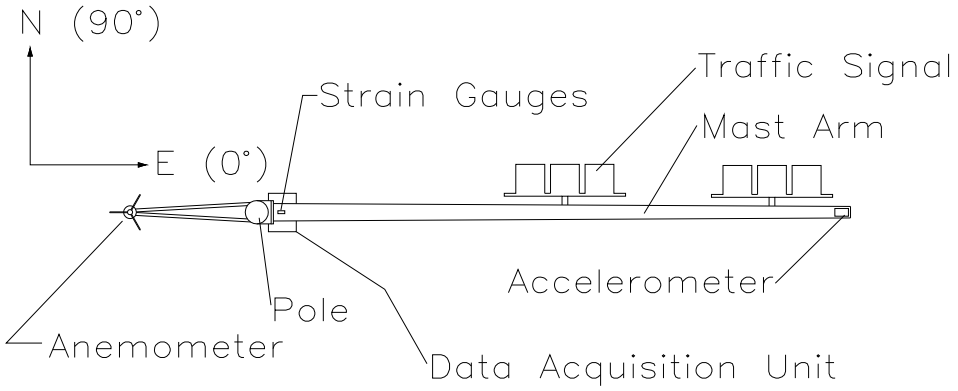

Figure 4.2: Plan view of equipment layout on typical traffic signal structure (axes shown correspond to anemometer data)

4.2.2 Strain Gauges

The strain gauges were temperature-compensating type FLA-3-11-3LT, made by TML of Tokyo, Japan. Each gauge was 3 millimeters in length, had a resistance of 120 Ohms, and was accurate up to 3 percent strain. For each setup, the two strain gauges were mounted longitudinally on the mast arm near the pole-to-arm connection, 1 to 2 in. from the fillet weld. One was mounted on

the top of the arm and the other was mounted on the side of the arm, as seen in Figure 4.3. Precise measurements were taken to ensure the gauges were placed directly on the top and side of each circular cross section.

To attach the strain gauges, a small area of the mast arm was sanded to remove the galvanization and then cleaned thoroughly with acetone. The gauges were carefully lined up and initially attached to the mast arm with a special type of Scotch tape, which was not affected by the adhesive. Peeling the tape back to reveal the gauge, a couple of drops of the adhesive, cyanoacrylate, was placed on the gauge, and then it was pressed on the mast arm for 30 seconds to cure. To waterproof and protect the gauges, the Scotch tape was removed and an acrylic coating was applied. Then the gauges were covered with a small piece of elastomeric pad and finally sealed with HVAC foil tape, as shown in Figure 4.4.

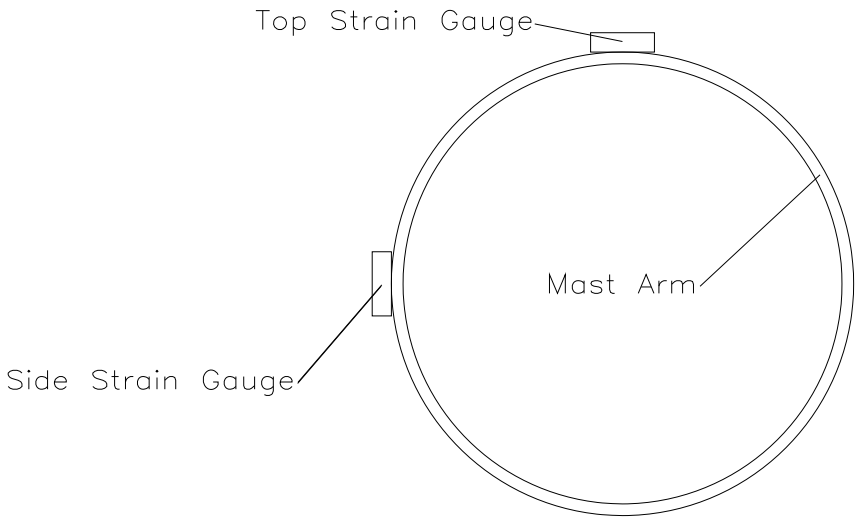

Figure 4.3: Cross section of mast arm near pole-to-arm connection

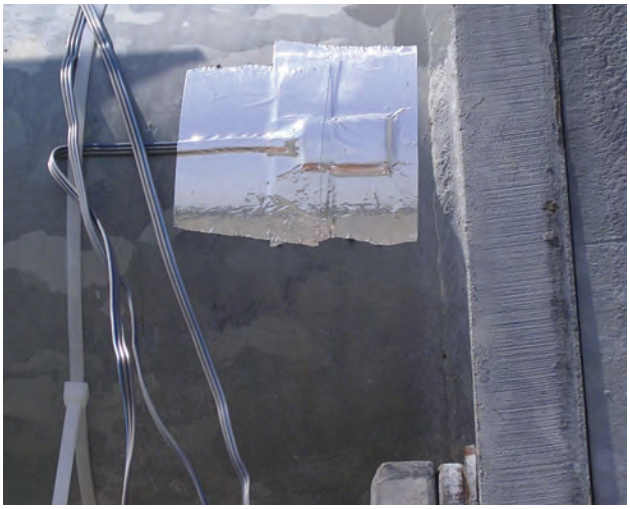

Figure 4.4: Strain gauge attached to mast arm and weatherproofed

4.2.3 Accelerometer

A Crossbow Technology piezoelectric 3-axis accelerometer, model number CXL10LP3, was used. The accelerometer had a range of ±10g. Although this model of accelerometer has been reported to drift with temperature changes, this was not a problem in this study because data were collected over brief intervals and the offset was easily removed. The accelerometer was placed at the tip of the mast arm such that the *x*-axis referred to the out-of-plane lateral acceleration, the *y*-axis referred to the in-plane lateral acceleration, and the *z*-axis referred to the vertical acceleration, as depicted in Figure 4.1. It was attached firmly to the mast arm with hose clamps, shown in Figure 4.5, to prevent any motion independent from the arm. The acceleration data was converted to displacements at the tip of the mast arm using the methodology described in Chapter 3.

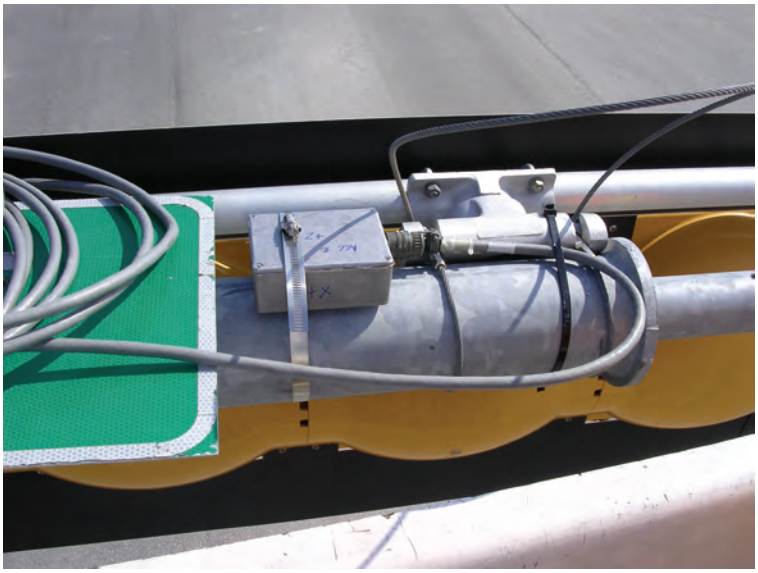

Figure 4.5: Accelerometer enclosed in weatherproof case and attached to tip of mast arm

4.2.4 Anemometer

An RM Young 81000 Ultrasonic Anemometer was used to capture wind speed data. The 3-axis ultrasonic anemometer was chosen for its ability to capture instantaneous wind velocity changes, which could play an important role in the determination of galloping potential. Since wind velocity varies with height, the anemometer was placed at the same height as the mast arm. It was attached in a direction opposite to the mast arm and 4 ft from the pole (as can be seen in Figures 4.6 and 4.7), a distance chosen to minimize both the turbulent effects that may be caused by the pole and the effects of relative velocity caused by the movement of the structure on recorded wind speeds. The anemometer was always instrumented so that north was aligned with the front side of the traffic signals and parallel to the roadway, as seen in Figure 4.2. Therefore, a “north” wind would come from the front of the traffic signals perpendicular to the mast arm, while an “east” wind would come from the side of the mast arm and act parallel to the arm.

Figure 4.6: Anemometer and data acquisition unit connected to pole

Figure 4.7: Ultrasonic anemometer attached to the pole

4.2.5 Data Acquisition Unit and Collection Program

A Campbell Scientific CR23X Micrologger data acquisition unit was used to gather data from all of the devices. This system was capable of recording twelve channels, which was more than was required here. The maximum continuous sampling rate for the eight channels utilized was 26 Hz, which was sufficient for the structures being monitored, which had natural fundamental frequencies of around 1 second. This unit was primarily chosen for its compact size, its ease in installation, and its ability to be conveniently attached to the traffic signal structure in a weatherproof encasing without being obtrusive. AC power was provided at each site by a cable running out at the top of the pole. A Sony Ericsson GM28 dual-band wireless modem was connected to the CR23X to allow remote communication with the data acquisition unit. In this

way, data was able to be automatically downloaded to a computer at the Ferguson Structural Engineering Laboratory each evening using the Campbell Scientific PC208W datalogger support software. The data acquisition system can be seen in Figure 4.8.

The program used to monitor each site and capture galloping events was designed to record wind and strain information at fixed intervals, only recording continuous data if a galloping event occurred. For this study, a galloping event was characterized by repetitive large-amplitude vertical displacements at the tip of the arm. Since the strain at the top of the mast arm at the connection is proportional to the tip displacement, the top strain gauge was used as a trigger to determine if a galloping event occurred. The top strain gauge was continuously measured at 100 Hz, while the two horizontal wind velocities were measured at 1 Hz. Every 5 seconds, the wind data for each direction was averaged and recorded, while the strain range, the difference between the maximum and minimum strain in each cycle, was recorded. If the strain range remained larger than 100 microstrain for three consecutive recordings (15 seconds), then a galloping event was assumed to be occurring and continuous recording would initiate. This occurrence is referred to in this report as a galloping event, whether or not actual galloping was the cause of the high strains. In a continuous recording mode for a galloping event, data were captured in all eight channels with a sampling rate of 26 Hz and such a session lasted at least 2 minutes. If the strain range remained over 100 microstrain, the continuous recording would continue. By designing the program in this manner, gust-caused events were weeded out and the cumbersome downloading of large amounts of unimportant data was avoided. Also, the program provided continuous information of what was occurring at the site with regard to the horizontal wind and the vertical movement of the arm so that non-galloping events could be studied as well.

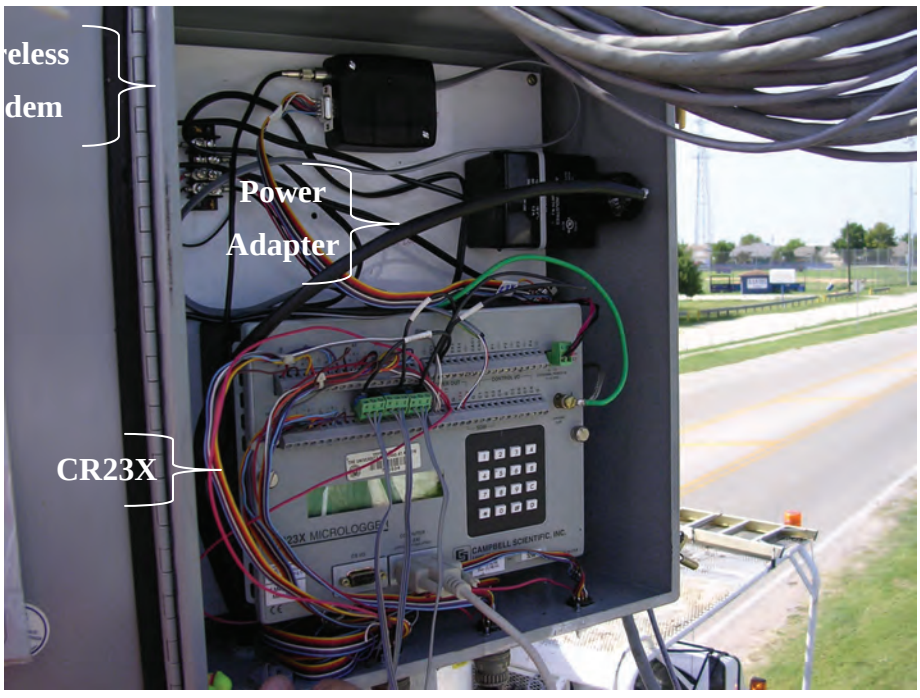

Figure 4.8: Data acquisition unit (CR23X), power adapter, and wireless modem in weatherproof encasement

4.3 Site 1: Pflugerville

4.3.1 General Site Information

The traffic signal structure in Pflugerville, shown in Figure 4.9, was located at the intersection of Oxford Drive and Immanuel Road, at the entrance of Pflugerville Elementary School. The structure that was monitored served southbound traffic on Immanuel Road, and was located at the southwest corner of the intersection. The site in Figure 4.9 was chosen because the traffic signal structure across the street, with its arm parallel to this one, failed in December 2003. Pictures of the failed structure are shown in Figures 1.1 and 1.2. The failure was due to fatigue, which is evident from rust that had formed in the crack around the upper half of the mast arm as noted in Figure 1.2. It was assumed that the failed structure had seen large-amplitude cyclic displacements. The signal structure that was chosen for monitoring was assumed to have a similar loading history, and therefore was a good candidate for studying the potential for galloping.

The mast arm was approximately 28 ft long and supported one sign and three traffic signal heads. The traffic signals had rounded backs and each one had a back plate. This configuration with signals mounted below the mast arm, as is evident in Figure 4.10, has been shown to be one of the most likely candidates for galloping, especially when the wind comes from the back of the signals (McDonald et al., 1995). This structure was monitored from August 5, 2004 to January 3, 2005.

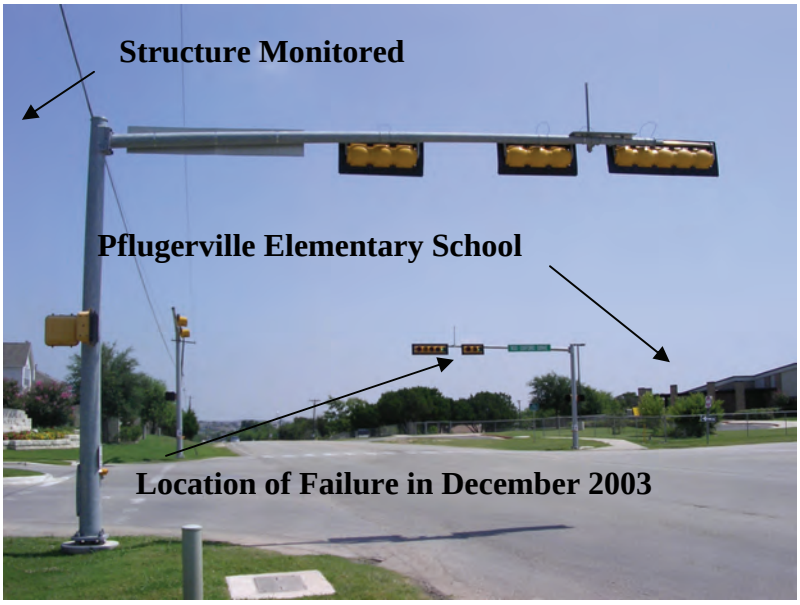

Figure 4.9: Location of monitored traffic signal structure in Pflugerville

Figure 4.10: The traffic signals have rounded backs and are below the mast arm

4.3.2 Pluck Test

While attaching the instrumentation, a pluck test was performed to determine the in-plane dynamic properties of the structure. To accomplish this, one member of the research team stood in a bucket truck near the tip of the pole, as seen in Figure 4.11, moved the tip of the arm directly downward and then suddenly let go. The structure vibrated in the vertical plane in its second mode (the first mode was determined to be out-of-plane), and time history data was collected. Using the vertical acceleration plot shown in Figure 4.12, *Equation 4-1* was used to determine the damping ratio, ζ, of the structure in this mode. The damping ratios of all the structures monitored were estimated in this fashion, and they are presented in Table 4.1.

$$\text{Equation 4-1:} \quad \zeta = \frac{1}{2\pi j} \ln \frac{\ddot{u}_i}{\ddot{u}_{i+j}}$$

where i and $i+j$ refer to two different time instants separated by exactly j cycles of oscillation in a time history plot for vertical acceleration, $\ddot{u}$, such as Figure 4.12.

Figure 4.11: A bucket truck is utilized to pluck the structure

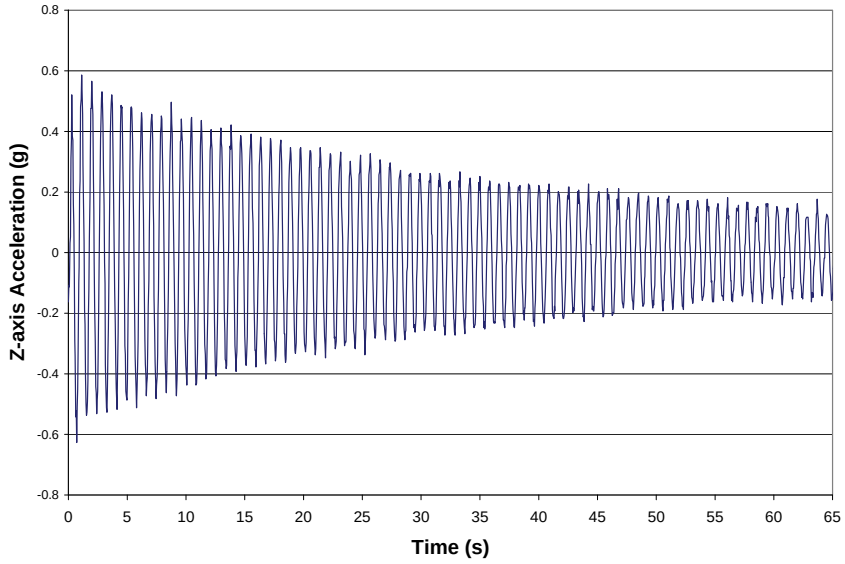

Figure 4.12: Vertical acceleration at tip of mast arm during pluck test

For traffic signal structures, the presence of wind during a free vibration test can affect the estimation of the damping ratio of the structure. If the wind velocity, especially perpendicular to the mast arm, is high during the pluck test, the aerodynamic damping ratio could be a part of the measured damping ratio, and lead to inaccurate conclusions regarding the structure's own damping properties. Therefore, the pluck test was performed when the perpendicular wind speeds were very low, as can be confirmed by studying Figure 4.13.

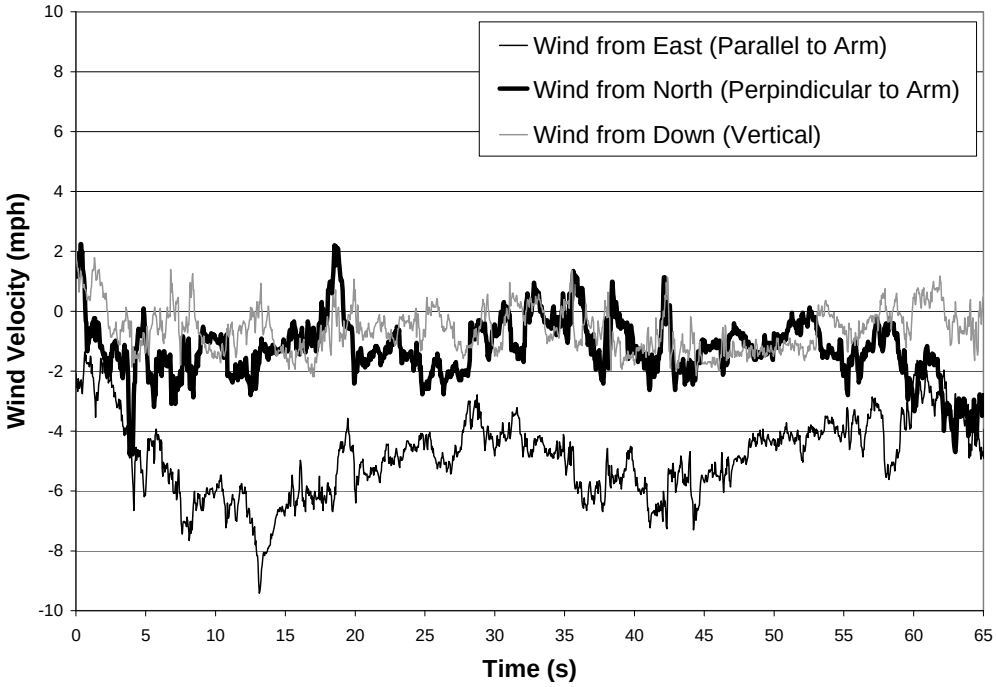

Figure 4.13: Wind velocities during the pluck test

The pluck test also allowed for a relationship to be established between the vertical displacement at the tip of the arm and the strain at the top of the arm at the pole-to-arm connection. (The displacements were calculated from the acceleration at the tip of the mast arm using the procedure described in Chapter 3.) The relationship can be studied in Figure 4.14, and was confirmed by a finite element model using SAP2000 with tapered members identical to the structure, and a vertical point load applied to the tip of the mast arm. The deformed shape of the finite element model can be viewed in Figure 4.15.

Figure 4.14 suggests that there is strong correlation between the vertical displacement at the tip of the arm and the longitudinal strain at the top of the arm at the pole-to-arm connection. The pluck test suggested roughly 36 microstrain per inch of tip displacement, whereas the finite element model calculated 39 microstrain per inch of tip displacement. This suggests that the tip of the mast arm needed to repeatedly displace vertically a total of about 2.75 inches for 15 seconds in order to initiate a “galloping” event as defined per our data collection protocol (see Section 4.2). Although this may not appear to require significant displacement amplitudes compared to previously witnessed galloping events, it was determined to be a good place to begin. It was felt that if the threshold were triggered too often for events that were not considered galloping, that the threshold would be raised at a later time.

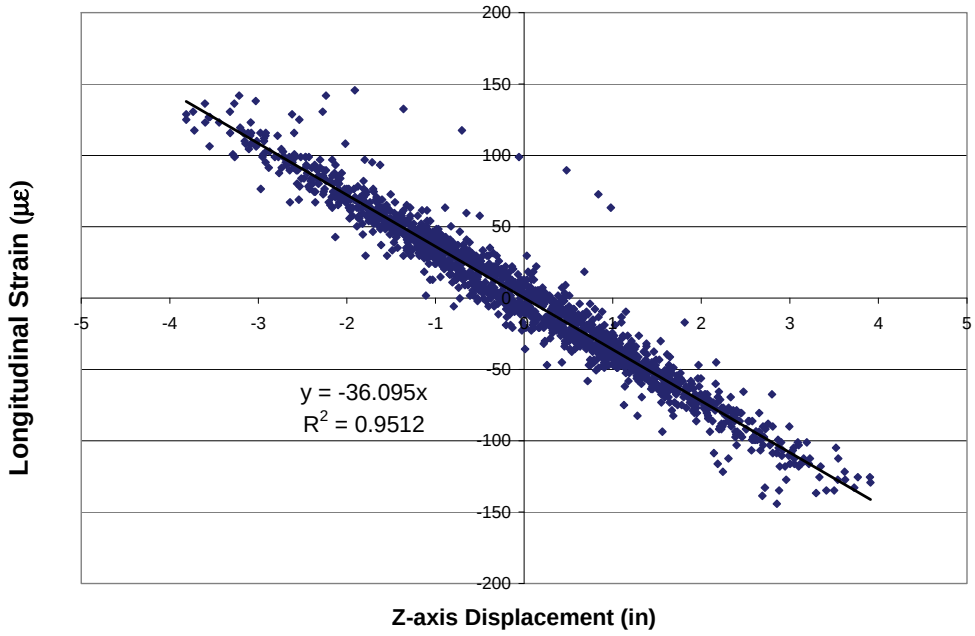

Figure 4.14: Relationship between the longitudinal strain at the top of the mast arm at the pole-to-arm connection and the vertical tip displacement

Figure 4.15: Deflected shape of finite element model of signal structure

4.3.3 Daily Wind and Strain Range Data

Overall, the strain ranges correlated fairly well with the wind velocity in the direction perpendicular to the mast arm for any 5-second period. If the perpendicular wind velocity and strain range are plotted together over an entire day, the peaks in the strain range can be clearly attributed to corresponding peaks in the wind velocity, as seen in Figure 4.16. This correlation was maintained whether the wind was coming from the front or the back of the mast arm, as can be confirmed by studying plots of the perpendicular wind speed versus the strain range in Figures 4.18 and from two different days. The strain range did not correlate as well with the velocity of the wind in a direction parallel to the mast arm, which is evident in plots presented in Figures 4.17 and 4.20.

Over the period of time when this site was monitored, significant winds were experienced from all directions. Although there is noticeably some relationship between wind velocities, wind direction, and strain ranges, none of the relationships are consistent. Therefore, the strain range for any given 5-second period must include other factors apart from wind speed and direction. It is known that the motion of the mast arm at any given time affects how the structure responds to wind; however, it was not possible to continuously capture this data.

Whenever the strain range reached a value corresponding to a stress range above 2.6 ksi, the CAFL (Constant Amplitude Fatigue Limit) stress range for the weld detail according to the current AASHTO specification corresponding to infinite life, the wind speed was consistently above 8 mph and the direction was generally slightly off from perpendicular to the mast arm; a few such events in a 2-week monitoring period are summarized in Figure 4.21. This CAFL stress range was exceeded, on average, sixteen times per week during the entire time the site was monitored. Statistical daily strain and wind speed data for a 2-week period in December are summarized in Table 4.2.

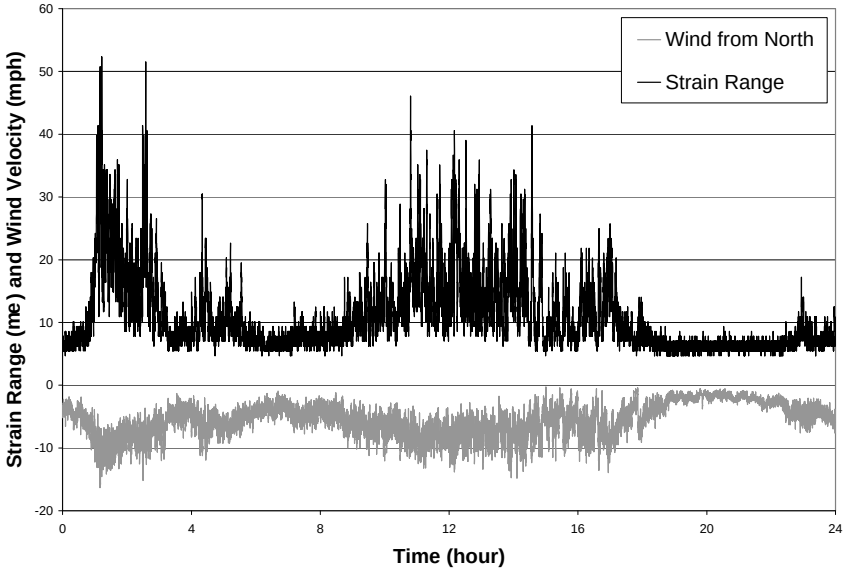

Figure 4.16: Plot of a typical day (October 20, 2005) showing the relationship between the perpendicular wind velocity and the strain range

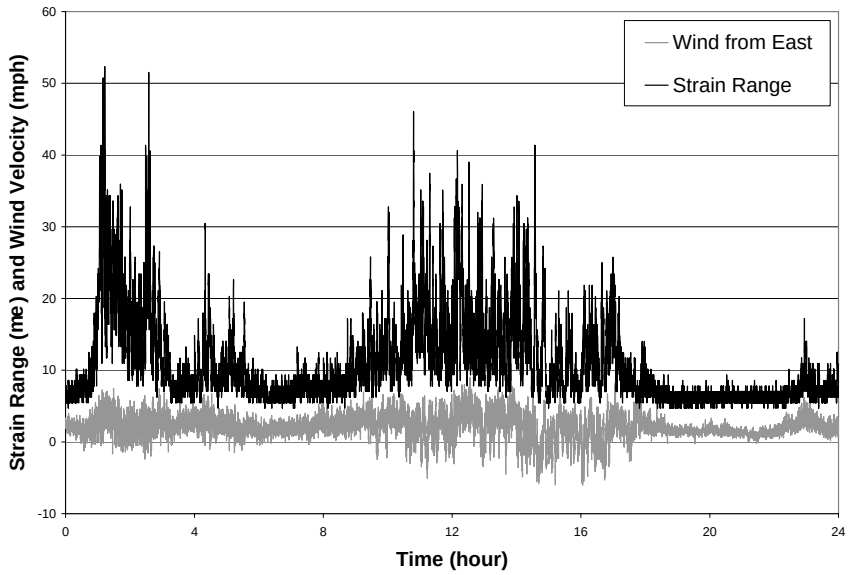

Figure 4.17: Plot of a typical day (October 20, 2005) showing the relationship between the parallel wind velocity and the strain range

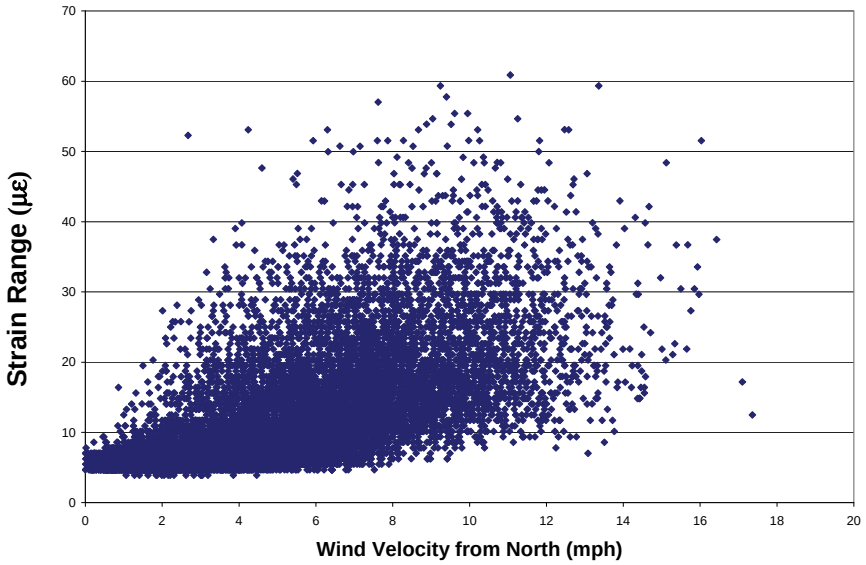

Figure 4.18: Plot of data from October 8, 2005, showing the strain range and the perpendicular wind from the front of the signals

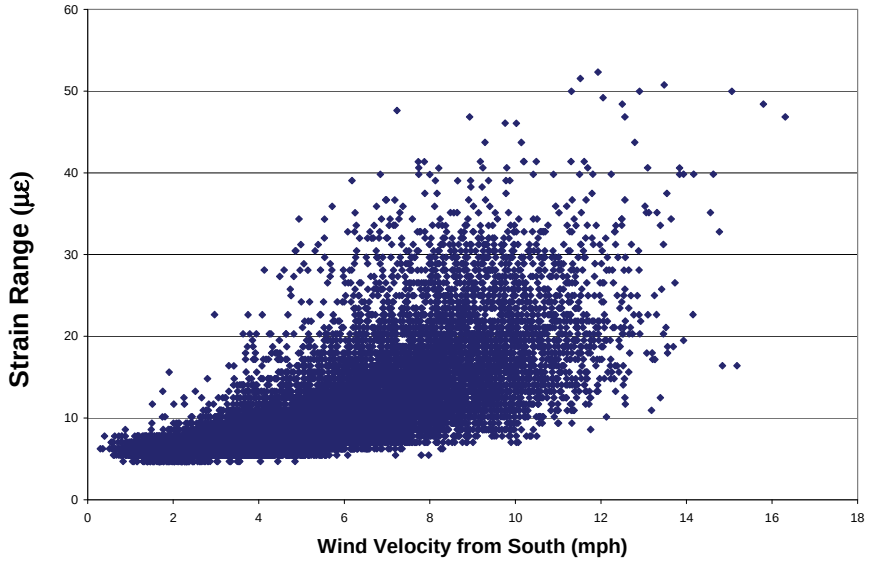

Figure 4.19: Plot of data from October 20, 2005, showing the strain range and the perpendicular wind from the rear of the signals

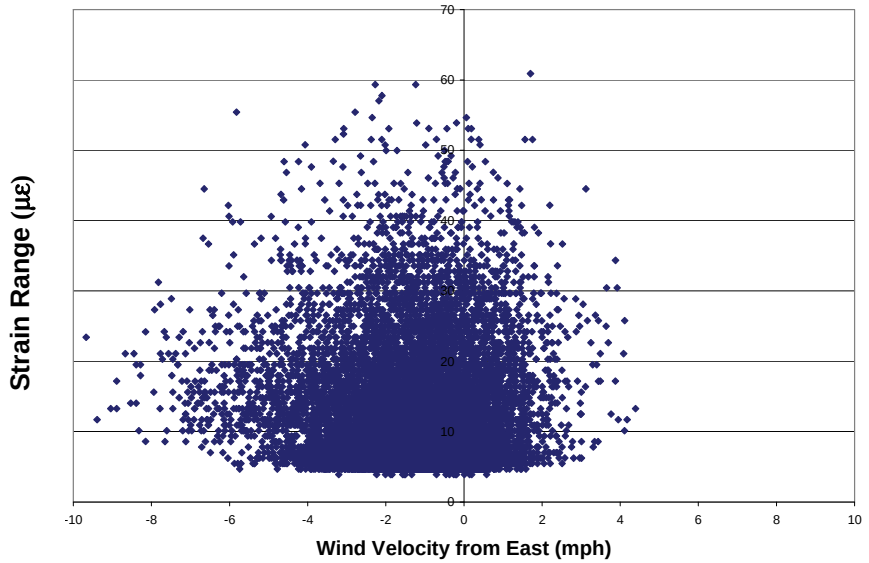

Figure 4.20: Plot of data from October 8, 2005, showing the relationship between the strain range and the wind parallel to the mast arm

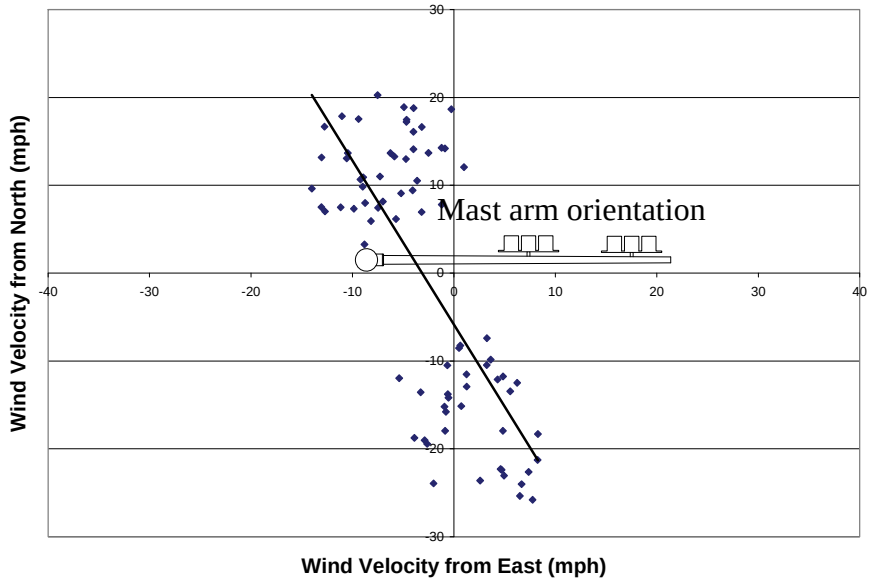

Figure 4.21: Plot of the wind resultant for each occurrence of a strain range over 87 microstrain during a 2-week period in December 2004

Table 4.2: Statistical summary of data taken every 5 seconds during a 2-week period in December 2004

	Mean of Absolute Daily Values			Maximum Daily Values		
Date	**Wind from East (mph)**	**Wind from North (mph)**	**Strain Range (με)**	**Wind from East (mph)**	**Wind from North (mph)**	**Strain Range (με)**
15-Dec-04	3.70	5.89	19.12	-5.12	25.67	148.70
16-Dec-04	1.93	3.27	8.05	10.22	19.56	59.47
17-Dec-04	3.31	4.22	10.55	15.88	-16.80	64.13
18-Dec-04	1.86	4.86	10.83	-10.25	18.43	147.00
19-Dec-04	2.84	2.67	6.65	-14.84	-11.98	26.59
20-Dec-04	4.82	2.18	8.14	-16.89	12.40	35.95
21-Dec-04	1.40	6.14	14.53	-13.30	-28.28	115.70
22-Dec-04	3.19	9.90	21.83	15.86	-31.97	111.80
23-Dec-04	4.12	4.67	15.35	-21.88	20.42	78.30
24-Dec-04	5.80	5.17	21.67	-22.35	21.96	125.30
25-Dec-04	2.78	8.09	24.24	-13.53	20.19	97.20
26-Dec-04	2.57	3.12	8.98	-11.94	16.58	65.03
27-Dec-04	1.42	3.11	6.22	9.01	-12.59	29.72
28-Dec-04	2.40	2.69	6.69	11.34	-11.74	34.42
29-Dec-04	4.04	4.14	9.53	13.14	-16.43	63.32

4.3.4 Galloping Events

Only one "galloping" event was registered during the time this site was monitored. It occurred on December 14, 2004 at 12:11 p.m. The event began with a large strain range measured on the top of the mast arm but quickly tapered off. Figure 4.22 shows that the strain range on the top of the mast arm was as large as 160 microstrain, while the strain range on the side of the mast arm only reached 20 microstrain. Figure 4.23 shows a zoomed-in view of the two strains plotted together. It is evident that they are almost perfectly out of phase. This suggests that the strain gauge on the side of the mast arm was sensing the strain caused by the vertical motion, not the lateral motion as expected.

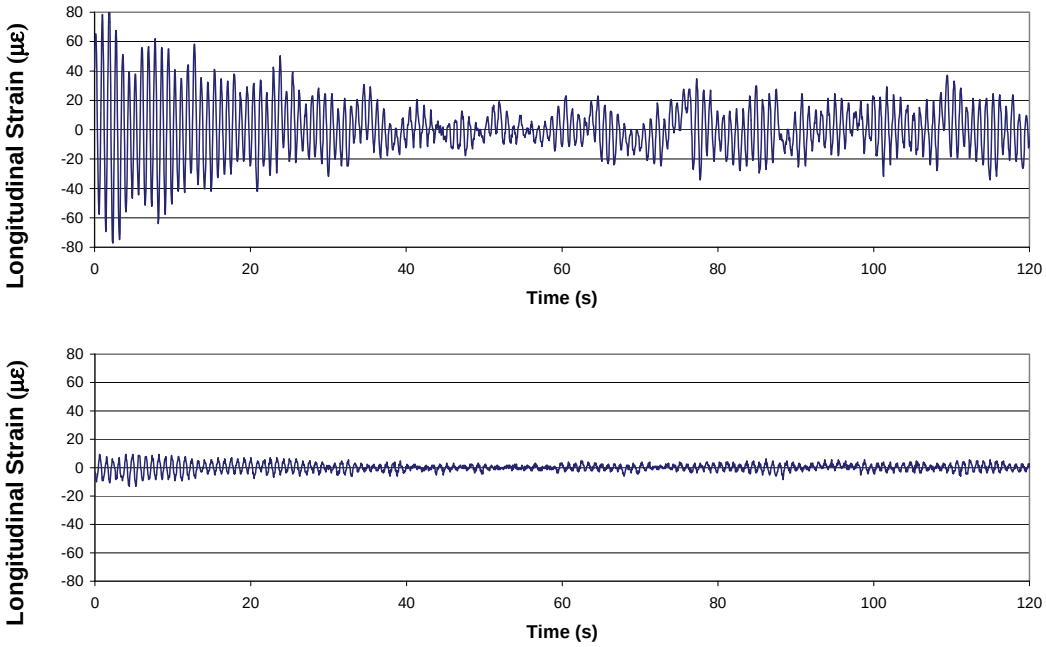

Figure 4.22: Longitudinal strain on the top of the mast arm (top) and the side of the mast arm (bottom)

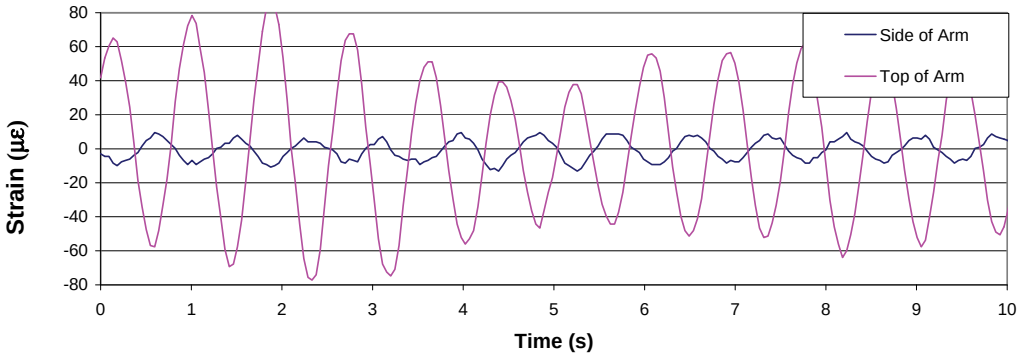

Figure 4.23: A 10-second close-up of the relationship between the longitudinal strain measured on the top and on the side of the mast arm

The displacements of the mast arm tip during the galloping event are shown in Figure 4.24. The vertical displacement has a maximum amplitude of approximately 2 in., which occurs at the beginning of the time series. The lateral out-of-plane displacement has a maximum amplitude of approximately 1.5 inches. This does not seem consistent with what would be expected from the small strain values recorded from the gauge on the side of the mast arm. When the two displacements are plotted against each other, as in Figure 4.25, a trace is created as if someone were looking at the tip of the mast from the opposite side of the street. The trace forms variously proportioned oval-shaped figures, but there is no apparent pattern.

However, it is very clear that the behavior does not resemble classical galloping, where the motion is strictly vertical and perpendicular to the wind direction.

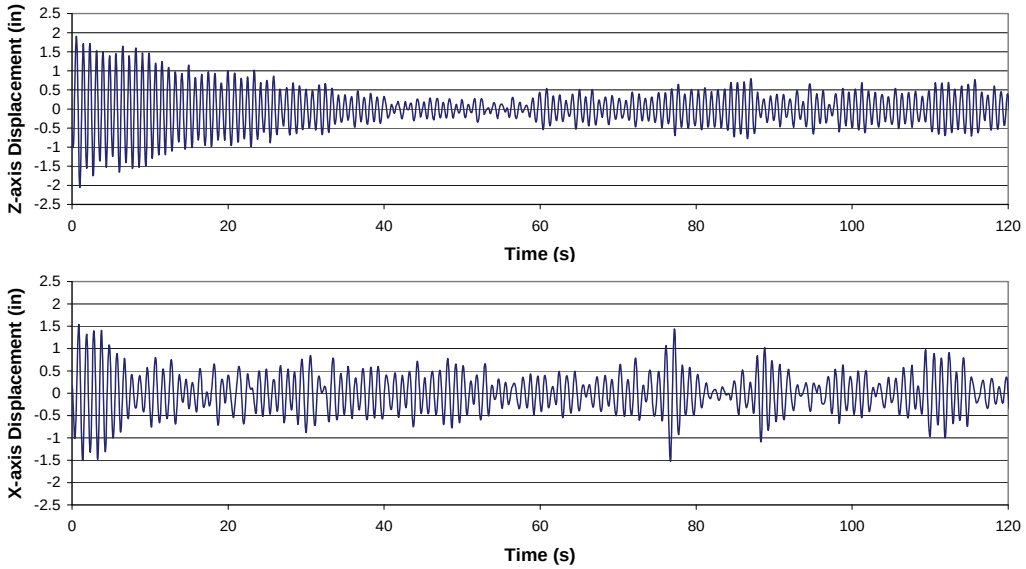

Figure 4.24: Vertical displacement (top) and lateral out-of-plane displacement (bottom) of the mast arm tip

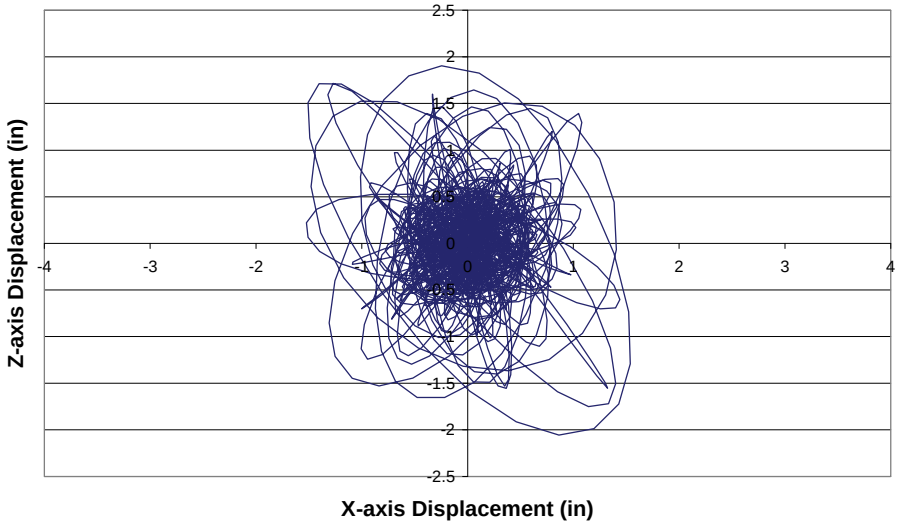

Figure 4.25: Vertical tip displacement versus lateral out-of-plane tip displacement

A relationship between the vertical tip displacement and the longitudinal strain can be derived as was done before with the pluck test. The relationship, as shown in Figure 4.26, is almost identical to that found during the pluck test, and suggests roughly 1 ksi of stress range per inch of tip displacement. Figure 4.27 shows that no clear correlation exists between the lateral out-of-plane tip displacement and the strain on the side of the mast arm. However, as described earlier and again in Figure 4.28, a rather clear relationship does exist between the vertical tip displacement and the strain on the side of the mast arm. These strain values, however, are quite small compared to the strain on the top of the mast arm.

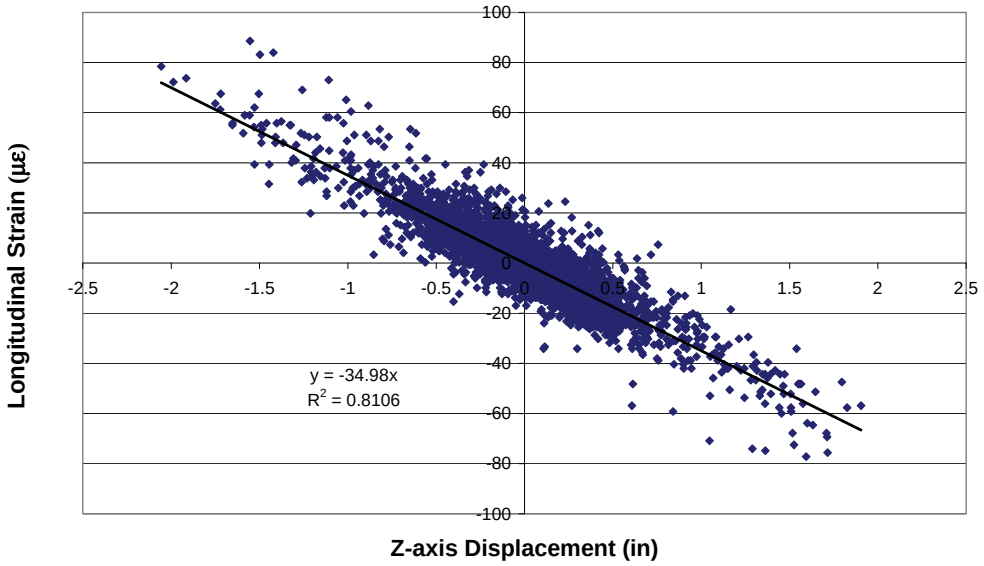

Figure 4.26: Relationship between vertical tip displacement and longitudinal strain on the top of the mast arm

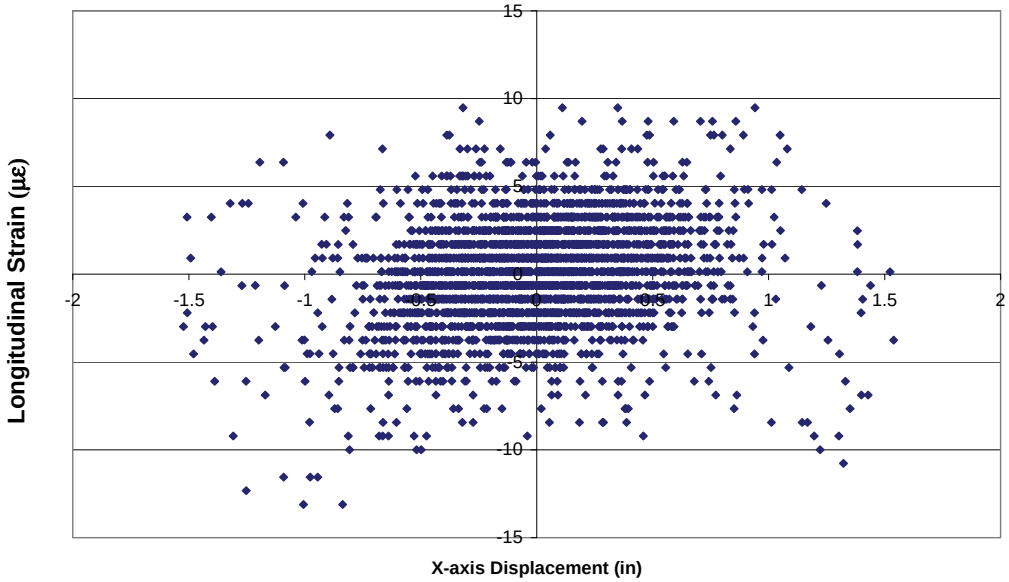

Figure 4.27: Relationship between lateral out-of-plane tip displacement and longitudinal strain on the side of the mast arm

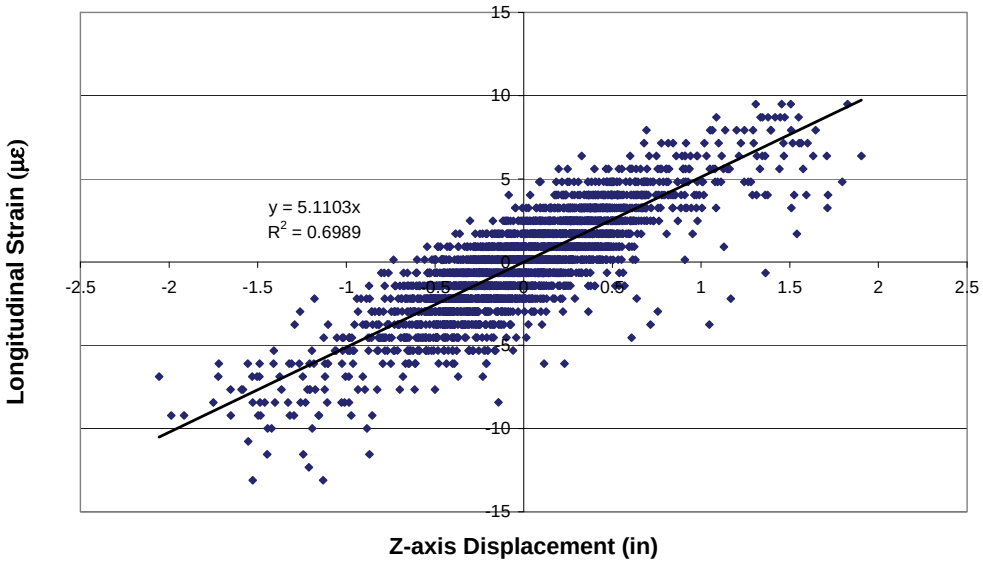

Figure 4.28: Relationship between vertical tip displacement and longitudinal strain on side of mast arm

The relationships identified between the strains and the displacements can be reinforced by studying the frequency content using power spectra of the data from each of the relevant channels. The strains on the top and the side of the mast arm both share the same principal frequency as the vertical acceleration at the tip of the mast arm. The lateral out-of-plane acceleration had a lower principal frequency than the others. The power spectra displaying the frequency content in each case are very clean and are all displayed in Figure 4.29

A dynamic analysis was run of the finite element model created in SAP2000. The model treated each connection as rigid, and accounted for the masses of the signal lights with offset point masses. The frequency of the in-plane mode matched up well with the actual structure, yielding a frequency of 1.18 Hz, compared to the 1.19 Hz suggested from the field measurements. However, the frequency of the out-of-plane mode was calculated to be 1.11 Hz, whereas the actual structure had a frequency of 1.02 Hz based on measurements. This discrepancy, apparent at all three sites, was studied in more depth and is reported in Chapter 5.

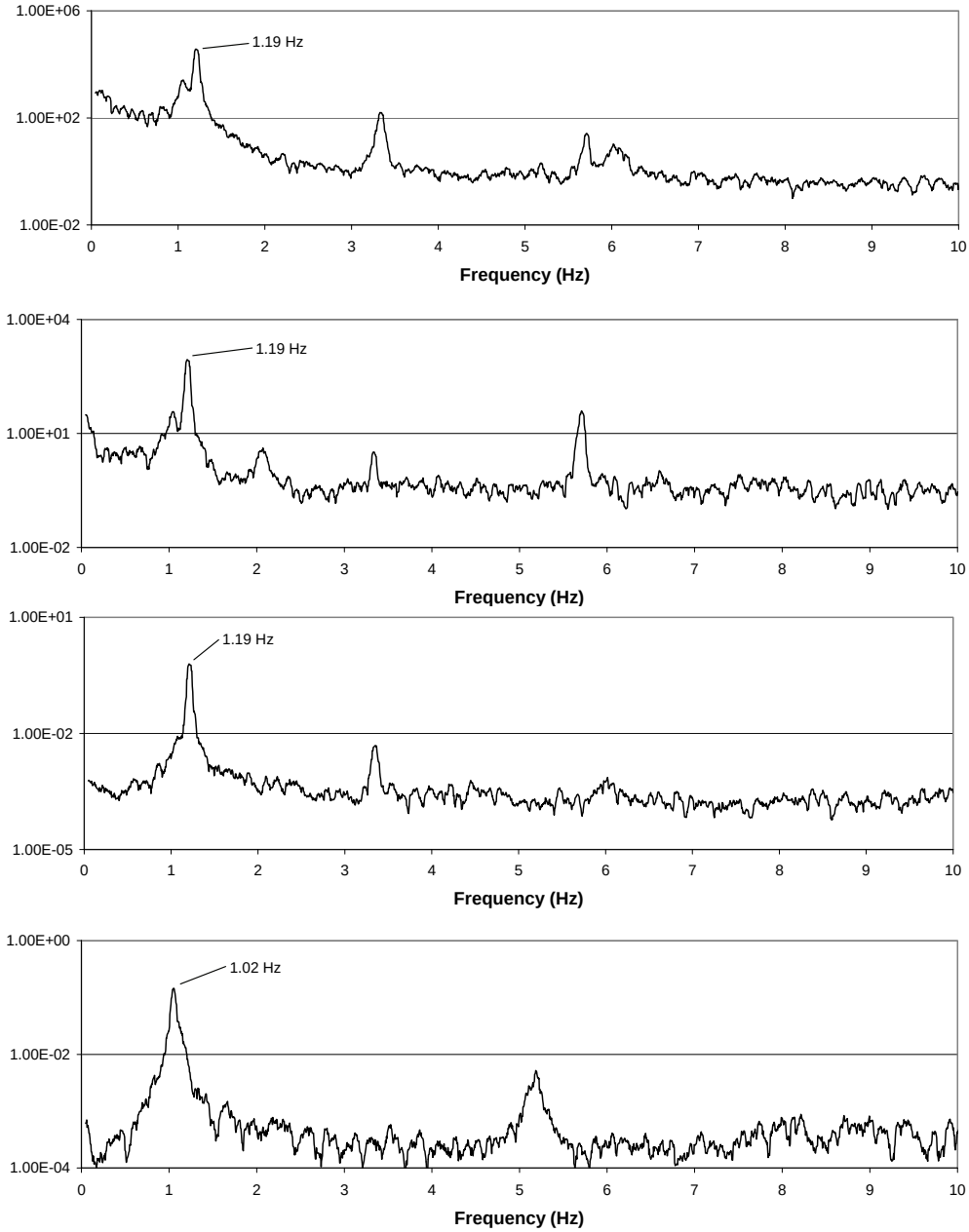

Figure 4.29: Power spectra of top strain, side strain, vertical acceleration, and lateral out-of-plane acceleration (from top to bottom)

The wind, combined with the behavior of the structure, is the primary factor in the displacements and strains experienced. Figure 4.30 shows the wind velocities for each of the three directions over the course of the single "galloping" event. Figures 4.31 and 4.32 clearly show that the direction of the wind was primarily from the northwest, and the wind speed typically varied between 10 and 25 mph. This is different from what was expected since traffic signals have typically been more susceptible to large-amplitude galloping-related displacements with wind coming straight from the rear of the signals, as stated earlier. The wind in this case not only came from the front, but came partly from the side as well. The vertical wind velocity component also played a critical role in the overall wind vector, creating angles of attack of up to 30 degrees with

wind speeds up to 15 mph. However, as shown in Figure 4.33, the angle of attack approaches zero as the wind speed gets close to 30 mph. It is hard to make very strong statements about the angle of attack at different wind speeds because the field data are naturally biased and fewer observations are obtained at higher wind speeds.

In a classical galloping situation, the vertical displacements have consistently large amplitudes over an extended period of time, and the wind speed and direction must stay relatively constant, as well. Therefore, although some sporadic galloping-type forces could have resulted on the structure, wind gusts with vertical components and their associated drag and lift forces probably acted on the structure as well, and likely also contributed to the large displacements observed. Since the large displacements quickly dissipated, none of the postulated loading scenarios (galloping or any other) acted on the structure in a sustained manner.

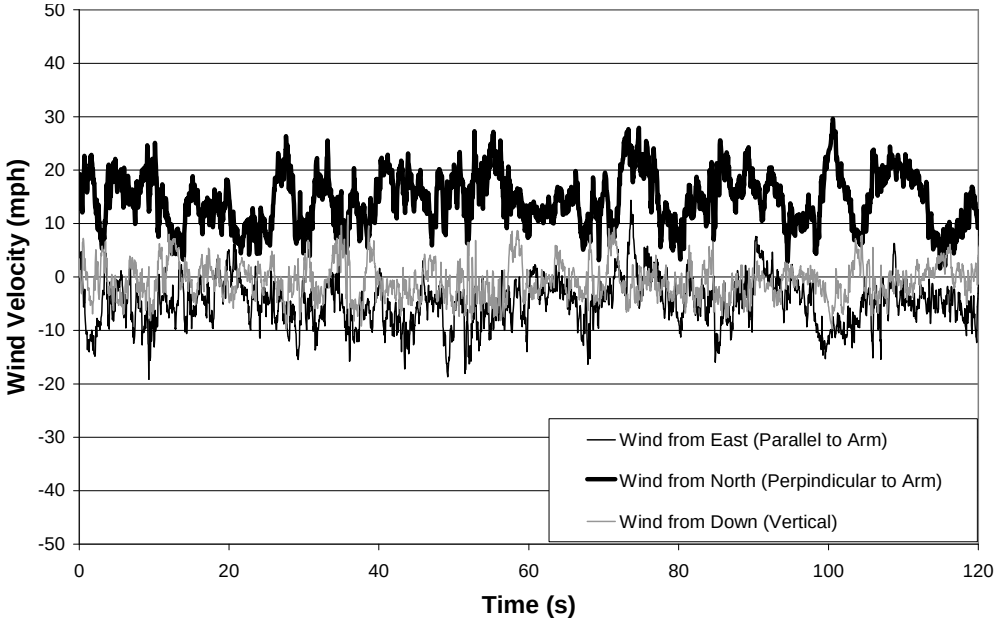

Figure 4.30: Wind velocities during galloping event

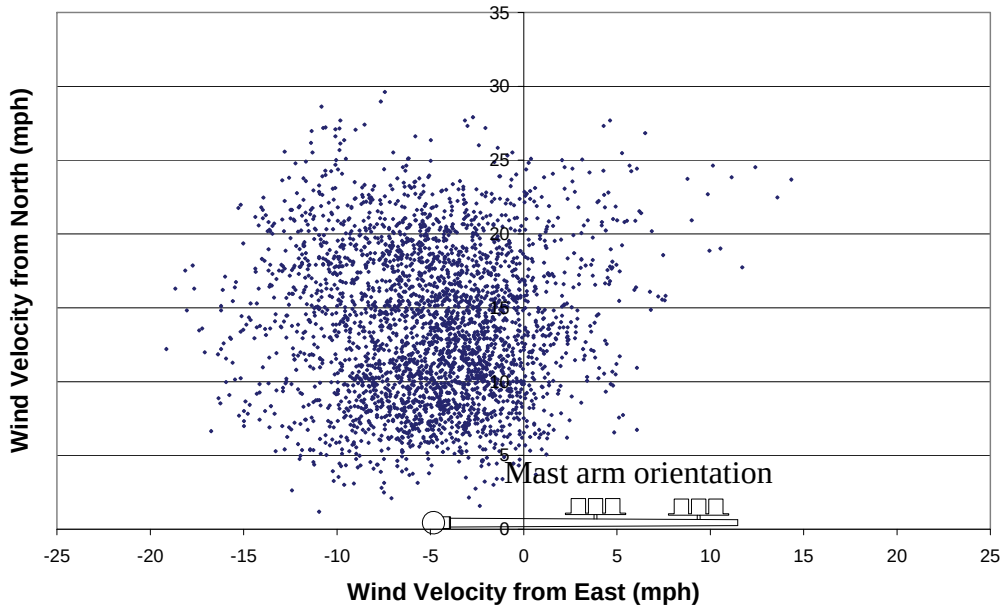

Figure 4.31: Wind resultants during galloping event

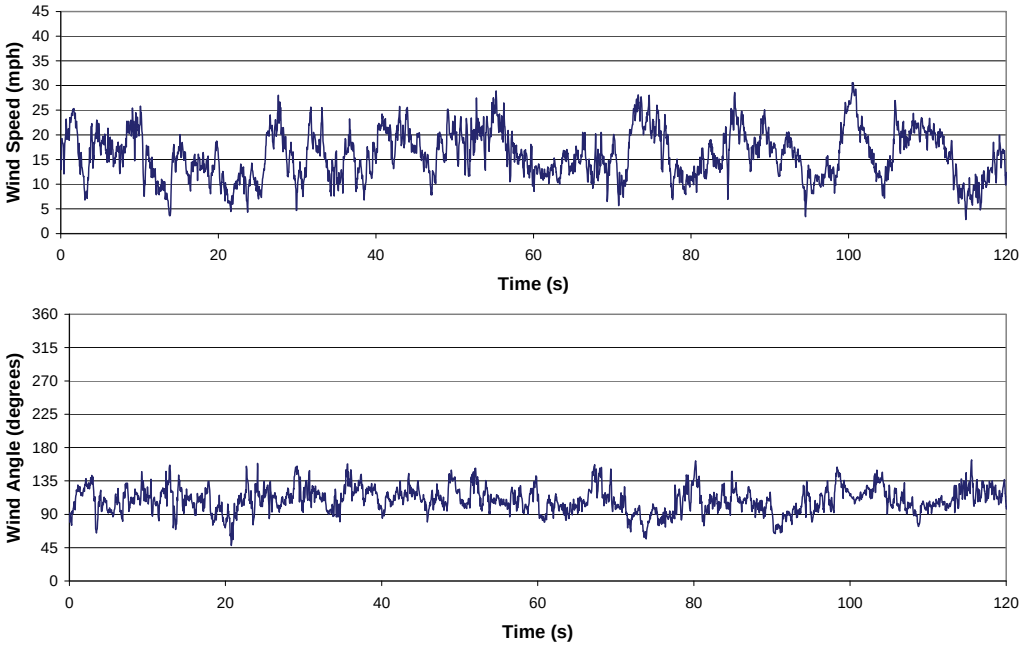

Figure 4.32: Wind speed and horizontal direction (0 degrees: from East; 90 degrees: from North) during galloping event

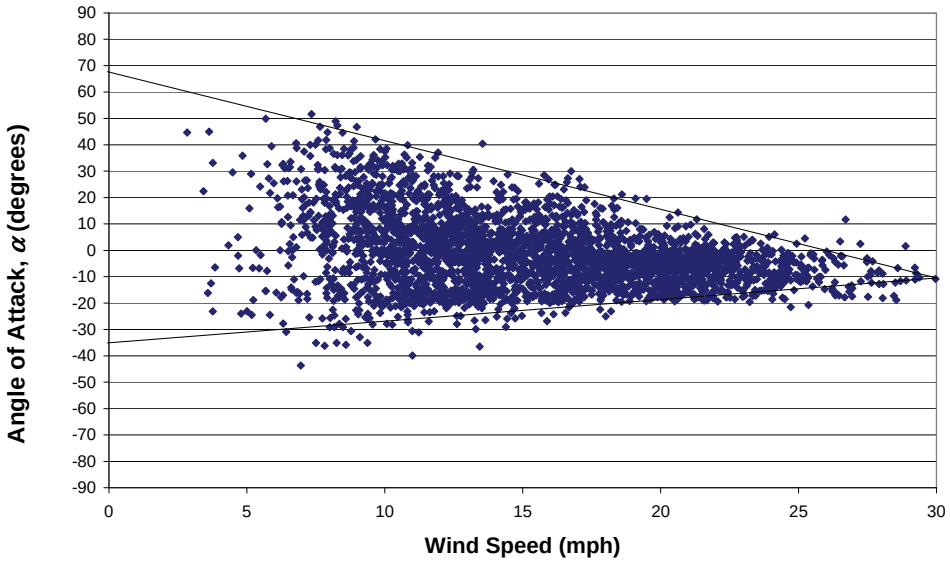

Figure 4.33: Relationship of wind speed and vertical angle of attack

4.4 Site 2: Round Rock

4.4.1 General Site Information

The traffic signal structure in Round Rock is shown in Figure 4.34. It was located at the intersection of Louis Henna Boulevard and A.W. Grimes Boulevard. In particular, the signal structure served southbound traffic on A.W. Grimes where it intersected with westbound traffic on Louis Henna (i.e., SH 45 Frontage Road). This structure was recommended by TxDOT because it had received called-in complaints due to large-amplitude displacements. Before moving all of the equipment to the site, the site was monitored for 4 days with a Microsafe fatigue rainflow cycle counting unit to determine the strain sizes reached on the top of the mast arm. Strains were sampled at 32 Hz, and strain ranges less than 5 microstrain were discarded. In one particular hour during the 4 days, the strain range equaled or exceeded the 155 microstrain bin 177 times. The histogram for the 4-day period can be seen in Figure 4.35. This histogram, combined with the fact that all of the adjacent roads contained the word “wind” in their names, such as Windy Park Circle, Windrift Way, Windsong Trail, and Windy Terrace Park, gave hope for galloping events at the Round Rock site.

The mast arm was approximately 34 ft long and supported one sign and two traffic signal heads. The traffic signals had more squared-off backs, visible in Figure 4.36, and each one had a back plate. Their configuration, mounted below the mast arm, was similar to the configuration of Pflugerville and presented a similar likelihood that galloping would occur with wind from the rear of the signals. This structure was monitored from January 7 to March 3, 2004. However, the accelerometer was not installed until January 19 because a bucket truck could not be obtained. Also due to the very limited time the bucket truck was available, no pluck test could be performed, and the damping ratio is not known for this particular structure. However, its

structural damping behavior is expected to be similar to the other structures, which are consistent to within 0.1 percent.

Figure 4.34: Traffic signal structure monitored in Round Rock

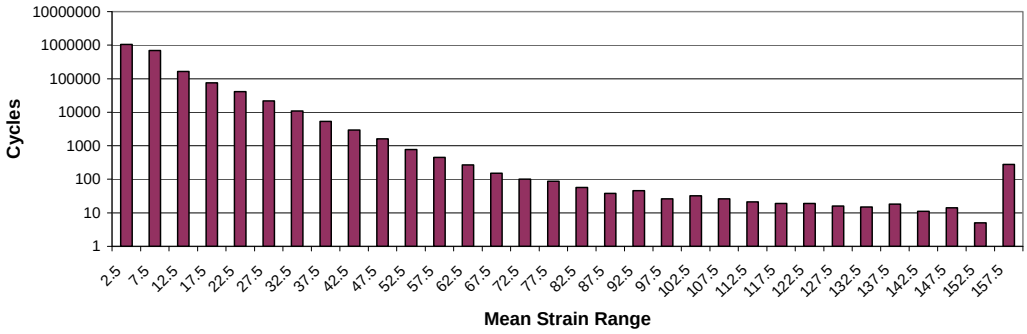

Figure 4.35: Rainflow data for 4-day period at Round Rock site

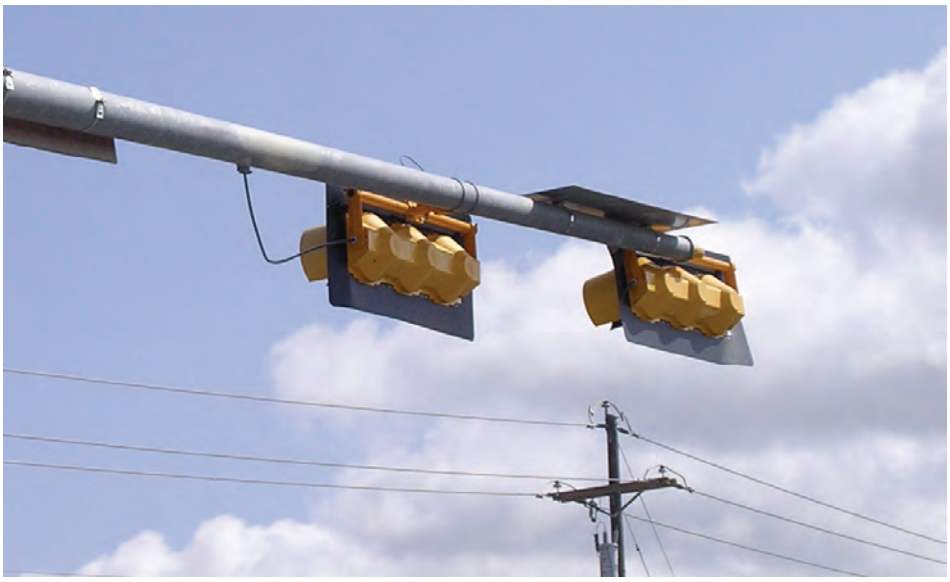

Figure 4.36: Traffic signals with squared-off backs attached to mast arm

4.4.2 Daily Wind and Strain Range Data

The behavior of the traffic signal at Round Rock on a daily basis was similar to that of the structure in Pflugerville. The strain range on the top of the mast arm increased with increased wind velocity perpendicular to the arm. This was true whether the wind came from the front of the signals or from the back. The relationship between the strain range and the wind velocity parallel to the mast arm did not have a clear trend. This behavior is expected when no galloping is present, and is not of particular interest. However, one trend of interest is that the structure in Round Rock did not witness strains as high as the Pflugerville site on a daily basis. This is evident in Table 4.3.

Table 4.3: Statistical representation of data taken every 5 seconds during a 2-week period in February 2005

	Mean of Absolute Daily Values			Maximum Daily Values		
Date	**Wind from East (mph)**	**Wind from North (mph)**	**Strain Range (με)**	**Wind from East (mph)**	**Wind from North (mph)**	**Strain Range (με)**
1-Feb-05	4.08	10.71	16.25	18.12	22.42	49.20
2-Feb-05	1.75	11.03	16.08	-10.94	26.81	56.23
3-Feb-05	2.37	6.52	9.58	14.00	21.15	44.51
4-Feb-05	1.64	1.45	3.86	7.95	8.70	14.05
5-Feb-05	2.88	5.13	7.62	13.39	-17.02	31.98
6-Feb-05	3.07	6.29	10.32	-13.26	-22.16	49.17
7-Feb-05	2.47	3.25	5.64	10.91	14.88	29.65
8-Feb-05	2.67	3.56	5.06	9.07	10.16	15.61
9-Feb-05	3.61	9.63	14.75	14.62	22.18	48.39
10-Feb-05	2.73	4.08	6.68	11.41	13.64	31.99
11-Feb-05	1.23	2.66	4.29	-6.58	-9.94	15.61
12-Feb-05	1.78	7.27	13.70	11.96	-24.44	74.10
13-Feb-05	6.24	5.28	10.52	-21.22	-24.91	56.16
14-Feb-05	1.78	3.21	4.77	9.71	-13.54	25.70

4.4.3 Galloping Events

Similar to the Pflugerville site, only one “galloping” event was registered during the time the Round Rock site was monitored. It occurred on January 12, 2005 at 6:36 a.m. The event began with a large strain range on the top of the mast arm, which held constant for about 20 seconds before tapering off. The strain range increased significantly again, but did not consistently maintain a large amplitude. Figure 4.37 shows that the strain range on the top of the mast arm was as large as 130 microstrain, while the strain range on the side of the mast arm only reached 30 microstrain. This behavior is similar to that previously witnessed in Pflugerville. Unfortunately, since the accelerometer was not in place at the time of the galloping event, no displacement data could be derived.

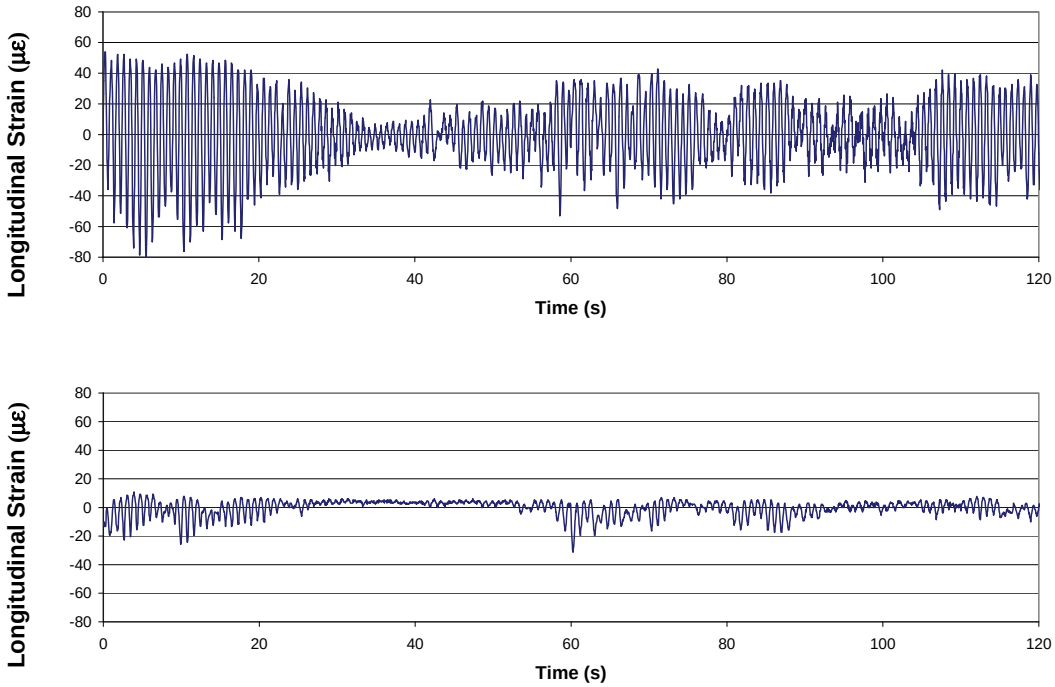

Figure 4.37: Longitudinal strain on the top of the mast arm (top) and the side of the mast arm (bottom)

The frequency content of the data from each strain gauge was inspected. The power spectrum of the strain on the top of the mast arm is very clean and shown in Figure 4.38. In the same figure, the power spectrum of the side strain can be seen to include frequency content from both the out-of-plane motion and the in-plane motion. The in-plane frequency was 1.23 Hz, and the out-of-plane frequency was 1.11 Hz. Once again, the out-of-plane mode has a lower frequency than the in-plane mode.

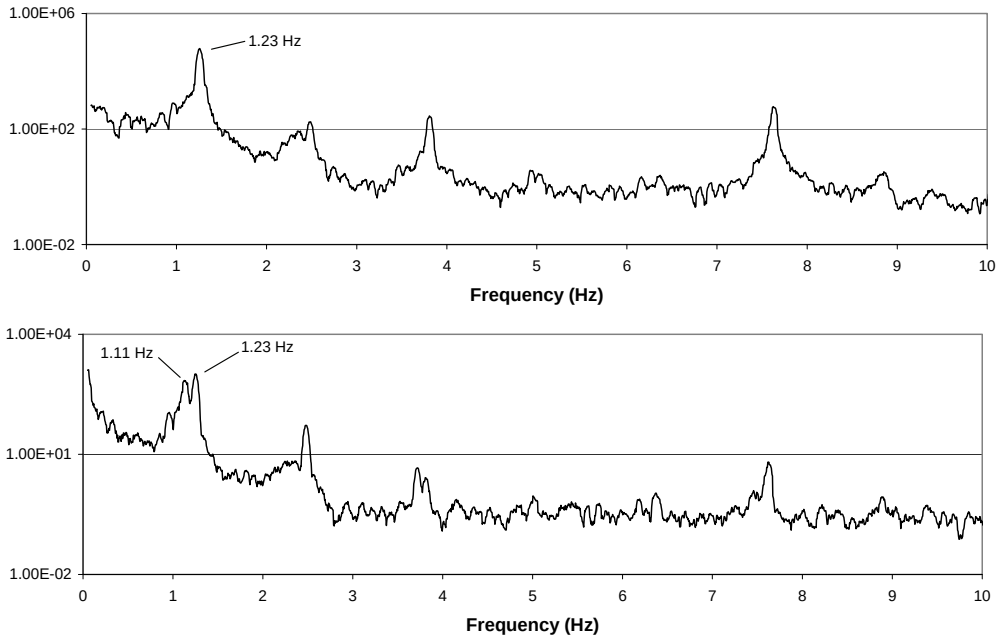

Figure 4.38: Power spectrum of strain on the top of the mast arm (top) and strain on the side of the mast arm (bottom)

The orientation of the wind during the galloping event at Round Rock was much different than the case in Pflugerville. The wind came almost directly from the back of the signals, as would be expected for the most probable galloping case. There is still a slight contribution from wind parallel to the mast arm, but the angle is not as severe as it was in Pflugerville. Figure 4.39 shows the wind velocities for each direction over the course of the galloping event. Figures 4.40 and 4.41 more clearly show that the direction of the wind was primarily from the south, and the wind speed typically varied between 15 and 35 mph. The velocities in this case were larger than was the case in Pflugerville, but they are equally gusty and not steady as would typically be the case in a galloping event.

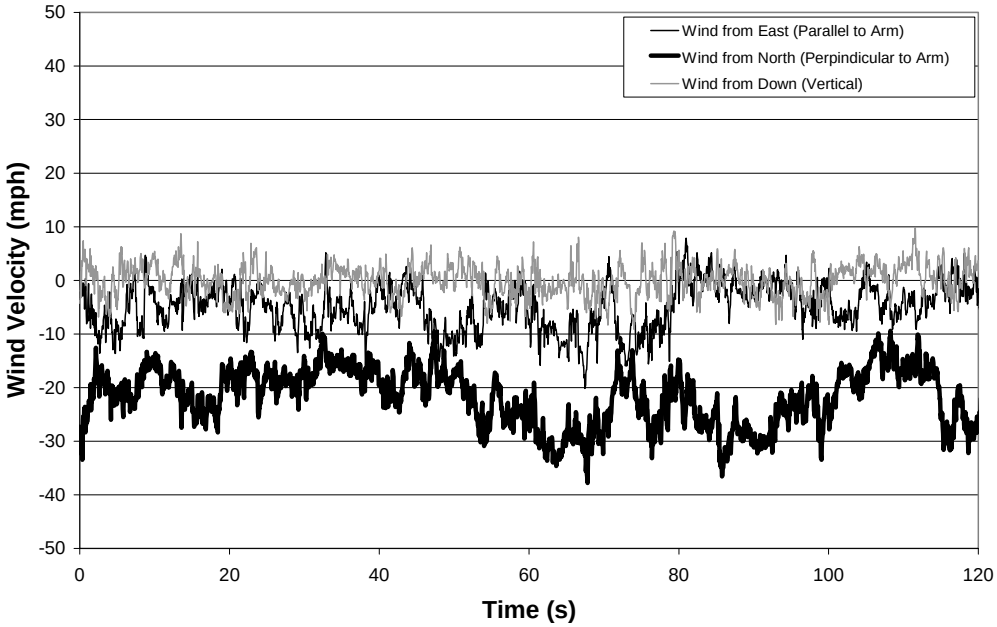

Figure 4.39: Wind velocities during galloping event

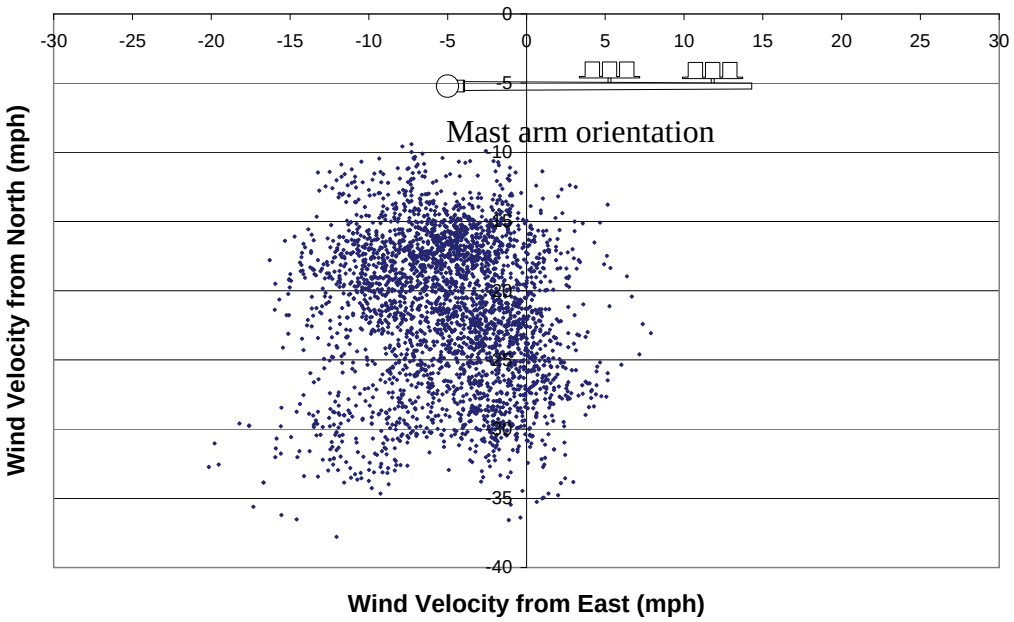

Figure 4.40: Wind resultants during galloping event

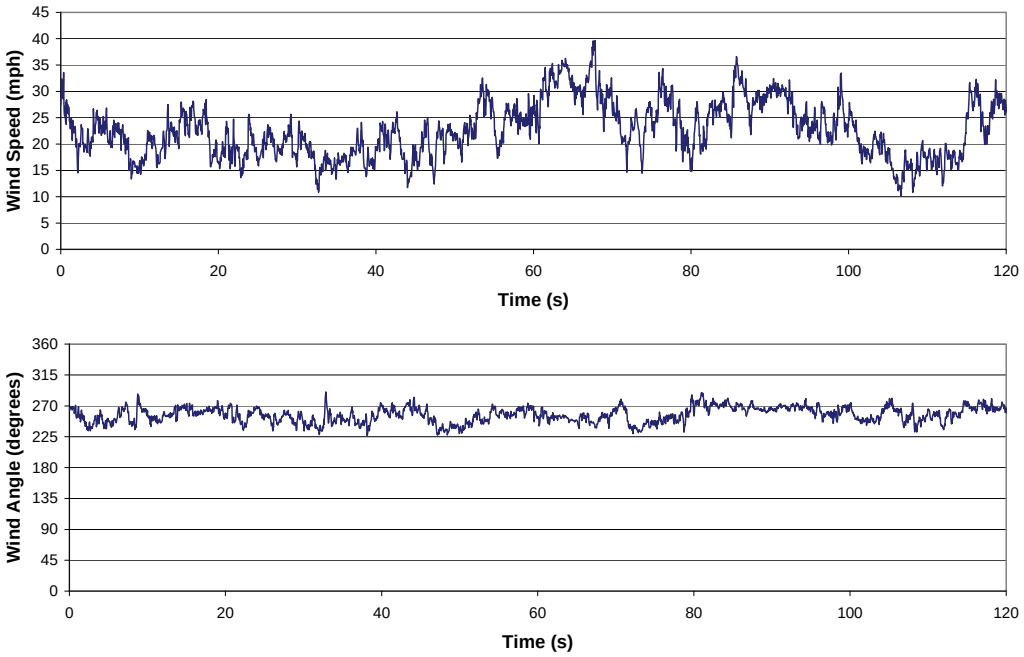

Figure 4.41: Wind speed and horizontal direction during galloping event

4.5 Site 3: Lubbock

4.5.1 General Site Information

The traffic signal structure in Lubbock is shown in Figure 4.42. It was located at the intersection of Slide Road and 69th Street, just south of Loop 289. The signal structure served southbound traffic on Slide Road. This site was recommended by Dr. Letchford at Texas Tech University and the City of Lubbock because of its history of frequently reported large-amplitude displacements. The City of Lubbock was especially helpful and interested in this research because they had a traffic signal structure fail in service due to fatigue a short time earlier. The equipment was installed on March 7, 2005.

The mast arm was approximately 45 ft long and supported two signs and three traffic signal heads. The traffic signals had V-shaped backs, visible in Figure 4.43, and each one had a back plate. Based on limited prior research, their configuration, mounted out in front and level with the mast arm was expected to have a higher probability of galloping with horizontal wind from the front of the signals. However, if the wind carried a large steady vertical component, it could cause galloping from the rear of the signals (McDonald et al., 1995). This structure was monitored for about two months starting on March 9, 2005. A pluck test determined the structure to have a damping ratio of 0.3 percent, and the in-plane frequency to be the same as displayed in Figure 4.48, which was taken during the galloping events.

Figure 4.42: Traffic signal structure monitored in Lubbock

Figure 4.43: Traffic signals with V-shaped backs attached to mast arm

4.5.2 Daily Wind and Strain Range Data

The daily behavior of the traffic signal at Lubbock was similar to that of the previous two structures. There was a clear trend of increased strain with increased wind velocity perpendicular to the mast arm. The wind parallel to the mast arm did not have a clear effect on the strain range. The structure in Lubbock, similar to Round Rock, did not consistently reach high strains on a typical day. This is summarized in Table 4.4.

Table 4.4: Statistical representation of data taken every 5 seconds during a 2-week period in March 2005

	Mean of Absolute Daily Values			Maximum Daily Values		
Date	**Wind from East (mph)**	**Wind from North (mph)**	**Strain Range (με)**	**Wind from East (mph)**	**Wind from North (mph)**	**Strain Range (με)**
11-Mar-05	3.6428	2.6435	6.9323	-20.4	-13.51	28.06
12-Mar-05	7.2169	2.4694	9.5684	-33.74	-14.22	39.75
13-Mar-05	6.2881	6.1123	11.7427	-23.18	24.84	51.53
14-Mar-05	6.3192	2.7617	7.3909	18.36	-17.35	34.34
15-Mar-05	7.842	4.3102	9.5054	22.67	17.68	36.72
16-Mar-05	3.0894	4.9069	7.2956	-12.87	16.1	28.92
17-Mar-05	3.6834	2.2841	7.7002	-23.96	-14.15	43.66
18-Mar-05	5.7415	3.0241	7.0673	-19.75	19.13	35.13
19-Mar-05	5.2938	2.5818	7.0382	21.13	-18.87	35.13
20-Mar-05	3.8367	2.3021	6.5995	-19.47	-13.47	31.95
21-Mar-05	8.5663	5.2836	12.2561	-35.6	28.23	65.51
22-Mar-05	5.6719	6.7593	11.899	-23.09	30.91	80.1
23-Mar-05	3.5272	8.3224	14.0169	17.45	-30.49	79.5
24-Mar-05	5.8422	2.0163	6.9127	-24.57	-14.09	32.76

4.5.3 Galloping Events

Two “galloping” events were registered during the time this site was monitored. The first one occurred on April 5, 2005 at 7:54 p.m. The second event occurred later that night on April 6, 2005 at 12:47 a.m. The first event maintained more constant-amplitude strains on the top of the mast arm for the entire duration as seen in Figure 4.44, but the range magnitude was only about 80 microstrain. The second event damped out more quickly, but at its initiation it experienced a strain range of about 130 microstrain. For both cases, the strain on the side of the mast arm behaved similarly to before, registering small strain ranges of only about 20 microstrain.

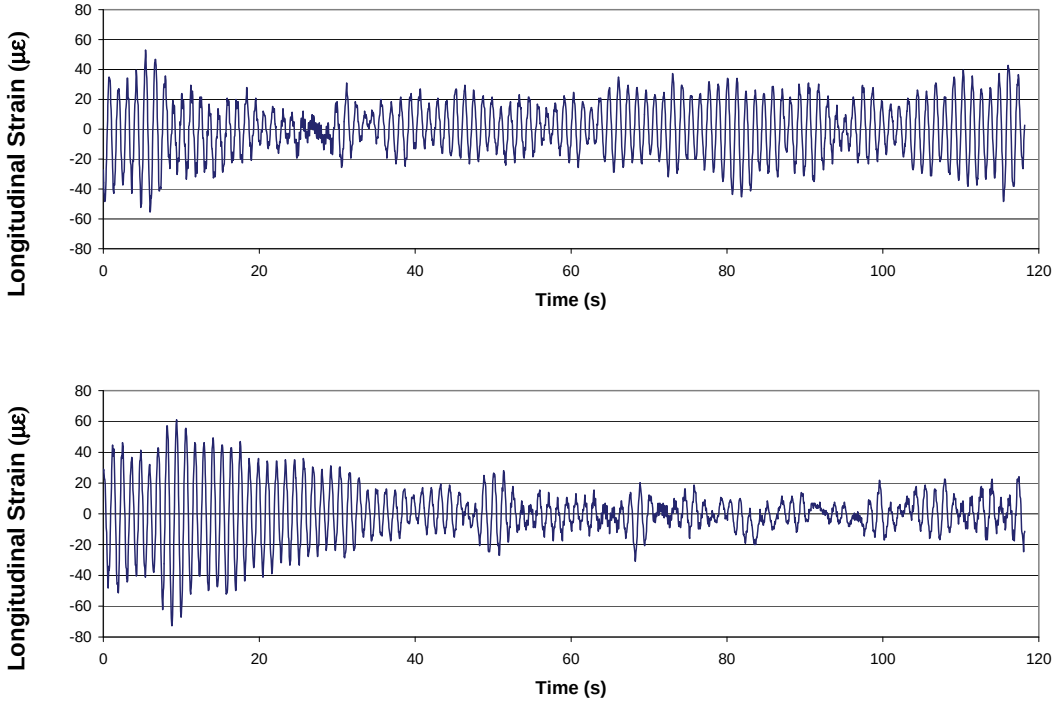

Figure 4.44: Longitudinal strain at the pole-to-arm connection on the top of the mast arm for the first (top) and second (bottom) galloping events

The vertical displacement of the mast arm tip for each case is shown in Figure 4.45. The amplitude is as large as 3.5 in. for the second event, while the first event only registered a maximum amplitude of 2.5 inches. The out-of-plane lateral displacement was larger than the vertical displacement for both cases. The trace of the mast arm tip can be seen in Figure 4.46, showing no clear relationship between lateral and vertical displacements. The relationship between the vertical tip displacements and strain on the top of the mast arm was consistent for both events. The first event showed a relationship of 17.0 microstrain per inch of displacement, and the second event, shown in Figure 4.47, measured the relationship to be 17.2 microstrain per inch of displacement. In both cases, the side strain matched the out-of-plane displacement better than at the previous two sites, and the side strain did not display a clear relationship with the vertical displacement.

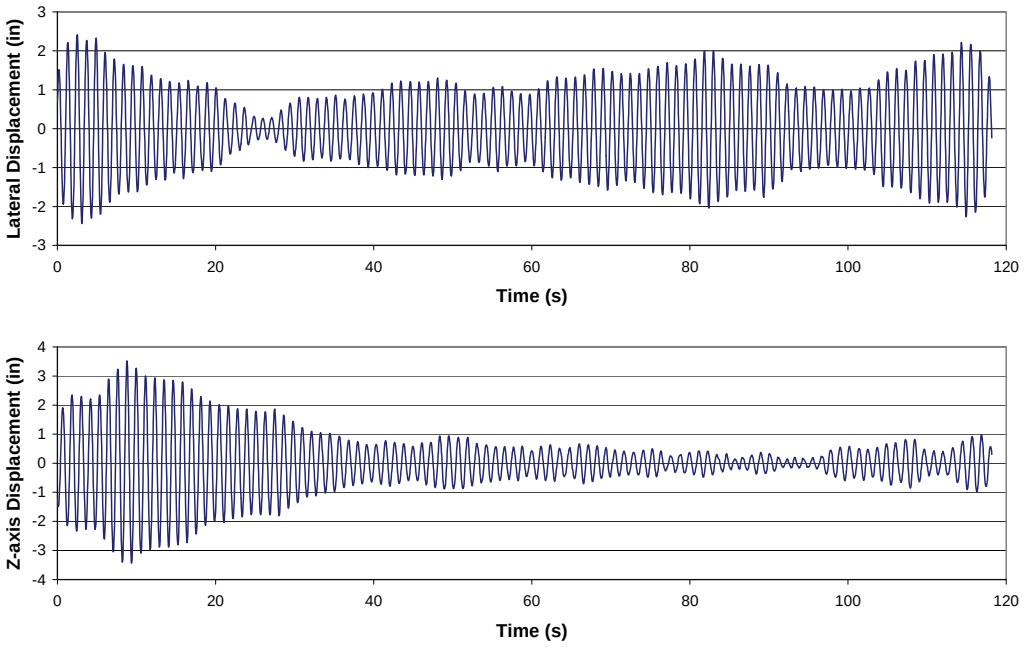

Figure 4.45: Vertical tip displacement of the first event (top) and the second event (bottom)

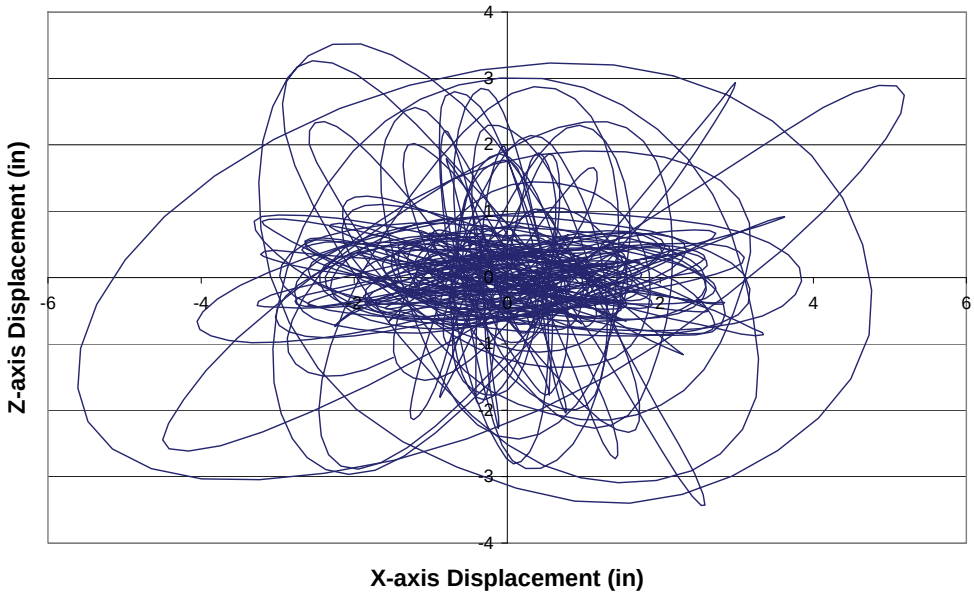

Figure 4.46: Vertical displacement versus lateral out-of-plane displacement for the second event

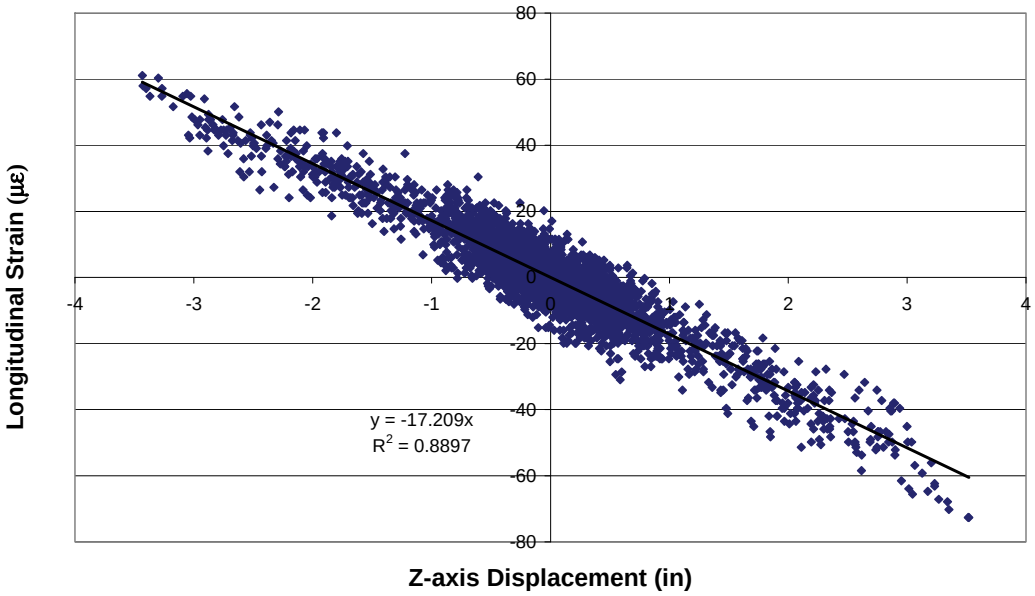

Figure 4.47: Relationship between vertical tip displacement and longitudinal strain on the top of the mast arm for the second event

The frequency content of each channel was practically identical for both cases. The principal out-of-plane frequency was determined to be 0.69 Hz. The principal in-plane frequency was determined to be 0.86 Hz. The power spectra are not as clean as at the previous sites, however, and several higher frequencies are noted for the tip acceleration data. The strain on the side of the mast arm has significant frequencies from both principal modes.

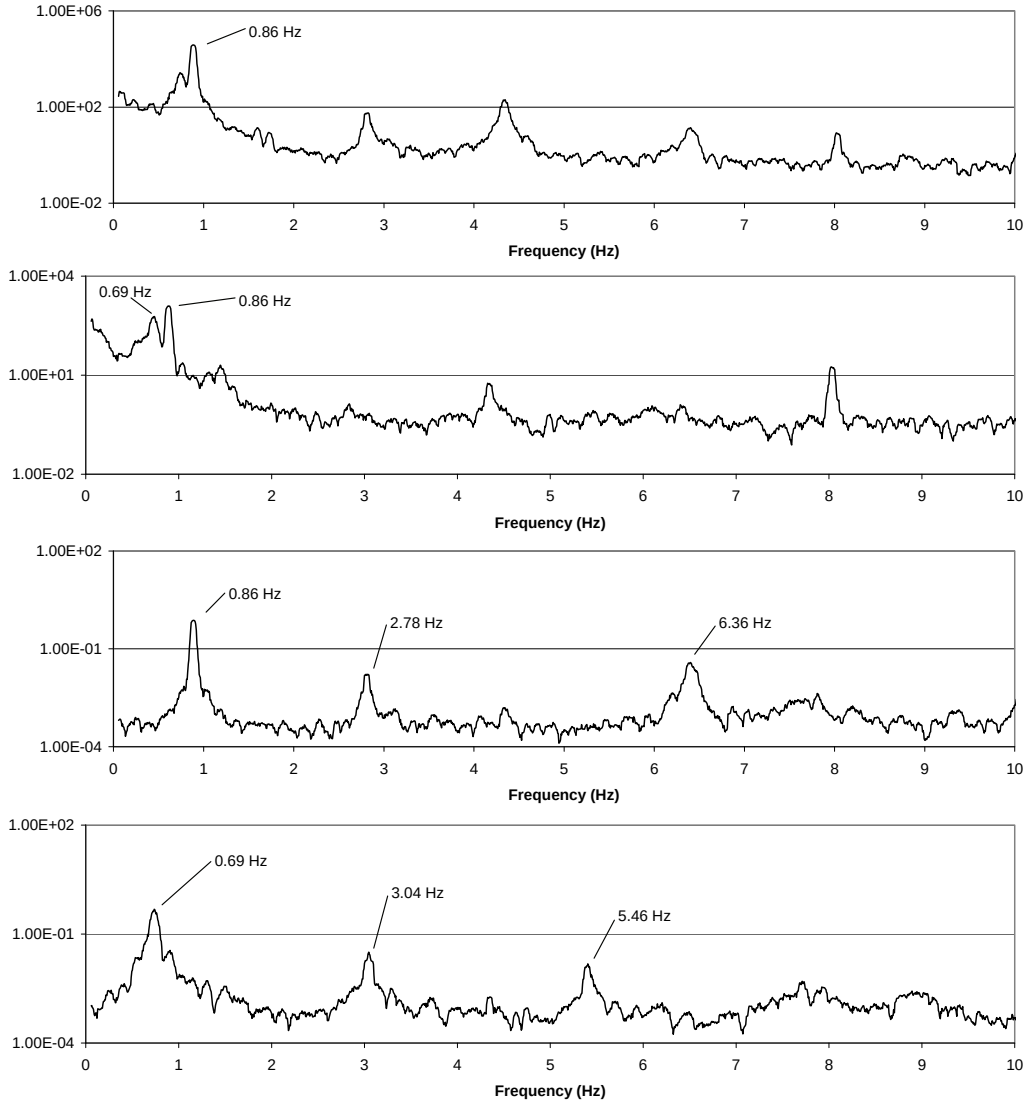

Figure 4.48: Power spectrum of top strain, side strain, vertical acceleration, and lateral out-of-plane acceleration (from top to bottom)

The wind behavior was similar for both "galloping" events. It was gusty and primarily came from the northwest with speeds between 10 and 35 mph. Figure 4.49 shows the wind velocities in their individual components over the duration of the second event, which is representative of both events. Figures 4.50 and 4.51 compare the wind resultants for each event. This underlines the observation from the other two sites that the signal structures tend to be more susceptible to large-amplitude displacements with winds that are not directly perpendicular to the mast arm. However, once again, these events were produced by sporadic wind patterns and arm displacements and are not representative of a true galloping scenario.

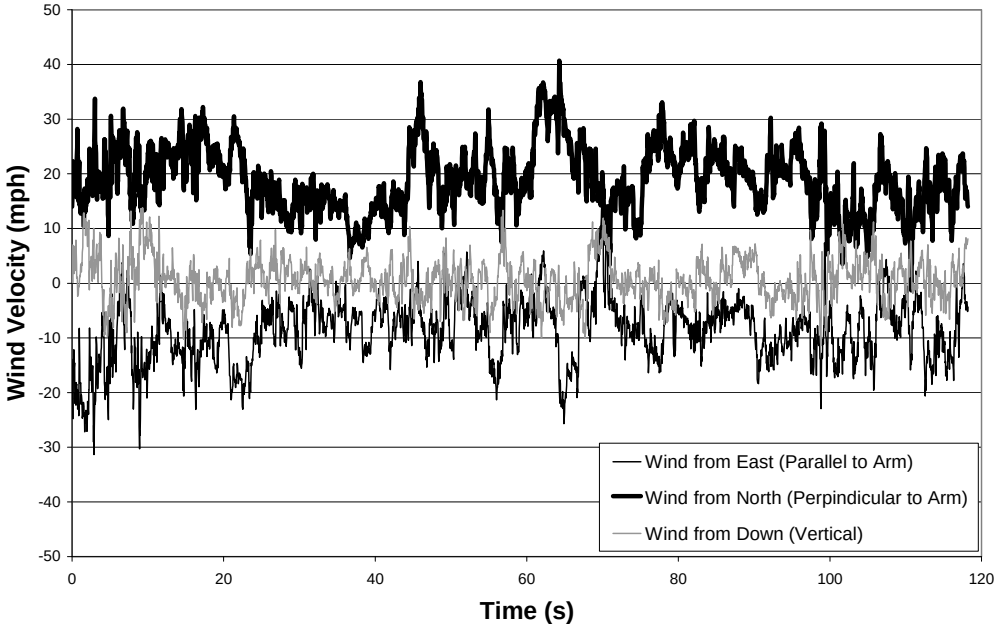

Figure 4.49: Wind velocities during the second galloping event

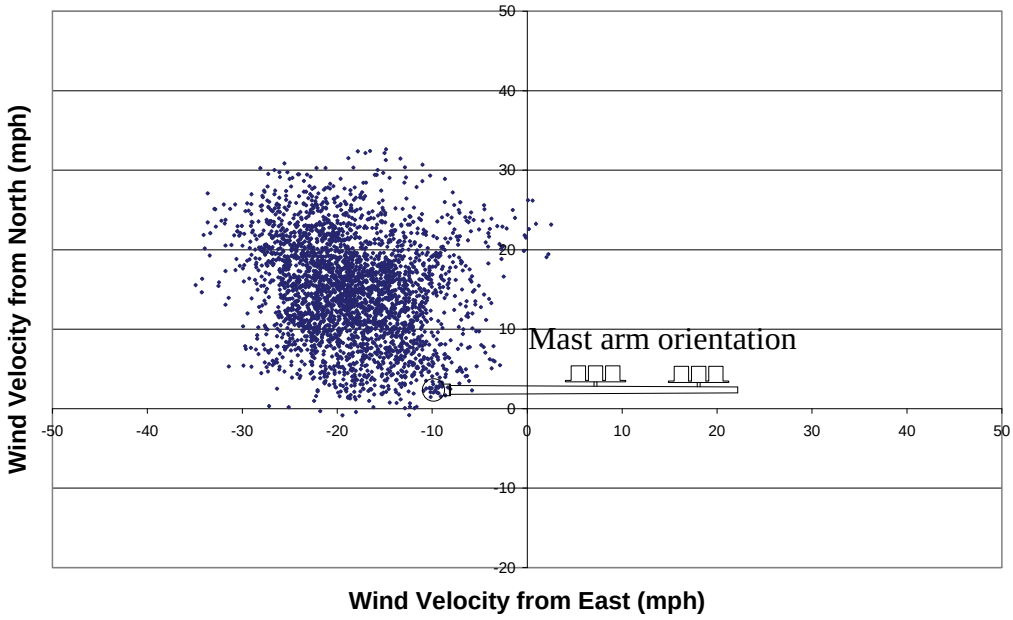

Figure 4.50: Wind resultants during first galloping event

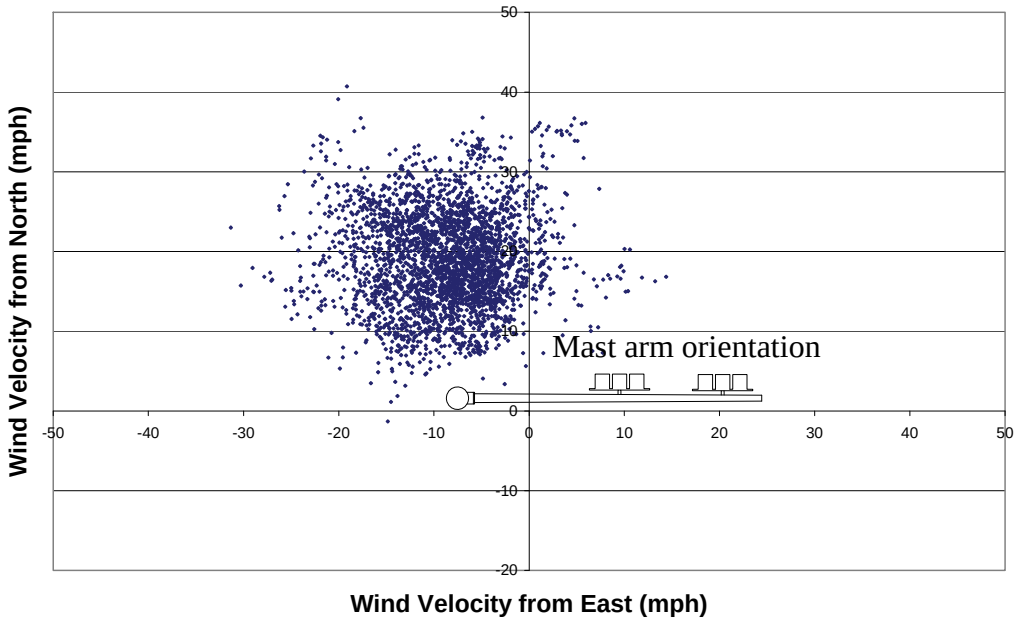

Figure 4.51: Wind resultants during second galloping event

4.6 Conclusions

Gathering data associated with galloping events in the field was not an easy or extremely fruitful task. Three traffic signal structures were instrumented and monitored for a total of about 9 months. Over 200 megabytes of data was downloaded over the wireless modem to continuously attempt to learn about the state of the wind at the site and the structure's response. Although four large-amplitude-displacement events were captured and gave insight into the behavior of the structures in windy conditions, none of them were determined to be true galloping events. Under uncontrolled conditions in the field, natural and random wind conditions determine if one will have the critical conditions required for galloping. In the tests carried out, such conditions did not occur frequently. An internal system at TxDOT to report and catalog incidents with signal structures that experience galloping behavior might improve the possibility of capturing a galloping event if such field tests are attempted in the future.

Chapter 5. Discussion of Results

5.1 Design for Galloping

5.1.1 Infrequent Galloping Confirmed

Prior to performing the field tests, it was known that galloping is only possible for certain structures whose negative aerodynamic damping has the potential to exceed any available structural damping and bring about instability. This requirement appears to be met by very few traffic signal structures, since most signal configurations have been shown to have only positive aerodynamic damping capability (McDonald et al., 1995). In addition to the need for sources of negative aerodynamic damping, the structure must also be subjected to a specific sustained wind condition for galloping to occur, and the probability that both of these criteria are met is not high. Hence, galloping traffic signal structures are not seen very often. The field tests confirmed that galloping is a rare occurrence and is not easily predictable in an uncontrolled setting. This underlines the fact, then, that it is theoretically not necessary to design all traffic signal structures to sustain galloping loads. However, since it is not currently possible to determine which signal structures might gallop, all such structures are required to be designed to resist galloping forces.

5.1.2 Comparison of Field Data with AASHTO Specifications

The strain data collected during the field tests can be utilized to compare the loads experienced during the "galloping" events with the current AASHTO design specifications. Assuming a linear strain gradient at the location of the strain gauge, the moment at the connection can be calculated as follows:

Equation 5-1: $M = S \cdot \sigma$

where M is the moment at the section, S is the section modulus, and σ is the longitudinal stress of interest.

The maximum stress ranges experienced at each site are presented along with the calculated moments in Table 5.1. An equivalent static pressure applied to each sign and signal attached to the arm can then be back-calculated using the load pattern assumed per the AASHTO specifications. The equivalent static pressures from the field tests are compared to the AASHTO requirements (for different Importance Factors) in Table 5.2.

Table 5.1: Maximum stress range, section modulus, and calculated moment experienced at each site

Test Site	Maximum Stress Range, σ (ksi)	Section Modulus, S (in^3)	Moment, M (kip-in)
Pflugerville	4.8	8.99	43.2
Round Rock	4.1	9.07	37.2
Lubbock	4.1	13.76	56.4

Table 5.2: Comparison of equivalent static pressures experienced in field tests with required design pressure per the AASHTO specifications

Test Site	Equivalent Static Pressure (psf)	Equivalent Pressure Required by AASHTO (psf)		
		I_F = 1.0	I_F = 0.65	I_F = 0.30
Pflugerville	4.9	21	13.7	6.3
Round Rock	5.3			
Lubbock	3.7			

Although the equivalent static pressures calculated above relate the findings in the field to the current requirements, they cannot be used to conclude that the requirements are conservative for the following three reasons. The first and most important reason is because the specimens in the field test never really experienced sustained galloping, and so the equivalent pressures calculated do not represent the most severe case of galloping-induced loads on the structure. Secondly, only three configurations of light signals on a structure were tested; more tests with a range of different parameters are necessary to make definitive conclusions. The last reason is that the pressures derived from the field tests may not be accurate due to the assumption of a linear strain gradient near the connection. The tests themselves showed that this assumption is completely invalid in the lateral direction. In the vertical direction, the direction of interest, the assumption was considered valid since the strain on the top of the arm appeared to be quite close to the finite-element model predictions for our test sites; however, no precise calibration was performed in the field.

A better method of calibration would consist of hanging different known weights from the tip of the mast arm (this could be done from a bucket truck to avoid closing lanes) and allowing it to come to rest. Multiplying each weight by the precise distance to the strain gauge would help to create a plot of moment versus strain from which the linear strain gradient assumptions at the connection can be checked, and the true relationship between moment and strain can in fact be directly derived.

5.1.3 Two Possible Design Approaches

As discussed in Chapter 2, all future traffic signals designed by TxDOT may have back plates. Therefore, TxDOT must design their traffic signal structures to resist the additional forces likely

to result because of these attachments. Both configurations of traffic signals with back plates that were studied at Texas Tech University (McDonald et al., 1995) have the potential to cause negative aerodynamic damping. Given the low structural damping of traffic signal structures, these signals could potentially experience galloping under the right conditions. Thus, basically two design options exist: (i) continue designing all traffic signal structures for galloping loads; or (ii) eliminate the potential of galloping by modifying the properties of the structure.

Design to Resist Galloping Forces

The loads caused by galloping are not well known. Theoretically, under optimal wind conditions and for signals with back plates that could see a continuous linear plot such as the one shown in Figure 5.1, galloping could cause increasing loads until the structure either yields or fractures. Tests have never shown galloping forces to reach this intensity, but only a very limited number and variety of controlled tests have been performed, and the worst case has most likely not been studied and subjected to the necessary wind conditions.

As discussed in Chapter 1, tests that have been done to determine galloping loads in the past have not been consistent. Some tests have even measured loads that were nearly twice the maximum required loads currently required by AASHTO for design, suggesting that the specifications may not be conservative in some cases. Part of this inconsistency comes from the fact that each structure has a unique maximum displacement amplitude caused by galloping, depending on its geometry and the aerodynamic properties of its attachments. Another part of this inconsistency comes from the fact that the equation for galloping in the current AASHTO specifications does not accurately capture the distribution of loads during a galloping event. The equation applies the same static pressure to each sign and signal. Even if all of the signs and signals were to have the same aerodynamic properties, the pressures would be greater towards the tip of the arm, for reasons explained in Chapter 2.

If tests are to be compared by back-calculating equivalent static pressure, an equation that captures this behavior should be used. In the end, determining an average maximum galloping load will not be very helpful in improving the current design requirements since some cases will still be unconservative, and it would still require all traffic signal structures to be designed to resist these galloping loads.

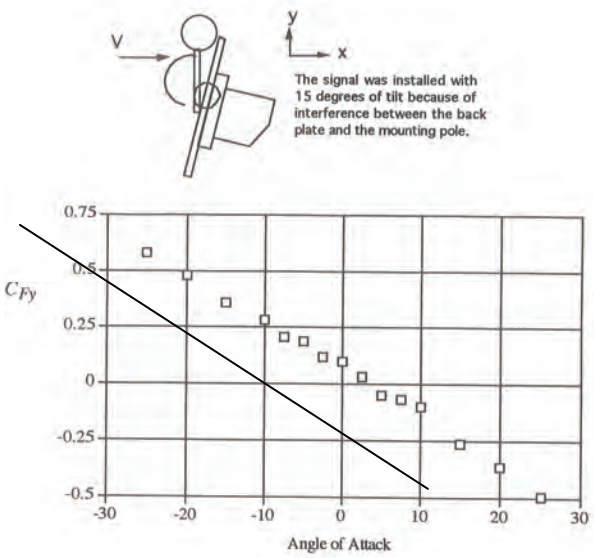

Figure 5.1: Continuously negative slope creates unlimited galloping potential

Eliminate Galloping Potential and Design Requirements

Another valid option, when faced with the possibility of galloping for traffic signal structures, would be to eliminate the possibility of it completely by modifying the properties in a way that overall negative aerodynamic damping is not possible. In this way, the galloping design criteria could be ignored, and only loads caused by natural wind gusts, vortex shedding, and truck-induced gusts would need to be considered during design. To accomplish this, an aerodynamic damper that would counteract the negative aerodynamic effects of the signals must be attached to the structure.

As discussed in Chapter 2, a horizontal sign blank, or wing, attached to the tip of the mast arm appears to be the most efficient and cost-effective solution to this problem. This option is also preferable because it could be applied to traffic signal structures that are already in service to eliminate future galloping and hence serve as a retrofit solution. One configuration of a damping wing has been subjected to tests from which specific aerodynamic damping data was retrieved. However, there have not been sufficient tests done on a variety of wings and configurations to know how to design the wings for the various conditions that exist with traffic signal structures. Additional research on the aerodynamic properties of damping wings is needed to be able to design them efficiently and with confidence in their effectiveness.

5.2 Unexpected Behavior during Field Tests

5.2.1 Diagonally Oriented Wind

The wind direction that caused the largest displacements and triggered all the four “galloping” events was not perpendicular to the mast arm. Traditionally, galloping potential has been studied only in two dimensions and determined for a cross section with wind blowing directly from the side, equivalent to a horizontal wind blowing perpendicular to the mast arm of a traffic signal

structure. The tow tank tests performed at Texas Tech University (McDonald et al., 1995) studied 3-dimensional traffic signals, but the fluid flow was still only considered in a direction perpendicular to the mast arm. Although the structures monitored during the field tests may not have ever experienced sustained galloping, they did experience large-amplitude displacements with a definite trend suggesting that the worst-case wind scenario does not always act perpendicular to the mast arm. Since galloping behavior is sensitive to the shape of the traffic signal and its orientation on the mast arm, additional testing would be needed to confirm that wind approaching at an angle might produce the worst case for traffic signals structures in general. However, it is evident that the wind parallel to the mast arm cannot be ignored when studying galloping of traffic signal structures.

5.2.2 Low Out-of-Plane Frequencies

Another unexpected behavior of the traffic signal structures was the fact that the out-of-plane frequency was, on average, 80 percent of the in-plane frequency. Finite element models of several typical traffic signal structures showed the in-plane and out-of-plane frequencies to be consistently within 5 percent of each other. One potential cause of the lower out-of-plane frequency in the field tests was thought to be the handhole near the base of the poles of all of the structures. Each of the three structures monitored had a 24 in. by 4 in. handhole cutout, as shown in Figure 5.2, which is useful for the installation and maintenance of electrical cables.

A closed cross section, like that of a pipe, is very rigid in torsion compared to a cross section of a pipe with a cut through one side. The effect of this cutout was not suspected to be as drastic as directly comparing the two cross sections because of the boundary conditions posed by the relatively short length of the handhole. However, a finite element model of a traffic signal pole with a 1-in. mesh size was created in ABAQUS both with and without the handhole present. The model with the handhole proved to be 20 percent more flexible in twisting when torsion was applied at the top of the pole than the model without the handhole.

An exaggerated distortion of the pipe near the handhole caused by the torsion can be viewed in Figure 5.3, where the model is cropped and turned on its side for visibility. This suggests that the handholes in the poles may be causing the reduced out-of-plane frequencies. Other characteristics that could contribute to this phenomenon are the potential slipping of the bolts in the slotted bolt holes at the base of the structure and a non-fixed condition at the pole-to-arm connection caused by warping of the mast arm’s base plate.

Figure 5.2: A handhole is typically cut out of the steel pipe near the base of the pole

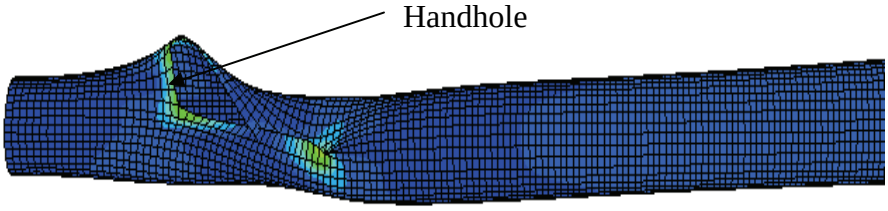

Figure 5.3: Finite element model of handhole near base of pole

5.2.3 Strain-Displacement Inconsistencies

During the field tests, inconsistencies between the displacement at the tip of the mast arm and the strain measured at the pole-to-arm connection were found. This was especially noticeable with the out-of-plane motion and the strains on the side of the mast arm. The inconsistency and unpredictability of strains near the connection may be a serious issue for traffic signal structures and could be the cause of many of their failures.

Previous research has demonstrated the strains around the cross section of the mast arm and pole near the connection to their base plate (Koenigs, 2003 and Connor, 2004) do not match the prediction based upon simple beam theory. The stress concentration appears to be unpredictable and can be caused by the flexibility of the base plate, loose bolts at the connection, and poor quality welding, among other factors. In particular, the change in stress produced by variation in bolt tension may explain why two identical structures subjected to the same wind environment at an intersection do not undergo the same fatigue damage.

Chapter 6. Conclusions

6.1 Summary of Work

The research documented in this report was part of a joint project with Texas Tech University aimed at investigating the load effects caused by galloping. The work performed on this topic at The University of Texas at Austin was broken up into two concentrations: analytical modeling and field tests.

A computer program created from the analytical model developed was utilized in parametric studies and to investigate the galloping potential of the structures at the specific field test sites. The analytical model showed that modifying a traffic signal structure's aerodynamic properties is the most effective method to eliminate galloping potential. This can be achieved by attaching traffic signals that only have positive aerodynamic damping potential, or by attaching a damping wing (also known as a sign blank) to the tip of the mast arm to counteract the negative aerodynamic damping of the signals. The latter option appears to be more desirable because it could be implemented on traffic signal structures already in service, and it would allow for back plates to be attached to the traffic signals, which is TxDOT's currently adopted practice. Although some insights on effective placement and length of damping wings were gained through parametric studies, limited data was available to perform the studies. Additional tests need to be run to determine the aerodynamic properties of variably oriented wings to be able to efficiently design them. The wings that have currently been installed on many signal structures throughout Texas tend to be very short and are attached directly to the mast arm. These attachments, in general, are probably not reducing the galloping potential of the structure at all, and a more effective application of the damping wings should be investigated and implemented.

For the field tests, three different sites, chosen because of the history of prior observed large-amplitude displacements there, were instrumented and monitored for a total of 9 months. During this time, some large-amplitude displacements occurred, but no sustained galloping events took place. These findings underline the fact that galloping is an infrequent occurrence. In fact, galloping is not even possible for many traffic signal structures, and therefore it is not necessary to design all structures to resist galloping forces. However, one must determine which structures will not gallop in order to know which structures do not need to be designed for galloping. Thus, both the aerodynamic properties of signals and damping wings need to be investigated in more detail.

During the field tests, some unexpected behavior was also observed. The first observation was that at all three sites, the largest amplitude vibrations were caused by wind not directly perpendicular to the mast arm, but occurring at an angle to the arm. The possibility of this wind condition producing the worst-case scenario for galloping has typically not been included in past research, and should be taken into consideration in future work. Another observation in the field was that the strains near the welded connection of the mast arm to its base plate were unpredictable and appeared to have concentrations at various locations. This phenomenon has been detected in previous research, but the stress concentration has never been explored in the field. These stress concentrations, unique to each structure, may be a key factor in traffic signal structure failures since quite often nearby signal structures have experienced similar loading

conditions but have not failed. The stress concentrations near the connection should be considered in future research studies of traffic signal structures.

6.2 Suggested Revision to AASHTO Specifications

With specific reference to the design equation for galloping (Eq. 11-1) in Section 11.7.1 of the AASHTO Specifications, no actual galloping events were recorded in the field tests of the present study from which one can assess the acceptability of the equivalent static pressure used for design. However, on the basis of the analytical studies conducted as part of the present study, it was shown that the forces induced by galloping depend on the location of the attachments (signals, panels, etc.) on the arm. Greater forces are expected at locations closer to the tip of the arm. The expectation is that Eq. 11-1 in the Specifications should probably recognize that a panel of the same area at different locations along the arm will likely not experience the same vertical shear range. Additional work in this area is suggested so that the design equation may be appropriately modified in the future.

Appendix D presents and discusses this suggested revision.

6.3 Ongoing and Future Research

At The University of Texas at Austin, the effects of truck gusts on the fatigue life of traffic signal structures have also been recently studied in the field as a continuation of the research performed for this report. If TxDOT is interested in utilizing damping wings to mitigate galloping, then the effects of truck gusts on the wings may be of interest as well. Researchers at Texas Tech University have also performed controlled tests on traffic signal structures to determine the loads caused by vortex shedding with a variety of traffic signal configurations.

Utilizing the findings of the research described in this report, two important topics that currently lack data are recommended for future research. The topics include a study of the aerodynamic properties of signals and damping wings, and the stress concentrations at the pole-to-arm connection of traffic signal structures.

The aerodynamic properties of signs, traffic signals, and damping wings with various geometries and configurations should be studied to help determine which structures cannot gallop and therefore should perhaps not be required to be designed for galloping loads. These studies could be carried out in a tow tank or a wind tunnel, but they should be thorough and well planned so that the final data could be utilized to design damping wings and to retrofit structures already in service.

Stress concentrations near the pole-to-arm connection are known to exist but have not been studied in depth. Warping of the end plate and variability in bolt tension may be key factors in these stress concentrations. Their effect on fatigue life, in turn, may also be considerable. Field investigations to sample the variation in bolt tension and to investigate the warping of the end plates of mast arms in service are recommended to provide insight into this potential problem.

References

American Association of State Highway and Transportation Officials. 2002 Interim to Standard Specification for Structural Supports for Highway Signs, Luminaires and Traffic Signals. AASHTO, 4th Edition, 2003.

Chopra, Anil K. Dynamics of Structures. Upper Saddle River: Prentice Hall, 2nd Edition, 2001.

Connor, Robert J et al. Laboratory and Field Fatigue Investigation of Cantilevered Signal Support Structures in the City of Philadelphia. Lehigh University, 2004.

Cook, Ronald A. and Bloomquist, David. Design, Testing, and Specification of a Mechanical Damping Device for Mast Arm Traffic Signal Structures. University of Florida, 2000.

Den Hartog, J.P. Mechanical Vibrations. New York: McGraw Hill, 4th Edition, 1956.

Dyrbye, Claës and Hansen, Svend O. Wind Loads on Structures. New York: John Wiley and Sons, 1997.

Hamilton, H.R. III, et al. Increased Damping in Cantilevered Traffic Signal Structures. University of Wyoming. Journal of Structural Engineering, V 126, Apr 2000, pp. 530-537.

Kaczinski, M.R. et al. NCHRP Report 412: Fatigue-Resistant Design of Cantilevered Signal, Sign and Light Supports. Washington D.C.: National Academy Press, 1998.

Koenigs, Mark T. et al. Fatigue Strength of Signal Mast Arm Connections. The University of Texas at Austin, 2003.

McDonald, James R. et al. Wind Load Effects on Signs, Luminaires and Traffic Signal Structures. Texas Tech University, 1995.

Pulipaka, Narendra et al. On Galloping Vibration of Traffic Signal Structures. Journal of Wind Engineering and Industrial Aerodynamics. V 77-78, Sep-Dec 1998, pp. 327-336.

Wu, Jingning et al. Wind-Induced Stresses on Traffic Signal Mast Arms: Case Studies. University of Missouri-Columbia, 2000.

Appendix A

Program to determine galloping potential of traffic signal structures as explained in Chapter 2.

User Input:

Units:

All units are in **inches, pounds,** and **seconds**

Overall:

ζ_s is the percentage of critical damping of the structure

$\zeta_s := 0.4$

Vertical Pole:

h is height of the pole up to the pole-arm connection
$\mathbf{t_p}$ is the pipe wall thickness of the pole
$\mathbf{D_{pBase}}$ is the outer diameter of the pole at its base
$\mathbf{D_{pTop}}$ is the outer diameter of the pole at the connection

$h := 218$ $t_p := .179$ $D_{pBase} := 11.62$ $D_{pTop} := 9.29$

Horizontal Arm:

L is the total length of the arm
$\mathbf{t_a}$ is the pipe wall thickness of the arm
$\mathbf{D_{aArm}}$ is the outer diameter of the arm at the pole-arm connection
$\mathbf{D_{aTip}}$ is the outer diameter of the arm at its tip

$L \equiv 340$ $t_a := .179$ $D_{aBase} := 8.26$ $D_{aTip} := 4.20$

Traffic Signals and Signs:

Exist requires a 1 if it exists and a 0 if not
Weight is the total weight of the signal or sign with brackets
Length is the length of the sign parallel to the arm
Location is the distance from the pole-arm connection to the center of the sign or signal
$\mathbf{dC_{Fy}}$ is the slope of the "C_{Fy} vs.α of attack" graph around the α of interest, usually at $\alpha = 0$
Drag is the drag coefficient measured at the same angle of attack

Sign or Signal 1:

$Exist_1 := 1$ $Weight_1 := 20$ $Length_1 := 102$ $Height_1 := 16$

$Location_1 := 68$ $dC_{fy1} := -0.5$

Sign or Signal 2:

$Exist_2 := 1$ $Weight_2 := 50$ $Length_2 := 52$ $Height_2 := 23$

$Location_2 := 166$ $dC_{fy2} := -0.5$

Sign or Signal 3:

$Exist_3 := 1$ $Weight_3 := 50$ $Length_3 := 52$ $Height_3 := 23$

$Location_3 := 263$ $dC_{fy3} := -0.5$

Sign or Signal 4:

$Exist_4 := 1$ $Weight_4 := 80$ $Length_4 := 80$ $Height_4 := 23$

$Location_4 := 348$ $dC_{fy4} := -0.5$

Sign or Signal 5:

$Exist_5 := 1$ $Weight_5 := 20$ $Length_5 \equiv 21$ $Height_5 := 9$

$Location_5 \equiv L - \frac{Length_5}{2}$ $dC_{fy5} := 4.6$

Calculations:

Pipe Properties:

$\rho s_s := .285$ $g := 386.4$ $\rho := \frac{\rho s_s}{g}$ $\rho = 7.376 \times 10^{-4}$ $E := 29600000$

Pole Properties:

$D_{po} := D_{pBase} - t_p$ $D_{ph} := D_{pTop} - t_p$

$D_p(y) := D_{po} - \left(\frac{D_{po} - D_{ph}}{h}\right) \cdot y$

$$I_p(y) := \left(\frac{\pi}{8}\cdot D_p(y)^3\right)\cdot t_p \text{ float},4 \rightarrow 7.032\cdot 10^{-2}\cdot\left(11.44 - 1.069\cdot 10^{-2}\cdot y\right)^3$$

$$A_p(y) := D_p(y)\cdot t_p\cdot\pi \text{ float},4 \rightarrow 6.435 - 6.011\cdot 10^{-3}\cdot y$$

$$M_p(y) := \rho\cdot A_p(y) \text{ float},4 \rightarrow 4.746\cdot 10^{-3} - 4.434\cdot 10^{-6}\cdot y$$

Arm Properties:

$$D_{ao} := D_{aBase} - t_a \qquad D_{aL} := D_{aTip} - t_a$$

$$D_a(x) := D_{ao} - \left(\frac{D_{ao} - D_{aL}}{L}\right)\cdot x$$

$$I_a(x) := \left(\frac{\pi}{8}\cdot D_a(x)^3\right)\cdot t_a \text{ float},4 \rightarrow 7.032\cdot 10^{-2}\cdot\left(8.081 - 1.194\cdot 10^{-2}\cdot x\right)^3$$

$$A_a(x) := D_a(x)\cdot t_a\cdot\pi \text{ float},4 \rightarrow 4.543 - 6.714\cdot 10^{-3}\cdot x$$

$$M_a(x) := \rho\cdot A_a(x) \text{ float},4 \rightarrow 3.351\cdot 10^{-3} - 4.952\cdot 10^{-6}\cdot x$$

Sign and Signal Properties:

$$M_1 := \frac{Weight_1}{Length_1\cdot g} \quad Mt_1 := \frac{Weight_1}{g} \quad a_1 := Location_1 - \frac{Length_1}{2} \quad b_1 := Location_1 + \frac{Length_1}{2}$$

$$M_2 := \frac{Weight_2}{Length_2\cdot g} \quad Mt_2 := \frac{Weight_2}{g} \quad a_2 := Location_2 - \frac{Length_2}{2} \quad b_2 := Location_2 + \frac{Length_2}{2}$$

$$M_3 := \frac{Weight_3}{Length_3\cdot g} \quad Mt_3 := \frac{Weight_3}{g} \quad a_3 := Location_3 - \frac{Length_3}{2} \quad b_3 := Location_3 + \frac{Length_3}{2}$$

$$M_4 := \frac{Weight_4}{Length_4\cdot g} \quad Mt_4 := \frac{Weight_4}{g} \quad a_4 := Location_4 - \frac{Length_4}{2} \quad b_4 := Location_4 + \frac{Length_4}{2}$$

$$M_5 := \frac{Weight_5}{Length_5\cdot g} \quad Mt_5 := \frac{Weight_5}{g} \quad a_5 := Location_5 - \frac{Length_5}{2} \quad b_5 := Location_5 + \frac{Length_5}{2}$$

Shape Functions:

The shape functions are based on the shape due to a vertical load on the arm tip equal to one, with the arm and pole each prismatic and constructed with its average diameter . This is chosen to represent the assumed shape of the structure during a galloping event . Then, the shape is normalized so the arm tip deflection is equal to unity.

$$M_{pole} := L \qquad \phi_p(y) := \frac{M_{pole}}{E \cdot I_p\left(\frac{h}{2}\right)} \qquad \theta_p(y) := \int_0^y \phi_p(a)\, da \qquad \delta_p(y) := \int_0^y \theta_p(b)\, db$$

$$V_a(x) := -1 \qquad M_{arm}(x) := \int_0^x V_a(b)\, db + L \qquad \phi_a(x) := \frac{M_{arm}(x)}{E \cdot I_a\left(\frac{L}{2}\right)}$$

$$\theta_a(x) := \int_0^x \phi_a(a)\, da + \theta_p(h) \qquad \delta_a(x) := \int_0^x \theta_a(b)\, db \qquad Factor1 := \delta_a(L) \qquad Factor1 = 0.04$$

$$\Psi_p(y) := \frac{\delta_p(y)}{Factor1} \qquad \Psi_a(x) := \frac{\delta_a(x)}{Factor1}$$

$$d\Psi_p(y) := \frac{d}{dy}\Psi_p(y) \text{ float}, 4 \rightarrow 3.806 \cdot 10^{-6} \cdot y$$

$$dd\Psi_p(y) := \frac{d}{dy}d\Psi_p(y) \text{ float}, 4 \rightarrow 3.806 \cdot 10^{-6}$$

$$d\Psi_a(x) := \frac{d}{dx}\Psi_a(x) \text{ float}, 4 \rightarrow -\left(2.740 \cdot 10^{-8}\right) \cdot x^2 + 1.863 \cdot 10^{-5} \cdot x + 8.297 \cdot 10^{-4}$$

$$dd\Psi_a(x) := \frac{d}{dx}d\Psi_a(x) \text{ float}, 4 \rightarrow -\left(5.480 \cdot 10^{-8}\right) \cdot x + 1.863 \cdot 10^{-5}$$

Calculate Generalized Mass:

$$M_{ta} := \int_0^L M_a(x)\, dx + Mt_1 \cdot Exist_1 + Mt_2 + Mt_3 + Mt_4 + Mt_5 \cdot Exist_5$$

$$Me_0 := \int_0^h \Psi_p(y)^2 \cdot M_p(y)\,dy + \Psi_p(h)^2 \cdot M_{ta} + \int_0^L \Psi_a(x)^2 \cdot M_a(x)\,dx \qquad Me_0 = 0.19$$

$$Me_1 := \int_{a_1}^{b_1} M_1 \Psi_a(x)^2\,dx \cdot Exist_1 \qquad Me_1 = 7.233 \times 10^{-4}$$

$$Me_2 := \int_{a_2}^{b_2} M_2 \Psi_a(x)^2\,dx \cdot Exist_2 \qquad Me_2 = 0.016$$

$$Me_3 := \int_{a_3}^{b_3} M_3 \Psi_a(x)^2\,dx \cdot Exist_3 \qquad Me_3 = 0.063$$

$$Me_4 := \int_{a_4}^{b_4} M_4 \Psi_a(x)^2\,dx \cdot Exist_4 \qquad Me_4 = 0.222$$

$$Me_5 := \int_{a_5}^{b_5} M_5 \Psi_a(x)^2\,dx \cdot Exist_5 \qquad Me_5 = 0.048$$

$$\alpha := 1.5$$

$$Me := Me_0 + \left(Me_1 + Me_2 + Me_3 + Me_4 + Me_5\right) \cdot \alpha \qquad Me = 0.716$$

Calculate Generalized Stiffness:

$$Ke := \int_0^h E \cdot I_p(y) \cdot dd\Psi_p(y)^2\,dy + \int_0^L E \cdot I_a(x) \cdot dd\Psi_a(x)^2\,dx \qquad Ke = 37.144$$

Calculate Natural Frequency of Assumed Mode Shape:

$$\omega := \sqrt{\frac{Ke}{Me}} \qquad \omega = 7.204$$

$$f := \frac{\omega}{2 \cdot \pi} \qquad f = 1.147$$

compare frequency to measured value from field and adjust α above until matching

Calculation of minimum wind speed for galloping to occur:

$$F_1 := Height_1 \cdot dC_{fy1} \cdot \int_{a_1}^{b_1} \Psi_a(x)^2 \cdot Exist_1 \, dx \qquad F_1 = -11.404$$

$$F_2 := Height_2 \cdot dC_{fy2} \cdot \int_{a_2}^{b_2} \Psi_a(x)^2 \cdot Exist_2 \, dx \qquad F_2 = -76.17$$

$$F_3 := Height_3 \cdot dC_{fy3} \cdot \int_{a_3}^{b_3} \Psi_a(x)^2 \cdot Exist_3 \, dx \qquad F_3 = -292.392$$

$$F_4 := Height_4 \cdot dC_{fy4} \cdot \int_{a_4}^{b_4} \Psi_a(x)^2 \cdot Exist_4 \, dx \qquad F_4 = -987.342$$

$$F_5 := Height_5 \cdot dC_{fy5} \cdot \int_{a_5}^{b_5} \Psi_a(x)^2 \cdot Exist_5 \, dx \qquad F_5 = 798.502$$

$$\rho_{air} := 1.141 \cdot 10^{-7} \qquad Factor_{mph} := \left(\frac{5280 \cdot 12}{3600}\right)^2 \qquad \frac{1}{2}\rho_{air} \cdot Factor_{mph} = 1.767 \times 10^{-5}$$

$$V_{gallop} := \frac{-4 \cdot Me \cdot \frac{\zeta_s}{100} \cdot \omega}{\rho_{air} \cdot Factor_{mph} \cdot (F_1 + F_2 + F_3 + F_4 + F_5)}$$

$V_{gallop} = 4.1$ **Velocity in MPH**

Appendix B

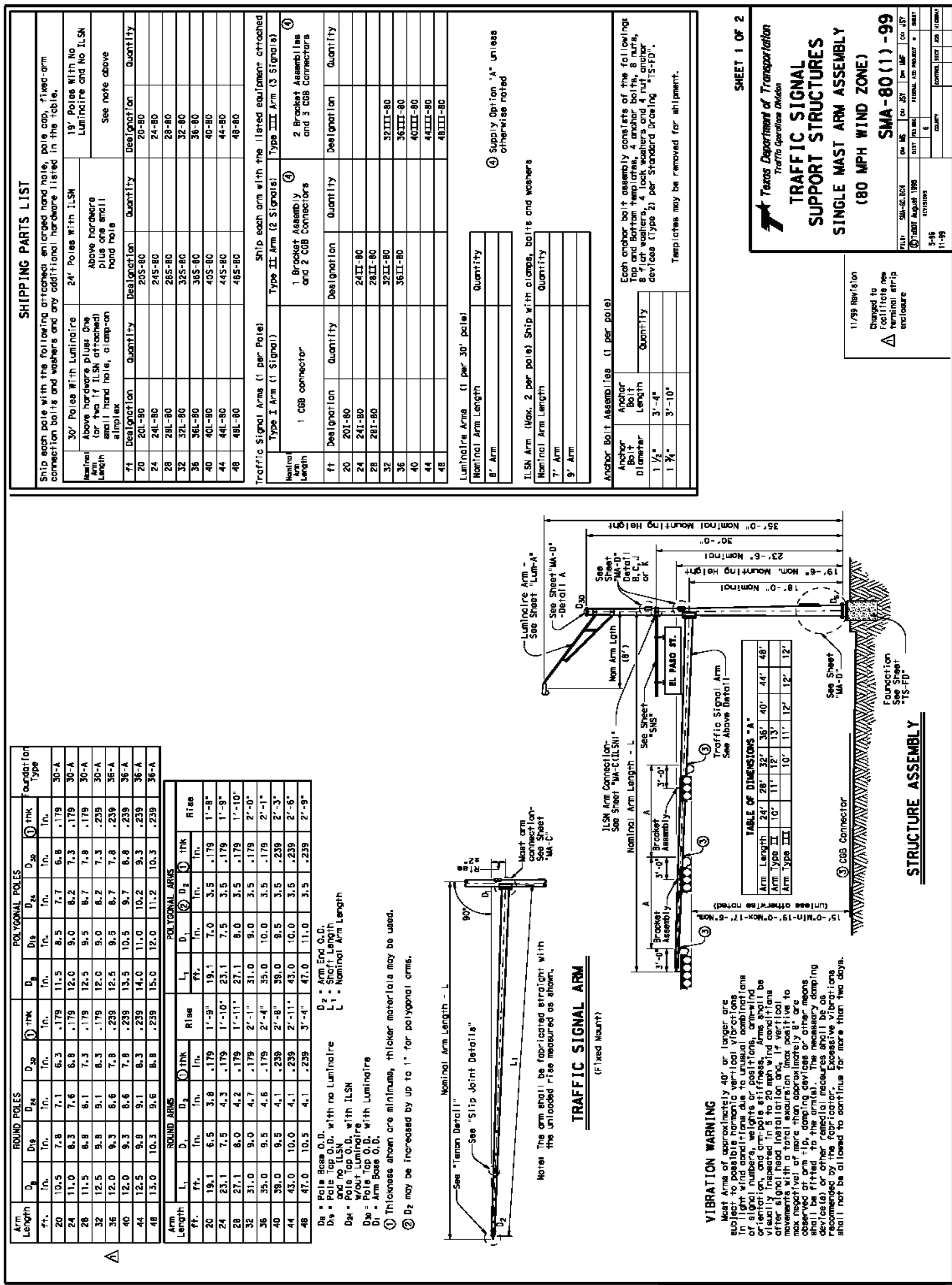

SHIPPING PARTS LIST

Ship each pole with the following attached: enlarged hand hole, pole cap, fixed-arm connection bolts and washers and any additional hardware listed in the table.

Nominal Arm Length	30' Poles With Luminaire: Above hardware plus: One (or two if ILSN attached) small hand hole, clamp-on simplex		24' Poles With ILSN: Above hardware plus one small hand hole		19' Poles With No Luminaire and No ILSN: See note above	
ft	Designation	Quantity	Designation	Quantity	Designation	Quantity
20	20L-80		20S-80		20-80	
24	24L-80		24S-80		24-80	
28	28L-80		28S-80		28-80	
32	32L-80		32S-80		32-80	
36	36L-80		36S-80		36-80	
40	40L-80		40S-80		40-80	
44	44L-80		44S-80		44-80	
48	48L-80		48S-80		48-80	

Traffic Signal Arms (1 per Pole) Ship each arm with the listed equipment attached

Nominal Arm Length	Type I Arm (1 Signal): 1 CGB connector		Type II Arm (2 Signals): 1 Bracket Assembly and 2 CGB Connectors ④		Type III Arm (3 Signals): 2 Bracket Assemblies and 3 CGB Connectors ④	
ft	Designation	Quantity	Designation	Quantity	Designation	Quantity
20	20I-80					
24	24I-80		24II-80			
28	28I-80		28II-80			
32			32II-80		32III-80	
36			36II-80		36III-80	
40					40III-80	
44					44III-80	
48					48III-80	

④ Supply Option "A" unless otherwise noted

Luminaire Arms (1 per 30' pole)

Nominal Arm Length	Quantity
8' Arm	

ILSN Arm (Max. 2 per pole) Ship with clamps, bolts and washers

Nominal Arm Length	Quantity
7' Arm	
9' Arm	

Anchor Bolt Assemblies (1 per pole)

Anchor Bolt Diameter	Anchor Bolt Length	Quantity
1 1/2"	3'-4"	
1 3/4"	3'-10"	

Each anchor bolt assembly consists of the following: Top and Bottom templates, 4 anchor bolts, 8 nuts, 8 flat washers, 4 lock washers and 4 nut anchor devices (Type 2) per Standard Drawing "TS-FD".

Templates may be removed for shipment.

Arm Length	ROUND POLES					POLYGONAL POLES					Foundation Type
	D_B	D_{19}	D_{24}	D_{30}	① thk	D_B	D_{19}	D_{24}	D_{30}	① thk	
ft.	in.	in.	in.	in.	in.	in.	in.	in.	in.	in.	
20	10.5	7.8	7.1	6.3	.179	11.5	8.5	7.7	6.8	.179	30-A
24	11.0	8.3	7.6	6.8	.179	12.0	9.0	8.2	7.3	.179	30-A
28	11.5	8.8	8.1	7.3	.179	12.5	9.5	8.7	7.8	.179	30-A
32	12.5	9.8	9.1	8.3	.179	12.0	9.0	8.2	7.3	.239	30-A
36	12.0	9.3	8.6	7.8	.239	12.5	9.5	8.7	7.8	.239	36-A
40	12.0	9.3	8.6	7.8	.239	13.5	10.5	9.7	8.8	.239	36-A
44	12.5	9.8	9.1	8.3	.239	14.0	11.0	10.2	9.3	.239	36-A
48	13.0	10.3	9.6	8.8	.239	15.0	12.0	11.2	10.3	.239	36-A

Arm Length	ROUND ARMS					POLYGONAL ARMS				
	L_1	D_1	D_2	① thk	Rise	L_1	D_1	② D_2	① thk	Rise
ft.	ft.	in.	in.	in.		ft.	in.	in.	in.	
20	19.1	6.5	3.8	.179	1'-9"	19.1	7.0	3.5	.179	1'-8"
24	23.1	7.5	4.3	.179	1'-10"	23.1	7.5	3.5	.179	1'-9"
28	27.1	8.0	4.2	.179	1'-11"	27.1	8.0	3.5	.179	1'-10"
32	31.0	9.0	4.7	.179	2'-1"	31.0	9.0	3.5	.179	2'-0"
36	35.0	9.5	4.6	.179	2'-4"	35.0	10.0	3.5	.179	2'-1"
40	39.0	9.5	4.1	.239	2'-8"	39.0	9.5	3.5	.239	2'-3"
44	43.0	10.0	4.1	.239	2'-11"	43.0	10.0	3.5	.239	2'-6"
48	47.0	10.5	4.1	.239	3'-4"	47.0	11.0	3.5	.239	2'-9"

D_B = Pole Base O.D.
D_{19} = Pole Top O.D. with no Luminaire and no ILSN
D_{24} = Pole Top O.D. with ILSN w/out Luminaire
D_{30} = Pole Top O.D. with Luminaire
D_1 = Arm Base O.D.
D_2 = Arm End O.D.
L_1 = Shaft Length
L = Nominal Arm Length

① Thickness shown are minimums, thicker materials may be used.

② D_2 may be increased by up to 1" for polygonal arms.

Note: The arm shall be fabricated straight with the unloaded rise measured as shown.

TRAFFIC SIGNAL ARM

(Fixed Mount)

VIBRATION WARNING

Mast Arms of approximately 40' or longer are subject to possible harmonic vertical vibrations in light wind conditions due to unusual combinations of signal numbers, weights or positions, arm-wind orientation, and arm-pole stiffness. Arms shall be visually inspected in 5 to 20 mph wind conditions after signal head installation and, if vertical movements with a total excursion (max positive to max negative) of more than approximately 8" are observed at arm tip, damping devices or other means shall be fitted to the arm(s). The necessary damping device(s) or other remedial measures shall be as recommended by the fabricator. Excessive vibrations shall not be allowed to continue for more than two days.

TABLE OF DIMENSIONS "A"							
Arm Length	24'	28'	32'	36'	40'	44'	48'
Arm Type II	10'	11'	12'	13'			
Arm Type III			10'	11'	12'	12'	12'

STRUCTURE ASSEMBLY

11/99 Revision
Changed to facilitate new terminal strip enclosure

SHEET 1 OF 2

Texas Department of Transportation
Traffic Operations Division

TRAFFIC SIGNAL SUPPORT STRUCTURES
SINGLE MAST ARM ASSEMBLY
(80 MPH WIND ZONE)

SMA-80(1)-99

FILE: SMA-80.DGN | DN: MS | CK: JSY | DW: LMF | CK: JSY
©TxDOT August 1995 | DIST | FED REG 6 | FEDERAL AID PROJECT | SHEET | COUNTY | CONTROL | SECT | JOB | HIGHWAY
REVISIONS 5-96 11-99

123A

Appendix C

```
MATLAB program to convert accelerations to displacements

%Remove all existing variables
clear all;

%Close all open diagrams so that windows open on plot command
close all;

%Read File
dlmread Pluck_For_FFT.txt;
Data=ans;
clear ans;

% Set variable Araw equal to Acceleration data in 3 axes
Araw=Data(:,6:8);
clear ans;
clear Data;

%Input the sampling rate in seconds
deltaT=0.0416984924623102;
SamFreq=1/deltaT;

%Convert acceleration data from G's to in/s^2
Araw=Araw*386.088;

% Determine original data size
AccSize=length(Araw);

%Find N from m, where vector length for FFT is N=2^m
i=1; m=0;
while i<2;
  if AccSize>2^m;
    m=m+1;
    i=1;
  else i=2;
  end
end
clear i;
N=2^m;
clear m;

% Create a matrix called time to correspond to each data value
for i=1:N;
  time(i,1)=(i-1)*deltaT;
end

%Perform fft of Accelerations, automatically pads with zeros to reach N
Aw=fft(Araw,N);

%Create frequencies that correspond to each fft entry
for i=0:N/2;
  Freq(i+1,1)=SamFreq*i/N;
end
for i=1:N/2-1
  Freq(N+1-i,1)=SamFreq*i/N;
end
```

```
% Create plots to see FFT of each channel, then input filter sizes to apply
figure(1);
plot(Freq(1:(N/SamFreq)*10),abs(Aw(1:(N/SamFreq)*10,1)));
filter1=input('Input the highest frequency you wish to filter out:');

figure(2);
plot(Freq(1:(N/SamFreq)*10),abs(Aw(1:(N/SamFreq)*10,2)));
filter2=input('Input the highest frequency you wish to filter out:');

figure(3);
plot(Freq(1:(N/SamFreq)*10),abs(Aw(1:(N/SamFreq)*10,3)));
filter3=input('Input the highest frequency you wish to filter out:');
close all;

% Apply filter to acceleration data in frequency domain
for i=1:N;
  if Freq(i)<filter1;
    Aw(i,1)=0;
  end
  if Freq(i)<filter2;
    Aw(i,2)=0;
  end
  if Freq(i)<filter3;
    Aw(i,3)=0;
  end
end

% Inverse fft, then take real values to eliminate insignificant data left
% behind by the added zeros
Afiltered=real(ifft(Aw));

% Integrate the acceleration data to get velocities
V(1,1:3)=0;
for i=2:AccSize;
  V(i,1)=.5*(Afiltered(i-1,1)+Afiltered(i,1))*deltaT+V(i-1,1);
  V(i,2)=.5*(Afiltered(i-1,2)+Afiltered(i,2))*deltaT+V(i-1,2);
  V(i,3)=.5*(Afiltered(i-1,3)+Afiltered(i,3))*deltaT+V(i-1,3);
end

%Perform fft of Velocities, automatically pads with zeros to reach N
Vw=fft(V,N);

% Plot FFT of each channel to ensure previous filter limits are ok
figure(1);
plot(Freq(1:(N/SamFreq)*10),abs(Vw(1:(N/SamFreq)*10,1)));
pause;

figure(2);
plot(Freq(1:(N/SamFreq)*10),abs(Vw(1:(N/SamFreq)*10,2)));
pause;

figure(3);
plot(Freq(1:(N/SamFreq)*10),abs(Vw(1:(N/SamFreq)*10,3)));
pause;
close all;
```

```
% Apply filters to velocity data in frequency domain
for i=1:N;
  if Freq(i)<filter1;
    Vw(i,1)=0;
  end
  if Freq(i)<filter2;
    Vw(i,2)=0;
  end
  if Freq(i)<filter3;
    Vw(i,3)=0;
  end
end

% Inverse fft, then take real values to eliminate insignificant data left
% behind by the added zeros
Vfiltered=real(ifft(Vw));

% Integrate the velocity data to get displacements
D(1,1:3)=0;
for i=2:AccSize;
  D(i,1)=.5*(Vfiltered(i-1,1)+Vfiltered(i,1))*deltaT+D(i-1,1);
  D(i,2)=.5*(Vfiltered(i-1,2)+Vfiltered(i,2))*deltaT+D(i-1,2);
  D(i,3)=.5*(Vfiltered(i-1,3)+Vfiltered(i,3))*deltaT+D(i-1,3);
end

%Perform fft of Displacements, automatically pads with zeros to reach N
Dw=fft(D,N);

% Plot FFT of each channel to ensure previous filter limits ok
figure(1);
plot(Freq(1:(N/SamFreq)*10),abs(Dw(1:(N/SamFreq)*10,1)));
pause;

figure(2);
plot(Freq(1:(N/SamFreq)*10),abs(Dw(1:(N/SamFreq)*10,2)));
pause;

figure(3);
plot(Freq(1:(N/SamFreq)*10),abs(Dw(1:(N/SamFreq)*10,3)));
pause;
close all;

% Apply filter to displacement data in frequency domain
for i=1:N;
  if Freq(i)<filter1;
    Dw(i,1)=0;
  end
  if Freq(i)<filter2;
    Dw(i,2)=0;
  end
  if Freq(i)<filter3;
    Dw(i,3)=0;
  end
end

% Inverse fft, then take real values to eliminate insignificant data left
% behind by the added zeros
```

```
Dfiltered=real(ifft(Dw));

% Plot displacements vs. time for each axis
figure (1);
plot(time(1:AccSize),Dfiltered(1:AccSize,1));
pause;

figure (2);
plot(time(1:AccSize),Dfiltered(1:AccSize,2));
pause;

figure (3);
plot(time(1:AccSize),Dfiltered(1:AccSize,3));
pause;

% Create a matix including time and displacements and write to file
for i=1:AccSize
  OutFile(i,1)=time(i);
  OutFile(i,2:4)=Dfiltered(i,1:3);
end

dlmwrite('Pluck_Displacements',OutFile, ',')

close all;
```

Appendix D

Product 1: Recommended Changes to the AASHTO Standard Specifications for Structural Supports for Highway Signs, Luminaires, and Traffic Signals (Section 11: Fatigue Design)

Based on the present study and another study on truck-induced gust loading (Albert et al., 2007), the following suggested revisions to the AASHTO specifications have been prepared.

2007 AASHTO BRIDGE COMMITTEE AGENDA ITEM

SUBJECT:

TECHNICAL COMMITTEE: T-12 – Structural Supports for Signs, Luminaires, and Traffic Signals

---

☒	**REVISION**	☐	**ADDITION**	☐	**NEW DOCUMENT**
☐	**DESIGN SPEC**	☐	**CONSTRUCTION SPEC.**	☐	**MOVABLE SPEC.**
☐	**LRFR MANUAL**	☐	**OTHER**		
☐	**US VERSION**	☐	**SI VERSION**	☒	**BOTH**

DATE PREPARED: November 7, 2007
DATE REVISED:

AGENDA ITEM:

- Append to the end of the following paragraph in the Commentary of Section 11.7.1:

"By combining wind tunnel tests and analytical calibrations to field data… …should be applied to the structure at the center of gravity of the sign panel."

the following sentences:

"A recent study (Florea et al., 2007) has shown that the equivalent static force that a sign panel of any dimension experiences depends on the location along the arm where the panel is attached. Equivalent static pressures or vertical shear ranges applied to the frontal area of each sign or traffic signal attachment are greater towards the tip of the arm. The specification ignores the effect of location upon the galloping force. Testing is necessary to verify this and to suggest location-specific ranges; at the present time, a static force of (1000 Pa × Area of Sign Panel in m^2 × I_F) in Newtons or (21 psf × Area of Sign Panel in ft^2 × I_F) in lb should be applied."

- Revise Section 11.7.4:

Replace the last paragraph,
"The truck-induced gust loading may be excluded for the fatigue design of overhead cantilevered traffic signal structures, as allowed by the owner."

with the following paragraph,
"The truck-induced gust loading may be excluded for the fatigue design of overhead cantilevered traffic signal structures."

This means the words "as allowed by the owner" should be deleted.

• Revise the Commentary to Section 11.7.4:

Replace the last paragraph,
"The given truck-induced gust loading may be excluded for the fatigue design of overhead traffic signal structures, as allowed by the owner. Many traffic signal structures are installed on roadways with negligible truck traffic. In addition, the typical response of cantilevered traffic signal structures from truck-induced gusts can be significantly overestimated by the design pressures prescribed in this article. However, some cantilever traffic signal structures have experienced large-amplitude vibrations from truck-induced gusts applied under the right conditions."

with the following,

"The given truck-induced gust loading may be excluded for the fatigue design of overhead traffic signal structures. Many traffic signal structures are installed on roadways with negligible truck traffic. In addition, the typical response of cantilevered traffic signal structures from truck-induced gusts is significantly overestimated by the design pressures prescribed in this article. This has been confirmed in a recent study (Albert et al., 2007) involving full-scale field tests where strains were monitored on cantilevered traffic signal structures. Over 400 truck events were recorded covering a variety of truck types and vehicle speeds; only 18 trucks produced even a detectable effect on the cantilevered traffic signal structures and the strains were very small relative to those associated with the design pressures in this article.

• Add the following references to Section 11.9

M. J. Florea, L. Manuel, K. H. Frank, and S. L. Wood, *Field Tests and Analytical Studies of the Dynamic Behavior and the Onset of Galloping in Traffic Signal Structures.* Report No. FHWA/TX-07/4586-1, Austin, Texas: Center for Transportation Research, Texas Department of Transportation, 2007.

M. N. Albert, L. Manuel, K. H. Frank, and S. L. Wood, *Field Testing of Cantilevered Traffic Signal Structures under Truck-Induced Gust Loads.* Report No. FHWA/TX-07/4586-2, Austin, Texas: Center for Transportation Research, Texas Department of Transportation, 2007.

OTHER AFFECTED ARTICLES:

None

BACKGROUND:

In a recently completed study on galloping of traffic signal structures, it was determined analytically that the forces induced by galloping depend on the location of the attachments (signals, panels, etc.) on the arm. Greater forces are expected at locations closer to the tip of the arm. While the cited study (Florea et al., 2007) involved extensive field studies on three different traffic signal structures, it was not possible to instrument multiple locations along the arm and it was also difficult to get the tested structures to experience galloping. Still, the expectation is that the design equation should probably recognize that a panel of the same area at different locations along the arm will likely not experience the same vertical shear range. Additional work in this area is suggested so that the design equation may be appropriately modified in the future.

In recently completed full-scale field tests (Albert et al., 2007) to evaluate truck-induced gust loadings on cantilevered traffic signal structures, it was found that recorded strains due to various truck types passing beneath these structures (and for a range of vehicle speeds) were negligibly small. While VMS structures might require truck-induced gust loading considerations for fatigue design, stresses generated by the passage of trucks under cantilevered signal structures are negligible.

ANTICIPATED EFFECT ON BRIDGES:

It is possible that elimination of the truck-induced gust loading design equation for cantilevered traffic signal structures will lead to more economical sections if the currently employed design equation controlled the design.

REFERENCES:

M. J. Florea, L. Manuel, K. H. Frank, and S. L. Wood, *Field Tests and Analytical Studies of the Dynamic Behavior and the Onset of Galloping in Traffic Signal Structures.* Report No. FHWA/TX-07/4586-1, Austin, Texas: Center for Transportation Research, Texas Department of Transportation, 2007.

M. N. Albert, L. Manuel, K. H. Frank, and S. L. Wood, *Field Testing of Cantilevered Traffic Signal Structures under Truck-Induced Gust Loads.* Report No. FHWA/TX-07/4586-2, Austin, Texas: Center for Transportation Research, Texas Department of Transportation, 2007.

OTHER: